Dissertation

submitted to the

Combined Faculty for the Natural Sciences and Mathematics

of the Ruperto Carola University Heidelberg, Germany

for the degree of

Doctor of Natural Sciences

Presented by

M.Sc. Karen Groß

Born in: Heidelberg, Germany

Oral examination: 28.10.2022

Embryonic and post-embryonic organogenesis in the medaka lateral line

Referees: Jun.-Prof. Dr. Lázaro Centanin

Dr. Sergio Acebrón

Abstract

Organs are functional units of multicellular organisms. Although the body can compensate for minor deficiencies in organ function in some cases, generally, survival of the organism depends on organ integrity. A critical step in the life of multicellular organisms is therefore organogenesis, which needs to be tightly regulated to prevent pathologic conditions. This thesis deals with the formation of stereotypic patterns on the organ and organ system level during embryonic and post-embryonic development of the Japanese rice fish medaka (*Oryzias latipes*).

The lateral line has been widely used as a model to study a variety of developmental processes. The lateral line is a sensory organ system of fish and aquatic amphibia that is used to detect water movement. It consists of small organs, so-called neuromasts, that are distributed bilaterally in stereotypic patterns across the entire surface of the animal. All embryonically formed neuromasts originate from specialized regions of head ectoderm (placodes) and from there populate the entire body via migrating primordia or sensory ridges. The lateral line can be divided into the anterior lateral line (aLL), including all neuromasts on the head, and the posterior lateral line (pLL), consisting of neuromasts on the tail.

While the embryonic development of pLL neuromasts via a migrating primordium has been extensively studied, the embryonic development of aLL neuromasts remains vastly understudied. This is potentially due to the complexity of the aLL system. I quantified position and number of aLL neuromasts of medaka in detail based on a previously published atlas, which defines nine distinct aLL sub-lines, according to innervation. Quantification of neuromast numbers revealed that some aLL sub-lines are characterized by variability in organ number, similar to the pLL, while other aLL sub-lines are highly stereotypic and display perfect symmetry among the left and right side of the same fish.

In addition, I started to uncover the developmental mechanisms building the aLL in medaka. Using live-imaging, whole-mount immunohistochemistry and *in situ* hybridization, I was able to identify sensory ridges as the tissue of origin for the majority of aLL neuromasts. The remaining few neuromasts are generated by a migrating primordium that relies on chemokine signaling via Cxcr4b, similar to the pLL primordium.

Furthermore, results from genetic and non-genetic perturbation experiments during embryonic development indicate that interactions with the surrounding tissue are an integral part of aLL development. Moreover, differential responses to perturbation in different aLL sub-lines suggest diverse developmental mechanisms within the aLL.

Like amphibians and some reptiles, fish display the remarkable feature of indeterminate growth. Neuromasts adjust to an ever-growing body by increasing in size, but also by generating additional organs post-embryonically from pre-existing neuromasts all over the body. The caudal neuromast cluster (CNC) is a group of neuromasts located on the caudal fin. Previous experiments from our lab have shown that in medaka all neuromasts in the CNC are derived from a single organ that was deposited on the caudal fin during embryonic development. The CNC is exceptionally well suited to study post-embryonic organogenesis due to its stereotypic location, accessibility for imaging and early onset of post-embryonic organogenesis. Using a combination of live-imaging, genetic tools and immunohistochemistry, I was able to start deciphering the mechanism of post-embryonic organogenesis on the tissue level. Briefly, a subset of neuromast stem cells that we termed organ-founder stem cells, undergoes an epithelial-to-mesenchymal transition (EMT), migrates out of a founder neuromast and generates a post-embryonic organ in a highly stereotypic manner.

The results acquired in this thesis indicate that stem cell migration is influenced by interactions with the surrounding tissue, specifically at the anterior side of the founder neuromast. Although the full mechanistic understanding of these tissue interactions remains elusive, my findings suggest that chemokine signaling via Cxcr4b and interaction with the vasculature are involved in the regulation of stem cell migration. I discuss these results in light of diseases in mammals. Possibly, molecular routes that are used under physiological conditions in fish, can be hijacked by cells in mammals, leading to pathologies.

Zusammenfassung

Organe sind funktionale Untereinheiten mehrzelliger Organismen. Obwohl der Körper in einigen Fällen in der Lage ist eine eingeschränkte Organfunktion auszugleichen, hängt das Überleben des Organismus im Allgemeinen von der Unversehrtheit der Organe ab. Daher ist die Organogenese ein wichtiger Vorgang im Leben mehrzelliger Organismen, der genau reguliert werden muss, um pathologische Zustände zu verhindern. Diese Dissertation befasst sich mit der Bildung stereotyper Muster auf Organ- und Organsystemebene des Seitenliniensystems während der embryonalen und post-embryonalen Entwicklung des Japanischen Reisfisches Medaka (*Oryzias latipes*).

Das Seitenliniensystem wurde bereits häufig als Modellsystem verwendet, um eine Vielzahl entwicklungsbiologischer Prozesse zu untersuchen. Es ist ein sensorisches Organsystem, das in Fischen und wasserlebenden Amphibien vorhanden ist, dessen Funktion es ist, Wasserbewegungen wahrzunehmen. Es besteht aus kleinen Organen, sogenannten Neuromasten, die beidseitig auf der gesamten Körperoberfläche in stereotypen Mustern angeordnet sind. Alle embryonal gebildeten Neuromasten stammen aus spezialisierten Regionen des Kopfektoderms (Plakoden) und besiedeln von dort den gesamten Körper über migrierende Primordia oder sogenannte sensorische Kämme. Das Seitenliniensystem kann unterteilt werden in das anteriore Seitenliniensystem (aLL), bestehend aus Neuromasten auf dem Kopf, und das posteriore Seitenliniensystem (pLL), welches die Neuromasten auf dem Schwanz beinhaltet.

Während die embryonale Entwicklung des posterioren Seitenliniensystems über ein migrierendes Primordium umfassend untersucht wurde, erfuhr die embryonale Entwicklung des anterioren Seitenliniensystems wenig Aufmerksamkeit. Möglicherweise lag das an der Komplexität des anterioren Seitenliniensystems. Ich quantifizierte deshalb, basierend auf einem zuvor veröffentlichten Atlas, der ausgehend von Innervierung neun verschiedene Unterseitenlinien bezeichnet, detailliert Position und Anzahl der Neuromasten des anterioren Seitenliniensystems in Medaka. Die Quantifizierung der Anzahl der Neuromasten offenbarte, dass sich einige Unterseitenlinien durch eine variable Anzahl an Organen auszeichnen, wohingegen andere durch beständige Anzahl an Organen und daher perfekte Symmetrie zwischen der rechten und linken Seite des gleichen Fisches gekennzeichnet sind.

Darüber hinaus begann ich, die entwicklungsbiologischen Mechanismen, die der embryonalen Entwicklung des anterioren Seitenliniensystems in Medaka zu Grunde liegen, zu untersuchen. Mit Hilfe der Lebendmikroskopie, Immunhistochemie und *In situ* Hybridisierung konnte ich sensorische Kämme als Ursprung der meisten Neuromasten des anterioren Seitenliniensystems identifizieren. Die wenigen übrigen Neuromasten werden, wie sich herausstellte, durch ein migrierendes Primordium gebildet, das auf ein Chemokinsignal über Cxcr4b angewiesen ist, ähnlich wie das Primordium des posterioren Seitenliniensystems.

Des Weiteren deuten Ergebnisse aus Experimenten mit genetischen und nicht-genetischen Störeinflüssen während der Embryonalentwicklung darauf hin, dass Interaktionen mit dem

umgebenden Gewebe eine wesentliche Rolle in der Entwicklung des anterioren Seitenliniensystems spielen. Außerdem deuten unterschiedliche Reaktionen der Unterseitenlinien auf Störeinflüsse darauf hin, dass verschiedene entwicklungsbiologische Mechanismen innerhalb des anterioren Seitenliniensystems vorliegen.

Fische zeichnen sich wie Amphibien und einige Reptilien durch die bemerkenswerte Eigenschaft unbegrenzten Wachstums aus. Neuromasten passen sich an einen ständig wachsenden Körper zum einen durch Wachstum des Organs, zum anderen aber auch durch Bildung zusätzlicher Organe auf der ganzen Körperoberfläche an. Diese entwickeln sich aus bereits bestehenden Organen während des post-embryonalen Lebens. Das caudale Neuromast-Cluster (CNC) ist eine Gruppe von Neuromastorganen auf der Schwanzflosse. Frühere Experimente unseres Labors haben gezeigt, dass alle Neuromasten des CNCs in Medaka aus einem einzigen Organ hervorgehen, das während der Embryonalentwicklung auf der Schwanzflosse gebildet wird. Aufgrund seiner stereotypen Position, seiner Erreichbarkeit für Mikroskopie und des frühen Beginns der post-embryonalen Organogenese ist das CNC außerordentlich gut geeignet, die post-embryonale Organogenese zu untersuchen. Mit Hilfe einer Kombination aus Lebendmikroskopie, genetischen Werkzeugen und Immunhistochemie, begann ich mit der Entschlüsselung des Mechanismus der post-embryonalen Organogenese auf Gewebeebene. Zusammengefasst stellt es sich so dar, dass ein Teil der Neuromaststammzellen, genannt organbildende Stammzellen, eine Epithelial-mesenchymale Transition (EMT) durchläuft, aus dem Ursprungsorgan auswandert und ein post-embryonales Organ auf sehr stereotype Art und Weise bildet.

Die in dieser Dissertation zusammengetragenen Ergebnisse weisen darauf hin, dass Zellmigration durch Interaktion mit dem umgebenden Gewebe, speziell an der anterioren Seite des Ursprungsorgans, mit gesteuert wird. Obwohl sich die mechanistische Grundlage dieser Gewebsinteraktionen noch nicht erschließt, deuten meine Ergebnisse darauf hin, dass ein Chemokinsignal über Cxcr4b und Interaktion mit Blutgefäßen die Regulation der Stammzellmigration mit beeinflussen. Interessant könnten diese Ergebnisse auch im Hinblick auf Krankheitsbilder in Säugetieren sein. Möglicherweise können molekulare Abläufe, die in Fischen unter regulären physiologischen Bedingungen stattfinden, in Säugetieren bei Störungen derselben zur Ausbildung bestimmter pathologischer Zustände führen.

Contents

Abbreviations

4-Di-2-ASP	4-(4-diethylaminostyryl)-1-methylpyridinium iodide
AG	anterior group
aLL	anterior lateral line
aLLn	anterior lateral line nerve
aLLp	anterior lateral line placode
aml	anterior mandibular line
Amp	ampicillin
ANC	anterior neuromast cluster
BC	border cell
BCIP	5-Brom-4-chlor-3-indoxylphosphat
BMP	bone morphogenetic protein
BSA	bovine serum albumin
Cas	CRISPR-associated system
CDS	coding sequence
CNC	caudal neuromast cluster
CRISPR	clustered regularly interspaced short palindromic repeats
Cxcl12a	CXC motif chemokine ligand 12a
Cxcr	CXC motif chemokine receptor
DAPI	4', 6-diamidino-2-phenylindole
DG	dorsal group
digUTP	digoxigenin deoxyuridine triphosphate
DNA	deoxyribonucleic acid
dpf	days post fertilization
dph	days post hatch
DR	dorsal ramus of the anterior lateral line nerve
E. coli	*Escherichia coli*
eGFP	enhanced green fluorescent protein
Egln3	Egl-9 Family Hypoxia Inducible Factor 3
EMT	epithelial-to-mesenchymal transition
ERM	embryonic rearing medium
EtOH	ethanol
Eya1	eyes absent 1

FGF	fibroblast growth factor
Fli1	friend leukemia integration 1
fwd	forward
GFP	green fluorescent protein
h	hour
HC	hair cell
HIF	hypoxia inducible factor
hl	horizontal line
HNT	hyomandibular nerve trunk
H2A	histone H2A
H2B	histone H2B
H_2O	water
Igf1r	insulin-like growth factor 1 receptor
INT	infraorbital nerve trunk
I-SceI	meganuclease I-SceI
K15	Keratin 15
l	liter
LB	lysogeny broth
lol	lower opercular line
M	molar
m	milli-
MC	mantle cell
mCFP	membrane cyan fluorescent protein
MeOH	methanol
min	minute
MP	multi-photon
mYFP	membrane yellow fluorescent protein
NBT	nitro blue tetrazolium
NGS	natural goat serum
PAM	protospacer adjacent motif
PBS	phosphate buffered saline
PCP	planar cell polarity
PCR	polymerase chain reaction
PEG	polyethylene glycol
PFA	paraformaldehyde
X	

PG	posterior groove organ
PGC	primordial germ cells
pLL	posterior lateral line
pLLp	posterior lateral line placode
PTW	phosphate buffered saline plus Tween 20
PVG	posteroventral group
rc	rostral commissure
RFP	red fluorescent protein
RNA	ribonucleic acid
RT	room temperature
rv	reverse
sdf1	stromal cell-derived factor 1
sec	second
SC	support cell
sgRNA	single guide RNA
SNT	supraorbital nerve trunk
TAE	tris-acetate-EDTA
TB	terrific broth
Tris	tris hydroxymethyl aminomethane
vegf	vascular endothelial growth factor
vegfr	vascular endothelial growth factor receptor
vol	ventral orbital line
Wnt	Wingless/Integrated
wph	weeks post hatch
wt	wildtype
x	-fold

1 Introduction

1.1 Medaka as a model system to study organogenesis

Organogenesis is a crucial step in the development of multicellular organisms. Without a set of functioning organs, multicellular organisms are compromised and, in many cases, not viable. Therefore, organogenesis and homeostasis of functional organs need to be tightly regulated to prevent pathologic conditions. The Japanese rice fish medaka (*Oryzias latipes*) is an excellent model system to study organogenesis for several reasons. The transparent embryos develop externally, enabling live-imaging during embryonic development, which is completed relatively fast within seven to nine days post fertilization. Furthermore, a plethora of genetic tools have been successfully established for medaka, such as transgenesis (Grabher and Wittbrodt, 2007), Cre/LoxP-based lineage tracing (Centanin et al., 2014; Okuyama et al., 2013) and CRISPR/Cas9-mediated mutagenesis (Ansai and Kinoshita, 2014; Stemmer et al., 2015).

An outstanding characteristic of fish, amphibia and some reptiles, as opposed to other vertebrates, is indeterminate growth. Unlike mammals, they continue to grow even after reaching sexual maturity. As a consequence, their organs need to adapt to the continuous increase in body size, to maintain functionality and ensure survival of the organism. There are two mechanisms to compensate for increased body size: Increase in organ size and increase in organ number. Both mechanisms can be found and studied in medaka, qualifying it as an outstanding model system to study organogenesis during embryogenesis, but also during the post-embryonic life. The medaka eye has been successfully used to address post-embryonic growth (Becker et al., 2021; Centanin et al., 2014; Tsingos et al., 2019). As the fish grow, the number of eyes stays constant, however, eye size is increased significantly. Stem cells are thought to be an integral part of this process. In the fish lateral line, increase in both organ size and number can be observed. This thesis contributes to elucidating mechanisms of embryonic development of the medaka lateral line and in addition generation of lateral line organs during post-embryonic development.

1.2 Morphology and function of the lateral line

The lateral line is a sensory organ system of fish and aquatic amphibia that is used to detect flow and pressure changes in the surrounding water (Dijkgraaf, 1963). It enables the animals to gather information about their environment to orient themselves, avoid predators or detect pray. The lateral line system consists of small sensory organs, so-called neuromasts, which are

distributed bilaterally across the entire surface of the animal body in a species-specific pattern. The system can be subdivided into the anterior lateral line (aLL), consisting of neuromasts on the head, and the posterior lateral line (pLL), entailing neuromasts on the tail (Fig. 1A). pLL neuromasts are arranged into two lines of organs on the tail: midline pLL neuromasts (secondary neuromasts) and ventral pLL neuromasts (primary neuromasts). Midline and ventral pLL neuromasts form an alternating pattern with a midline pLL neuromast in between two neighboring ventral pLL neuromasts (Fig. 1A). The neuromast pattern of the aLL is rather complex. Based on nerve connections, aLL neuromasts have been grouped into nine distinct aLL sub-lines, generating a first atlas of aLL neuromasts (Ishikawa, 1994). Quantification of aLL neuromasts performed in this thesis were based on an adapted version of this atlas. Neuromast organs of the aLL and pLL look indistinguishable at hatchling stages (Fig. 1B, C). Neuromasts are simple organs, consisting of only four different cell types (Fig. 1D). Sensory hair cells (HC) are located at the core of the organ. Deflection of the hair cell cilium results in a signal that is relayed to the brain. Mantle cells (MC) are bona fide neuromast stem cells, which was shown by lineage tracing and ablation experiments (Seleit, Krämer et al., 2017b). MC are arranged in a ring, enveloping support and hair cells. MC give rise to support cells (SC), which in turn divide to generate HC. Border cells (BC) have been shown to act as a physical niche for neuromast stem cells (Seleit, Krämer et al., 2017b). A number of reporter lines have been established in medaka to label different cell types within the neuromast. The promoters *Keratin 15* (*K15*) and *Eyes absent 1* (*Eya1*) have been shown to be active in neuromast cells. *Eya1* is expressed in fully differentiated HC and to a lower extent in SC and some MC (Fig. 1B, C) (Seleit et al., 2017a). *K15* is expressed in epithelial cells and MC, the stem cells of the system (Fig. 1B, C) (Seleit, Krämer et al., 2017b). Many transgenic lines used in this thesis were generated using these promoters, driving expression in epithelial cells, neuromast stem cells or differentiated cells.

Generation of transgenic reporter lines using different tagged fluorescent proteins facilitates visualization of cellular shape and its dynamics *in vivo*. Neuromasts display a typical, volcano-like shape (Fig. 2A, 90°). Neuromast stem cells (MC) are elongated along the apical-basal axis and appear epithelialized (Fig. 2B). They form an opening pore, through which HC cilia project towards the environment to fulfill their function in sensing water movement (Fig. 2A, 0°).

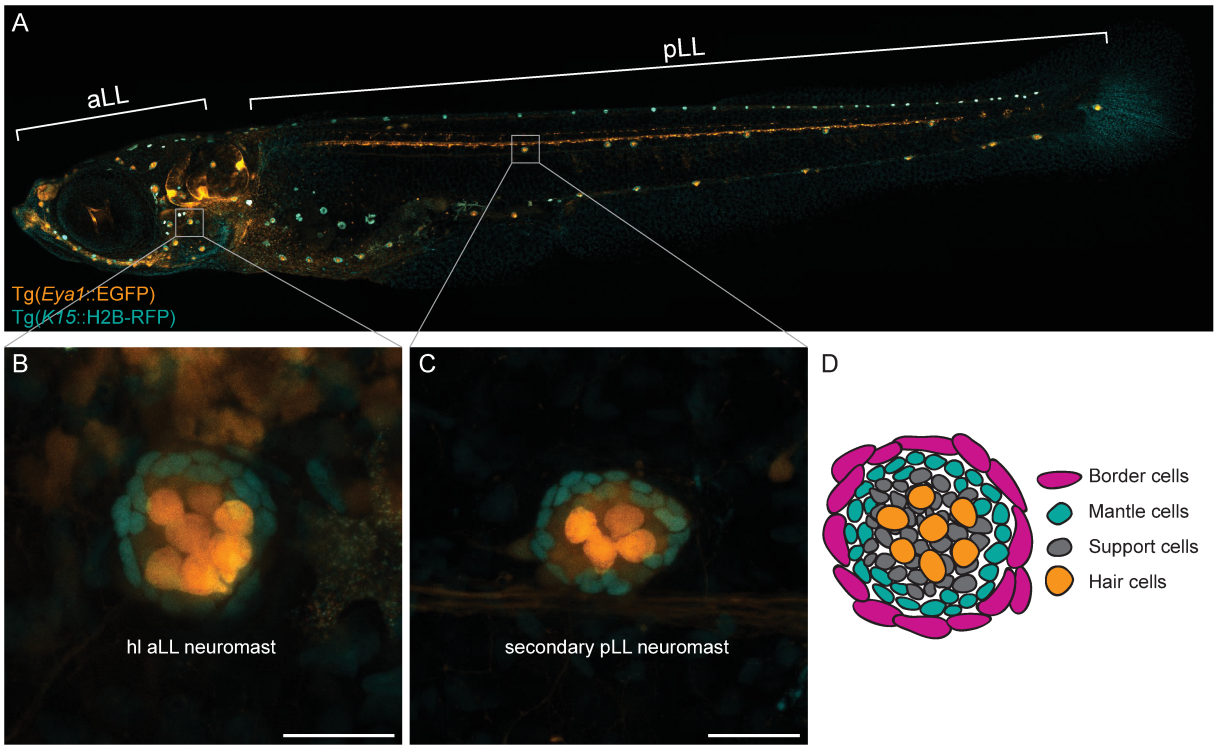

Figure 1: Morphology of the lateral line and its organs. A: The sensory lateral line system consists of neuromasts that are distributed across the entire body. The lateral line can be subdivided into the anterior lateral line (aLL) and posterior lateral line (pLL). B: Neuromast organ of the aLL. C: Neuromast organ of the pLL. aLL and pLL neuromasts are indistinguishable at juvenile stages. Scale bars = 20 µm. D: Schematic depiction of a neuromast organ consisting of four different cell types: Border cells (BC), mantle cells (MC), support cells (SC) and hair cells (HC). The scheme was adapted from (Seleit, Krämer et al., 2017b).

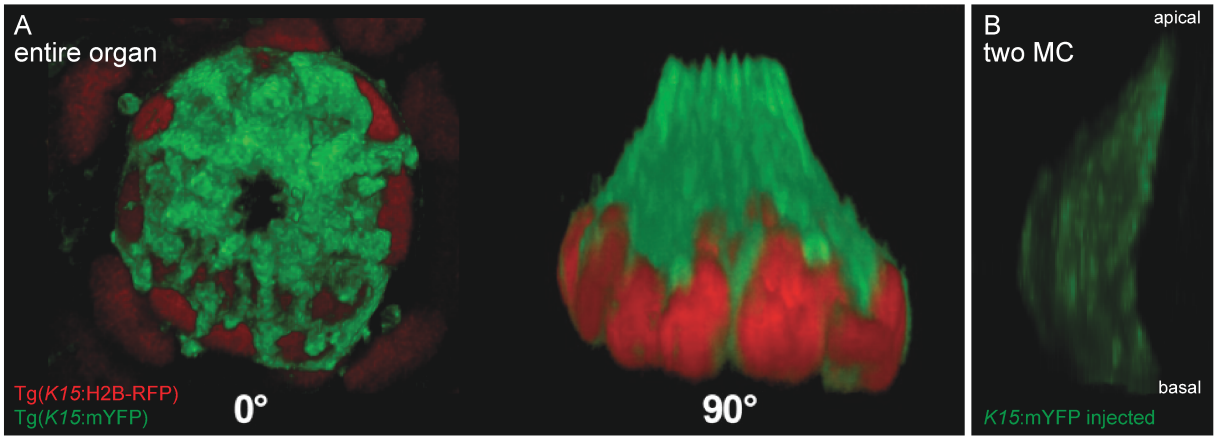

Figure 2: Neuromast stem cell morphology. A: 3D reconstruction of an entire neuromast organ. 0° shows an apical view on a neuromast organ (image taken by Jasmin Onistschenko). 90° shows a lateral view on a neuromast organ (image adapted from Seleit, Krämer et al. (2017b)). Neuromast stem cells are elongated and appear epithelialized with an apical and basal pole. They form a pore for protruding hair cell cilia. B: 3D reconstruction of two isolated neuromast stem cells. Using mosaic expression of *K15*:mYFP via injection of a plasmid, single stem cells were labelled. The shape indicates polarization along the apical-basal axis.

1.3 Embryonic development of the lateral line

1.3.1 Origin of lateral line tissues

The lateral line is derived from ectodermal placodes, evolutionary innovations of vertebrates (Northcutt, 1996). During embryonic development, a horseshoe-shaped panplacodal area is specified in cranial ectoderm adjacent to the anterior region of the neural plate (Schlosser, 2002a, 2007, 2010). The panplacodal area is induced after gastrulation and depends on activation of FGF signaling together with attenuation of BMP and Wnt signaling (Litsiou et al., 2005; Nikaido et al., 2017). Apart from the lateral line placodes, the panplacodal area gives rise to the adenohypophyseal, olfactory, lens, trigeminal, profundal, otic and epibranchial placode. It is thought that different placodes are successively specified from the panplacodal area (Schlosser, 2006). Together with the otic and epibranchial placodes, the lateral line placodes originate from the posterior Pax2/Pax8^{+} and Sox2/Sox3^{+} region of the panplacodal area in amphibians (Pieper et al., 2011; Piotrowski and Baker, 2014; Schlosser, 2010). So far, the mechanistic basis for lateral line placode induction is not well understood. Originally, there seem to have been six lateral line placodes, three pre-otic and three post-otic placodes. In different taxa however, some placodes might have been lost, fused or are difficult to distinguish morphologically (Northcutt et al., 1994; Piotrowski and Baker, 2014; Schlosser, 2002b). Placodes often appear as transient thickenings of the inner ectodermal layer and give rise to neuromast organs, as well as the neurons innervating them (Piotrowski and Baker, 2014; Schlosser, 2002a). Recently, it was discovered that aLL and pLL placode specification in zebrafish rely on different signaling pathways (Nikaido et al., 2017). Using genetic or pharmacological activators/inhibitors of Wnt, BMP, Fgf and retinoic acid signaling, it was shown that retinoic acid is required for pLL placode specification, while Fgf signaling is required for specification of aLL placodes. Additionally, Wnt and BMP were shown to negatively regulate pLL placode size (Nikaido et al., 2017). After specification, both aLL and pLL placodes undergo morphogenetic changes and generate neuromasts on the head and tail, respectively. These morphogenetic events are described in detail below.

1.3.2 Neuromast formation via migrating primordium

The development of the pLL after induction of the pLL placode has been extensively studied in various model organisms (Dona et al., 2013; Haas and Gilmour, 2006; Harrison, 1904; Seleit et al., 2017a; Valentin et al., 2007). A cluster of about 140 collectively migrating cells, called primordium, delaminates from the pLL placode and migrates posteriorly along the horizontal myoseptum until it reaches the caudal fin, along with the pLL nerve. While traveling along the

horizontal myoseptum, the primordium deposits protoneuromasts, immature neuromasts, in regular intervals (Ghysen and Dambly-Chaudiere, 2007; Haas and Gilmour, 2006; Seleit et al., 2017a). Work mainly conducted in zebrafish indicates that the primordium is patterned by the activity of Wnt and Fgf signaling. In the leading part of the primordium a Wnt signaling center, sustained by a positive feedback loop is established. Additionally, Wnt signaling induces the expression of the ligands Fgf3 and Fgf10a. At the same time Fgf signaling in Wnt^+ cells in the leading part of the primordium is inhibited. Fgf3 and Fgf10a bind to the Fgf receptor in the rear end of the primordium, where an Fgf signaling center is established (Aman and Piotrowski, 2008). In turn, Fgf signaling in the rear end of the primordium induces expression of Dkk1b, which inhibits Wnt signaling, restricting Wnt signaling to the leading part of the primordium (Aman and Piotrowski, 2008). Thus, two stable, mutually exclusive signaling centers are established within the primordium.

Fgf signaling in the rear end of the primordium controls the formation of protoneuromasts, by organizing primordium cells into epithelialized rosette-like structures. Fgf induces the expression of Atoh1a and DeltaD and thereby determines future hair cell progenitors in the middle of the rosette-like structures (Nechiporuk and Raible, 2008). At a given time-point during primordium migration, a number of protoneuromast rosettes are present in the rear end of the primordium, that successively stop migrating and are thereby deposited. These deposited protoneuromasts are connected by so-called interneuromast cells, that originate from the primordium as well.

So far, the mechanisms driving pLL primordium migration seem conserved among zebrafish and medaka (Dona et al., 2013; Haas and Gilmour, 2006; Seleit et al., 2017a; Valentin et al., 2007). Primordium migration from anterior to posterior is highly polarized and follows a trail of Cxcl12a ligand that is expressed along the horizontal myoseptum (Haas and Gilmour, 2006; Seleit et al., 2017a). Directionality is ensured by the expression of chemokine receptors Cxcr4b and Cxcr7 in the primordium, which both bind to and compete for the ligand Cxcl12a. While Cxcr4b is expressed throughout the primordium, expression of Cxcr7 is limited to the trailing part (Dambly-Chaudiere et al., 2007; Haas and Gilmour, 2006; Valentin et al., 2007). Restriction of Cxcr7 expression is due to the asymmetric activity of Wnt signaling in the primordium (Aman and Piotrowski, 2008). Binding of Cxcl12a to Cxcr4b results in intracellular signaling driving migratory behavior of primordium cells. In contrast to this, binding of Cxcl12a to Cxcr7, which appears to be more efficient, does not produce intracellular signaling (Dalle Nogare and Chitnis, 2017; Naumann et al., 2010). Instead, the receptor/ligand pair is internalized and the ligand is degraded, while the receptor is recycled (Naumann et al., 2010). Thereby, the concentration of Cxcl12a ligand that is available to the cell via Cxcr4b is higher

at the leading side of the primordium, generating a Cxcl12a gradient that drives posterior primordium migration. In this thesis I show that aLL development is largely independent from Cxcr4b-based chemokine signaling, with the exception of a single aLL sub-line, which is derived from a chemokine driven primordium, just like the pLL. Moreover, results obtained in this thesis suggest that Cxcr4b-dependent cell migration is not only restricted to embryonic development of the lateral line, but is also a factor driving post-embryonic neuromast formation in the pLL, albeit not in the aLL.

Cells at the leading edge of the primordium display a rather mesenchymal phenotype, while cells at the rear end appear more epithelialized (Dalle Nogare and Chitnis, 2017). It has recently been shown that cells of the primordium leading edge express Snail1b in response to Cxcl12a, inducing an EMT specifically in cells of the leading edge. Snail1b expression in the trailing edge is repressed by Fgf signaling (Neelathi et al., 2018).

Although seemingly self-organizing, pLL primordium and neuromasts are in constant exchange with their environment. It has been shown in zebrafish and medaka that interaction with the surrounding tissue is crucial for proper primordium migration and neuromast positioning. Disturbance of tissue interactions leads to halting or slowing of primordium migration and aberrant neuromast pattern (Nogare et al., 2019; Seleit et al., 2021). The findings of this thesis suggest that tissue interactions are not only crucial for embryonic development of the pLL, but are also instructive during embryonic development of the aLL and post-embryonic neuromast formation.

While the mechanisms driving primordium migration seem to be similar in zebrafish and medaka, there are differences in setting up of the pLL neuromast pattern. The embryonic zebrafish pLL is set up by several primordia that migrate consecutively and deposit neuromasts along the way (Ghysen and Dambly-Chaudiere, 2007). The embryonic medaka pLL is set up by only a single primordium that deposits primary neuromasts along the horizontal myoseptum. These primary neuromasts migrate ventrally after deposition to form the ventral posterior lateral line (vpLL). Primary neuromasts are connected via so-called interneuromast cells. Interneuromast cells, together with cells escaping from primary neuromasts, generate secondary neuromasts in between every pair of primary neuromasts. Secondary neuromasts migrate dorsally and localize to the midline (Seleit et al., 2017a). Thereby, the typical alternating pattern of neuromasts in the medaka pLL is formed (Fig. 1A).

Upon deposition by the primordium or formation from interneuromast cells, protoneuromasts undergo a maturation process to form fully functional neuromasts. This maturation process includes the recruitment of epithelial cells from the surrounding epithelium. Recruited epithelial

cells undergo morphological and gene expression changes and acquire border cell fate. Border cells then act as a physical niche for neuromast stem cells (Seleit, Krämer et al., 2017b).

1.3.3 Neuromast formation via sensory ridge

Although not extensively studied on a mechanistic level, it has been reported that neuromasts, in particular neuromasts on the head (aLL), are formed via sensory ridges in amphibia and cartilaginous fish (Balfour; Northcutt et al., 1994; Piotrowski and Baker, 2014; Winklbauer and Hausen, 1983). Like primordia, sensory ridges are derived from lateral line placodes. However, as opposed to migrating primordia, sensory ridges are not migratory, but stretch over the tissue mainly via proliferation, while remaining connected to their place of origin (Winklbauer and Hausen, 1983). Proliferation does not occur in specialized growth zones, but throughout the entire sensory ridge (Winklbauer and Hausen, 1983). Neuromast formation begins with rosette-like structures, similar to protoneuromasts in the pLL primordium, that are organized in the middle of the sensory ridge along its length and eventually erupt through the outer epidermal layer rather simultaneously (Northcutt et al., 1994; Winklbauer and Hausen, 1983).

Only recently was the mechanistic basis of neuromast formation on the head of zebrafish tackled on a molecular level (Iwasaki et al., 2020). In the development of the zebrafish aLL both migratory and non-migratory primordia were observed. Non-migratory primordia possibly correspond to sensory ridges. Neuromast formation via non-migratory primordia in the aLL of zebrafish was shown to rely on interactions with underlying tissues for proliferation and differentiation (Iwasaki et al., 2020).

The first part of this thesis gives a detailed description of the aLL pattern in medaka and moreover begins to elucidate the mechanistic basis for its development. The results indicate that most aLL lines in medaka are formed from sensory ridges and not migrating primordia. Moreover, distinct aLL sub-lines seem to rely on different developmental mechanisms, as suggested by differential reaction to different stimuli.

1.4 Post-embryonic growth of the lateral line

After embryonic development, fish and amphibia possess a certain number of lateral line organs. Throughout the lifetime of the animals, this number is increased immensely through post-embryonic organogenesis (Ghysen and Dambly-Chaudiere, 2007; Ledent, 2002; Nunez et al., 2009; Schlosser, 2002a; Wada et al., 2013; Wada et al., 2010). Post-embryonic organogenesis in the lateral line occurs all over the body with most embryonically generated neuromasts giving rise to additional organs. Post-embryonic neuromasts are formed from pre-

existing organs by a process termed stitching. So far, the mechanistic basis of stitching is not well understood. It has been shown that post-embryonic organogenesis in the zebrafish caudal fin depends on Wnt signaling induced by the pLL nerve (Wada et al., 2013).

In medaka, post-embryonic organogenesis has been described in the caudal neuromast cluster (CNC), a group of up to around 10 neuromasts on the caudal fin (Fig. 3B') (Seleit, Krämer et al., 2017b). Advantages of the CNC as a model system are its accessibility for imaging and stereotypic position, allowing unambiguous identification and iterative imaging. Ablation experiments have shown that the CNC is entirely derived from a single neuromast (P0-neuromast, Fig. 3A') that is deposited on the caudal fin by the pLL primordium during embryonic development (Seleit et al., 2017a; Seleit, Krämer et al., 2017b). Furthermore, lineage tracing experiments based on the Cre/LoxP system performed by Isabel Krämer in our lab suggest that the majority of cells in CNC neuromasts are derived from only a subset of cells within the P0-neuromast (Seleit, Krämer et al., 2017b).

With this thesis I contribute to elucidating the mechanistic basis for post-embryonic organogenesis in the CNC of medaka. Neuromast stem cells in the anterior part of the P0-neuromast undergo an EMT, migrate in anterior direction in a Cxcr4b-dependent manner and generate the first post-embryonic PE1-neuromast. The data suggest that this process heavily relies on tissue interactions with the surrounding microenvironment.

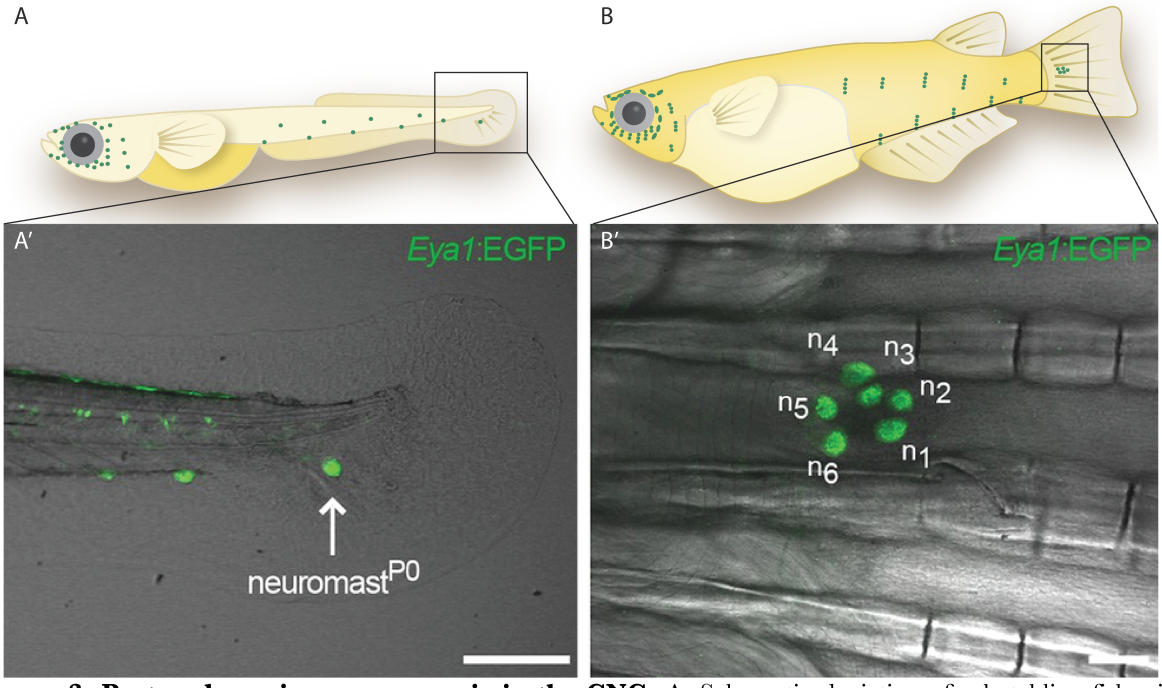

Figure 3: Post-embryonic organogenesis in the CNC. A: Schematic depiction of a hatchling fish with embryonically generated neuromasts. A': Embryonically generated P0-neuromast on the caudal fin. B: Schematic depiction of an adult medaka fish. The number of neuromasts increases with increased body size. B': CNC of an adult fish. Five post-embryonic organs have been generated from the P0-neuromast. All CNC organs are positioned in between the same fin rays. Images in A' and B' were adapted from (Seleit, Krämer et al., 2017b). Throughout this thesis, microscopy images are shown with the same orientation, if not otherwise specified: The anterior side faces left and the posterior side faces right.

1.5 Adult stem cells

Adult stem cells are the body's horn of plenty. By generating both new stem cells and differentiated cells they drive tissue growth, homeostasis and regeneration, while at the same time maintaining a constant stem cell pool. In contrast to embryonic stem cells, adult stem cells have a limited potency and only generate cells of the tissues in which they reside throughout the lifetime of an organism. Adult stem cells can be found in numerous tissues and are located in specialized microenvironments, termed niches (Morrison and Spradling, 2008). Niche is an abstract term describing all cellular and molecular factors that regulate stem cell behavior. Communication between niche and stem cells occurs bidirectionally and can be of different nature. Signaling between stem cells and their microenvironment has been shown to be transmitted via mechanical stimuli, secreted biochemical factors and direct cellular contacts (Chacon-Martinez et al., 2018; Manokawinchoke et al., 2021; Vining and Mooney, 2017; Wong et al., 2008). The sum of signals regulating cell behavior can be specific to particular stem cell/niche units.

How stem cells react to signals from the niche can be variable due to differences in stem cell intrinsic cues (such as variations in gene expression) and/or received signals from the microenvironment resulting in heterogeneous stem cell behavior in terms of cell fate, proliferative activity or division mode. It has been proposed that heterogeneous stem cell behavior is used as a mechanism to maintain a constant stem cell pool, while at the same time allowing stem cells to respond to differentiation signals (Graf and Stadtfeld, 2008). How stem cell heterogeneity is generated however, and how heterogeneous stem cells act together to form a functioning stem cell pool is not fully understood yet.

An example of heterogeneous behavior can be observed in neuromast stem cells. K15 has been used as a neuromast stem cell marker (Seleit, Krämer et al., 2017b). Stable transcriptional reporters driven by the *K15* promoter display rather homogeneous signals within stem cells (Fig. 4A). In order to confirm the observed expression pattern of *K15* transcriptional reporter lines, I performed an *in situ* hybridization against *K15*. While the expression pattern was well recapitulated by the transgenic lines, expression levels within neuromast stem cells, but also epithelial cells were heterogeneous (Fig. 4B). Using destabilized transcriptional reporters, Jasmin Onistschenko was able to confirm this finding and show that upregulation of *K15* correlates with epithelial cells and neuromast stem cells undergoing mitosis (Jasmin Onistschenko, unpublished). The neuromast as a very simple organ might therefore serve as a suitable system to address interactions between stem cells and their microenvironment *in vivo* to gain insight in the regulation of stem cell behavior.

This thesis deals with the heterogeneous regulation of migratory behavior of neuromast stem cells in the context of organ morphogenesis.

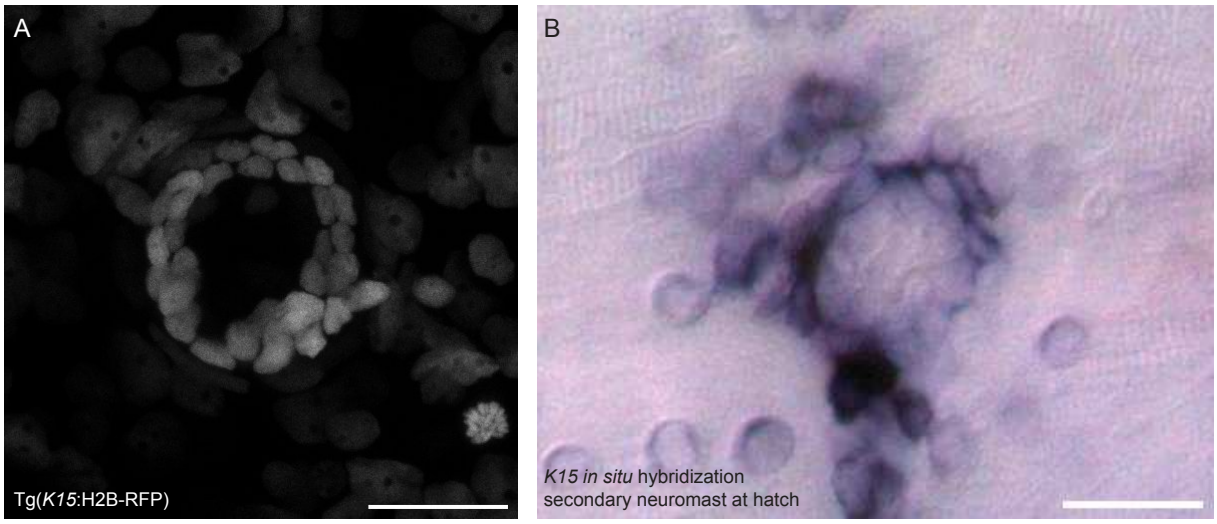

Figure 4: Heterogeneous gene expression in neuromast stem cells. A: Stable transgenic line Tg(*K15*:H2B-RFP). Signal within neuromast stem cells appears homogeneous. B: Via *in situ* hybridization, heterogeneous *K15* expression can be observed in neuromast stem and epithelial cells. Scale bars=20 µm.

Aims

The aim of this study was to shed light on two aspects of organogenesis in the lateral line of medaka:

1) Organ formation in the anterior lateral line during embryonic development

Although the lateral line has been a subject of research for over a century, surprisingly little is known about the anterior lateral line. Using live-imaging and whole-mount staining, I addressed the morphogenetic events leading to aLL formation during embryonic development. Furthermore, using different mutant lines, I tackled the question whether aLL and pLL development depend on similar pathways.

2) Organ formation during post-embryonic development

Among other organisms, teleost fish distinguish themselves by indeterminate growth. Their organs handle this challenge by increasing either in size, as can be seen in many organs, such as the eye, or in number. Increase in organ number can be observed in the lateral line. At the end of embryogenesis, fish possess a certain (variable) number of neuromast organs. This number is increased substantially over the life-time of the fish. So far, little is known about how new organs are formed and integrated into an already existing, functional system. In this study I examined post-embryonic organ formation in the caudal fin of medaka. I characterized the events of post-embryonic organogenesis using live-imaging at different stages. Moreover, using immunohistochemistry, laser ablation, ectopic gene expression tools and CRISPR/Cas9 I started to uncover the mechanistic basis of this process.

2 Results

2.1 Part I: Embryonic development of the anterior lateral line

2.1.1 Identification and quantification of aLL neuromasts

The lateral line has been a subject of research for over a century, tackling questions of directed cell migration, cell differentiation, patterning processes, organogenesis, etc. (Balfour; Haas and Gilmour, 2006; Harrison, 1904; Hofer, 1908; Leydig, 1850; Lush et al., 2019; Nechiporuk and Raible, 2008; Nogare et al., 2019; Sapede et al., 2002; Schulze, 1870; Seleit et al., 2021; Seleit et al., 2017a; Seleit, Krämer et al., 2017b; Stone, 1928, 1933). However, most studies focus on the posterior lateral line (pLL) and only few deal with the anterior lateral line (aLL) (Ishikawa, 1994; Iwasaki et al., 2020; Wada et al., 2010). This might be due to the complexity of the aLL pattern, which manifests both in organ number and position. The aLL system consists of a right and left aLL with neuromasts that are distributed all over the head. Due to the complex shape of the head and therefore neuromast pattern, visualization and characterization of the aLL poses a challenge. In this thesis I give a detailed description of the aLL pattern and quantification of aLL neuromast numbers, based on the nomenclature established previously (Ishikawa, 1994). Additionally, I included neuromasts of the anterior neuromast cluster (ANC) into the description and quantification of the aLL, based on nerve connections visualized in Tg(*KremenI*:mYFP) fish (transgenic line generated by Katharina Lust, AG Wittbrodt). This transgenic line in combination with Tg(*K15*:lifeAct-tRFP) allowed for easy identification of aLL neuromasts *in vivo* and facilitated aLL description and quantification of neuromast numbers immensely (Fig. 5A-D). Apart from neuromast stem cells, Tg(*K15*:lifeAct-tRFP) labels interneuromast cells connecting neuromasts of the same sub-line, easing assignment of sub-line affiliation of each neuromasts.

The aLL consists of ten sub-lines, that are located bilaterally in a highly stereotypic pattern, mainly around the eyes (Fig. 5D, E). Organ numbers among the different sub-lines vary between one and up to eleven organs. Quantification of organ numbers at hatchling stage within the distinct sub-lines revealed a low degree of variability in most sub-lines (Fig. 5E). In the sub-lines rc (rostral commissure), PG (posterior groove organ), lol (lower opercular line) and AG (anterior group), no variability among different fish or the left and right sides of the same fish can be detected. A minute degree of variability can be detected in the sub-lines DG (dorsal group), hl (horizontal line) and aml (anterior mandibular line). The highest degree of variability can be observed in the sub-lines PVG (posteroventral group) and vol (ventral orbital line). In the ANC either one or two neuromasts can be detected. The second ANC neuromast is formed from the

first embryonically generated ANC organ via migrating neuromast stem cells after the embryonic development of the aLL (more on this issue will follow in part II). Therefore, variability in ANC organ number is due to developmental timing and does not arise during embryonic, but post-embryonic development.

These results show that there are characteristic differences among the distinct aLL sub-lines, with some being highly stereotypic and others variable in organ number. This in turn might suggest that sub-lines with differing characteristics are formed differently and moreover might originate from different aLL placodes.

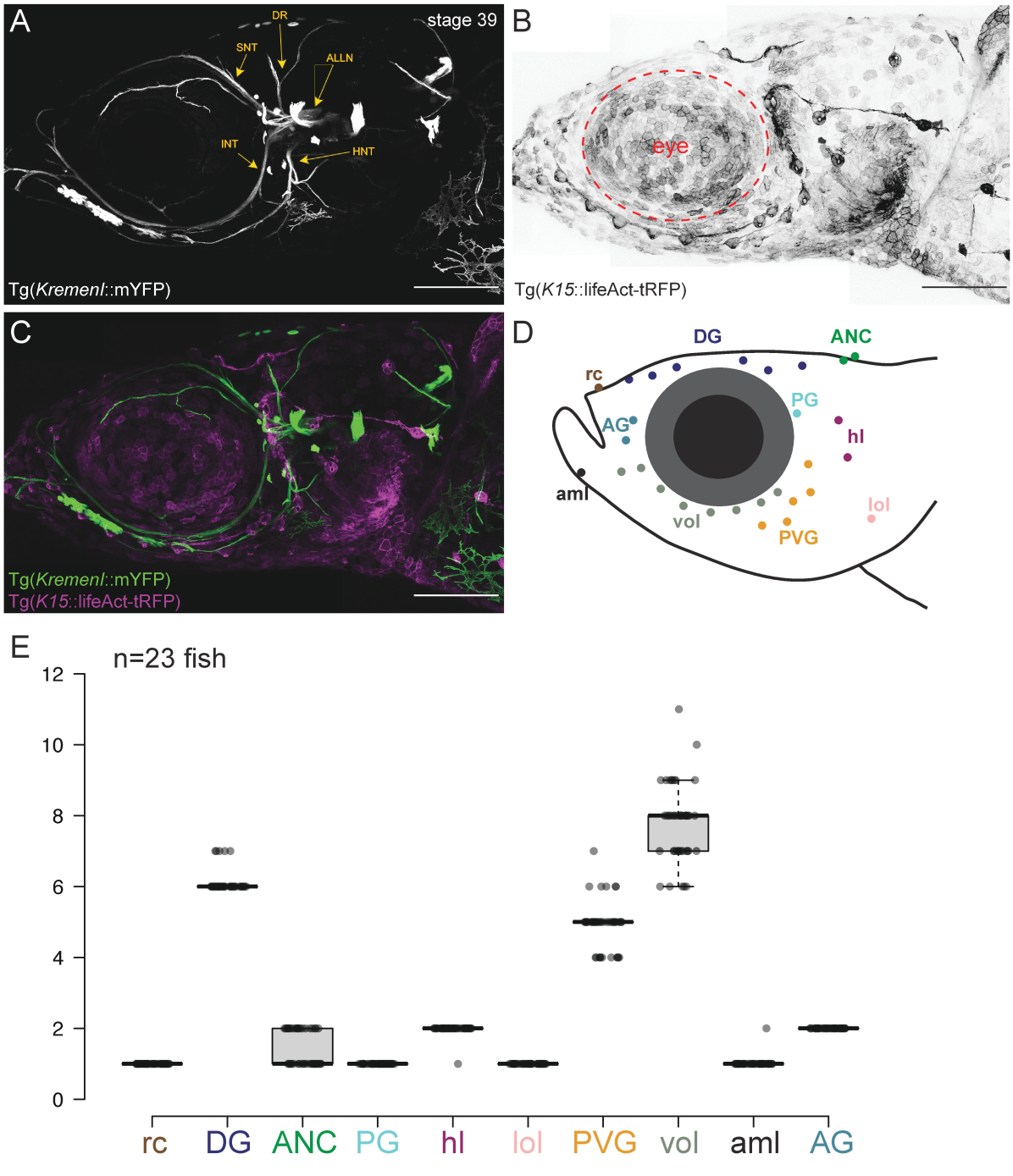

Figure 5: Description of the medaka aLL system. A: Confocal image of sensory neurons in the head using Tg(*KremenI*:mYFP) (transgenic line generated by Katharina Lust). Marked by yellow arrows are sensory neurons of the aLL system. ALLN: anterior lateral line nerve; DR: dorsal ramus of the anterior lateral line nerve; SNT: supraorbital nerve trunk; INT: infraorbital nerve trunk; HNT: hyomandibular nerve trunk. B: Confocal image of aLL neuromasts using Tg(*K15*:lifeAct-tRFP). For better visualization of neuromasts the signal was inverted using Fiji. C: Merge of A and B for easy identification and quantification of aLL neuromasts. Scale bars = 200 µm. D: Schematic description of aLL neuromast identity. Positions of aLL sub-lines are stereotypic. rc: rostral commissure, DG: dorsal group, ANC: anterior neuromast cluster, PG: posterior groove organ, hl: horizontal line, lol: lower opercular line, PVG: posteroventral group, vol: ventral orbital line, aml: anterior mandibular line, AG: anterior group E: Quantification of organ numbers within the distinct aLL sub-lines. No variability in sub-lines rc, PG, lol and AG. Low degree of variability in sub-lines DG, hl and aml. Higher degree of variability in sub-lines PVG and vol.

Work from Rebecca Kern during her Bachelor thesis in fact suggests that although all aLL sub-lines share a common origin in the panplacodal area (Schlosser, 2002a), some are closer related, meaning they share a common origin within the panplacodal area that is distinct from other aLL sub-lines. Rebecca Kern injected a plasmid containing an H2B-EGFP construct driven by the *K15* promoter at the medaka one- or two-cell-stage. Thereby, she generated chimeric fish containing both cells carrying the *K15*:H2B-EGFP transgene and cells that don't. At the end of embryogenesis, she quantified clones of *K15*:H2B-EGFP expression in aLL neuromasts. Quantification of the co-labeling proportion of neuromasts in different aLL sub-lines revealed that the sub-lines hl, PVG and PG most likely share a common origin, and are possibly generated from the same aLL placode.

2.1.2 aLL development is driven by different mechanisms using Cxcr4b-dependent and independent pathways

Development of the pLL depends on intact chemokine signaling via the receptors Cxcr4b and Cxcr7, which bind to the ligand Cxcl12a (sdf1) that is expressed along the horizontal myoseptum (Dona et al., 2013; Haas and Gilmour, 2006; Seleit et al., 2017a; Valentin et al., 2007). It has previously been reported that chemokine signaling via Cxcr4b is dispensable for aLL development in zebrafish (Ghysen and Dambly-Chaudiere, 2007; Piotrowski and Baker, 2014). In order to examine whether this holds true for medaka as well, I generated a *Cxcr4b* mutant line by injecting two gRNAs targeted against the *Cxcr4b* locus into Tg(*Eya1*:EGFP/*K15*:lifeAct-tRFP). I obtained a deletion of 625 base pairs (Fig. 6A). The resulting mutant line was therefore called *cxcr4b*^{D625}. The mutant fish display the same phenotype as the previously published *kazura* mutant (Yasuoka et al., 2004), lacking many or most pLL neuromasts (WT = 208 pLL neuromasts in 16 pLLs; n=8 fish; *cxcr4b*^{D625} = 24 pLL neuromasts in 18 pLLs; n=9 fish), due to disturbed primordium migration (Fig. 6 B, C). In order

to quantify aLL organ numbers in *cxcr4b*^{D625} mutants, only fish displaying a disturbed pLL pattern were used. As for zebrafish, most aLL sub-lines were present with wildtype organ-numbers (Fig. 6E-F), indicating that unlike pLL development, aLL development does not depend on intact Cxcr4b-mediated chemokine signaling. However, compared to the wildtype, organ numbers in the vol (P=0.00098; two-tailed unpaired t-test) and PVG (P=0.0049; two-tailed unpaired t-test) sub-lines are decreased, while organ numbers in the aml sub-line seem slightly increased (P=0.0315; two-tailed unpaired t-test). Despite the change in organ numbers, the vol, PVG and aml sub-lines were present in all fish, suggesting that initiation of sub-line development was unaltered. Strikingly, the rc sub-line is strongly affected in *cxcr4b*^{D625} mutant fish in comparison to the wildtype. Most mutant fish are lacking the rc neuromast (P<0.0001; two-tailed unpaired t-test), suggesting that development of this particular sub-line might in fact depend on chemokine signaling via Cxcr4b, similar to the pLL. Taken together, these results show that different aLL sub-lines react differently to a loss of Cxcr4b, once again showing diverse characteristics of aLL sub-lines. This in turn might point towards an origin from different aLL placodes.

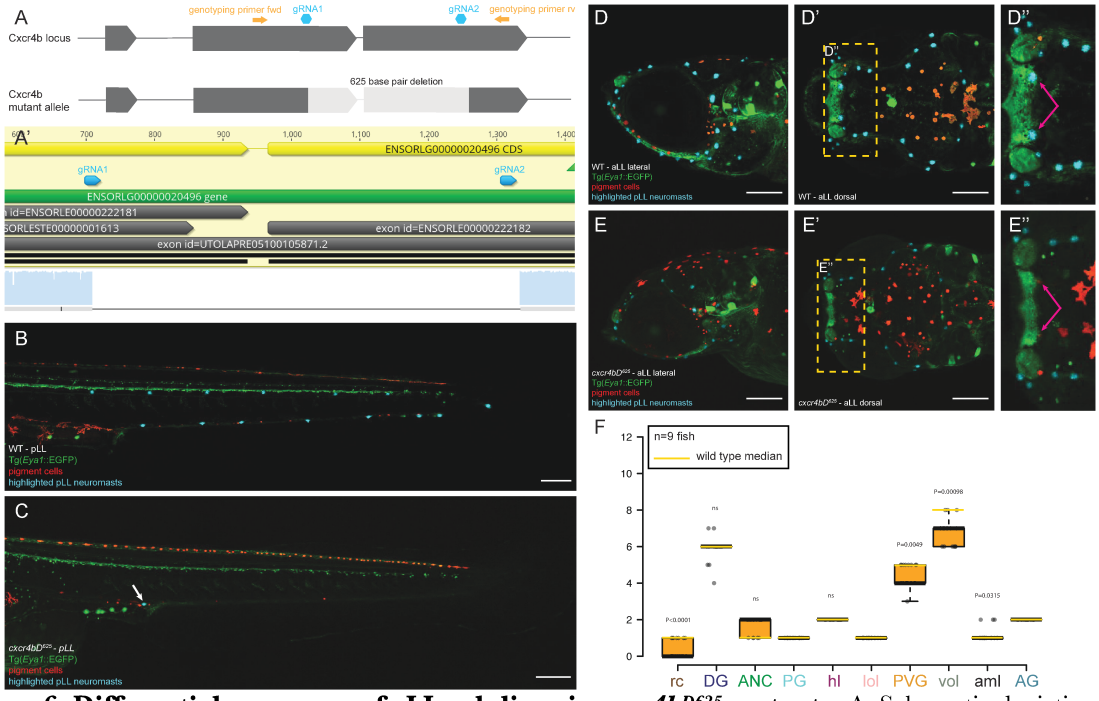

Figure 6: Differential responses of aLL sub-lines in *cxcr4b*^{D625} mutants. A: Schematic depiction of the wildtype and mutant *Cxcr4b* locus, including position of gRNAs and sequencing primers. A': Sanger-sequencing data visualizing 625 base pair deletion between gRNA1 and gRNA2. B: Wildtype pLL. Neuromasts are highlighted in cyan. pLL displays typical alternating pattern. Scale bar: 200 µm. C: *cxcr4b*^{D625} mutant pLL. Primordium migration is disturbed and pLL neuromast number therefore reduced substantially. Scale bar: 200 µm. D: Wildtype aLL from a lateral view. D': Wildtype aLL from a dorsal view. Scale bars = 200 µm. D'': Wildtype rc sub-line. E: *cxcr4b*^{D625} mutant aLL from a lateral view. Most aLL sub-lines are present and can be identified. E': *cxcr4b*^{D625} mutant aLL from a dorsal view. Scale bars = 200 µm. E'': *cxcr4b*^{D625} mutants lack rc neuromasts. F: Quantification of neuromast numbers in aLL sub-lines of *cxcr4b*^{D625} mutant fish. Sub-lines DG, ANC, PG, hl, lol and AG display wildtype numbers. Organ numbers in PVG and vol sub-lines are reduced, while they are slightly increased in the aml sub-line. Strikingly, most *cxcr4b*^{D625} mutant fish are lacking the rc sub-line.

2.1.3 aLL neuromasts are generated from sensory ridges

The relative robustness of most aLL sub-lines towards a loss of Cxcr4b begs the question as to how they are formed if not by a Cxcr4b-dependent primordium. Is has been described in sharks, skates, axolotls and recently in zebrafish that neuromasts can originate from sensory ridges or 'non-migratory primordia' instead of migrating primordia (Balfour; Ghysen and Dambly-Chaudiere, 2007; Gillis et al., 2012; Iwasaki et al., 2020; Northcutt et al., 1994; Piotrowski and Baker, 2014). In order to examine if this is the case for the medaka aLL as well, I performed live-imaging as well as whole-mount immunohistochemistry and *in situ* hybridization to elucidate the morphogenetic events leading to the formation of the distinct aLL sub-lines. Eya1 has been successfully used to visualize both early and late stages of neuromast development (Moody and LaMantia, 2015; Seleit et al., 2017a). Therefore, I performed a fluorescent *in situ* hybridization against *eya1* at 2 and 2.5 dpf to visualize initial stages of aLL development. Indeed, *eya1* signal could be detected anterior to the otic vesicle at 2 dpf (Fig. 7A, yellow arrow), an area that most likely contains the anterior lateral line placodes. The *eya1*$^+$ area seems fragmented, indicating the presence of multiple aLL placodes, which has been described in the literature for amphibia (Schlosser, 2002a). At 2 dpf, the pLL primordium has already delaminated from the pLL placode and travels posteriorly along the tail (Fig. 7A, magenta arrow). At 2.5 dpf, the primordium has travelled further and has started to deposit primary neuromasts, creating the pLL-specific discontinuous pattern (Fig. 7B, magenta arrow and asterisks). At 2.5 dpf the appearance of the presumed *eya1*$^+$ aLL placodes has changed substantially. The *eya1*$^+$ area has elongated along the dorsal and ventral side of the eye and appears to form continuous stripes (Fig. 7B, B', yellow arrows). *Eya1*$^+$ stripes can also be detected in live samples at 3 dpf using Tg(*Eya1*:EGFP) (Fig. 7C-C''). Interestingly, at 4 dpf neuromasts have appeared along the positions of *eya1*$^+$ stripes simultaneously (Fig. 8A-C'), indicating that the *eya1*$^+$ stripes are indeed sensory ridges that generate aLL neuromasts. At 6 dpf, embryonic development of the aLL is complete (Fig. 9A-C'). With a few exceptions, all embryonic aLL neuromasts seem to be generated from sensory ridges, as opposed to the embryonic pLL, which is exclusively formed by a migrating primordium. It seems extraordinary that neuromasts of the aLL and pLL are formed in different ways, yet their morphology is indistinguishable at early juvenile stages (Fig.1).

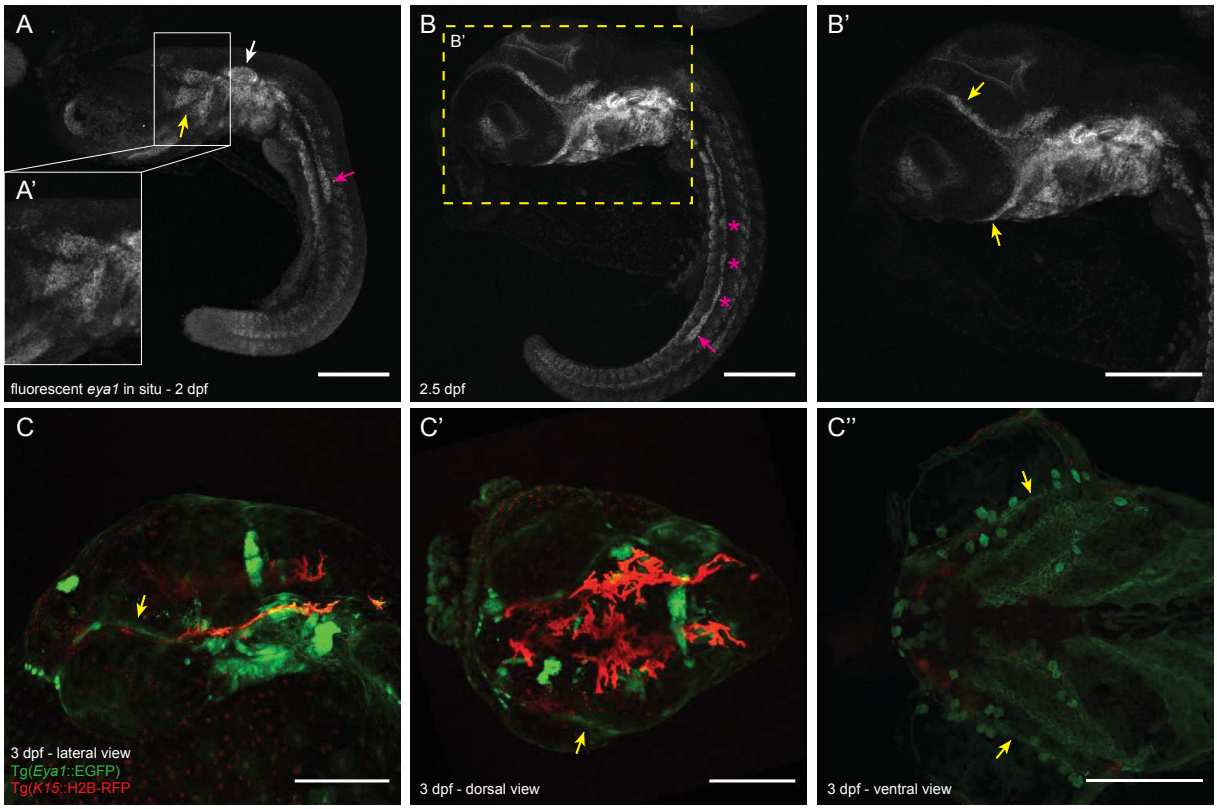

Figure 7: Formation of sensory ridges as precursors of aLL neuromasts. A: Fluorescent *eya1 in situ* hybridization at 2 dpf. aLL placodes (yellow arrow) can be seen anterior to the otic vesicle (white arrow). The pLL primordium has already delaminated from the pLL placode and started travelling along the tail (magenta arrow). A': Zoom in on the aLL placode region. B: Fluorescent *eya1 in situ* hybridization at 2.5 dpf. The pLL primordium (magenta arrow) has started to deposit primary pLL neuromasts (magenta asterisks) and displays its typical discontinuous pattern. B': Zoom in of B. *eya1*$^+$ area has elongated to form *eya1*$^+$ stripes (sensory ridges) that extend dorsal and ventral to the eye. C-C'': Tg(*Eya1*:EGFP)/Tg(*K15*:H2B-RFP) at 3 dpf. Sensory ridges can be seen dorsal and ventral (yellow arrows) to the eye. C'' is a whole-mount α-GFP immunostaining. The image was adapted from my master thesis. Sensory ridges can be seen ventral to the eye. Scale bars = 200 μm.

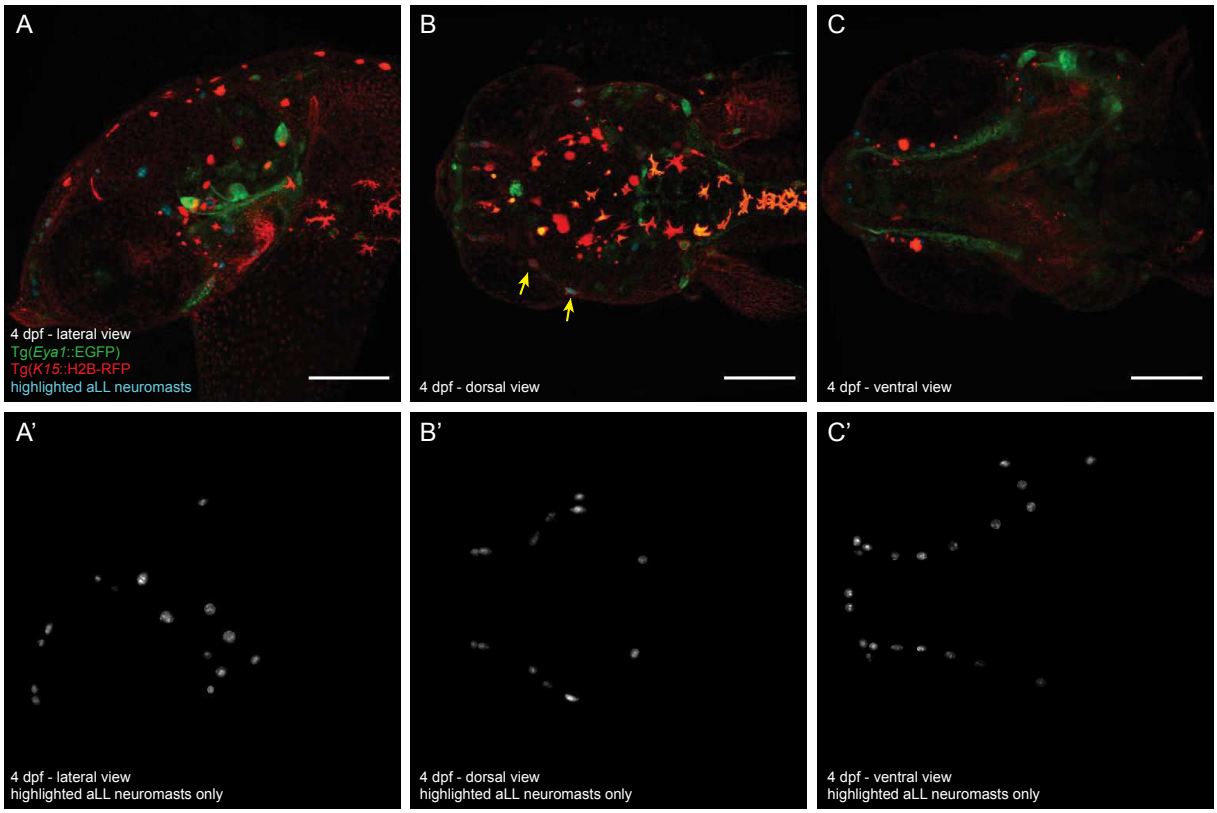

Figure 8: Neuromasts are simultaneously formed along sensory ridges. A-C: Tg(*Eya1*:EGFP)/Tg(*K15*:H2B-RFP) at 4 dpf from a lateral, dorsal and ventral view. Neuromasts have appeared along sensory ridges (yellow arrows). A'-C': Highlighted neuromasts extracted from A-C. Scale bars = 200 µm.

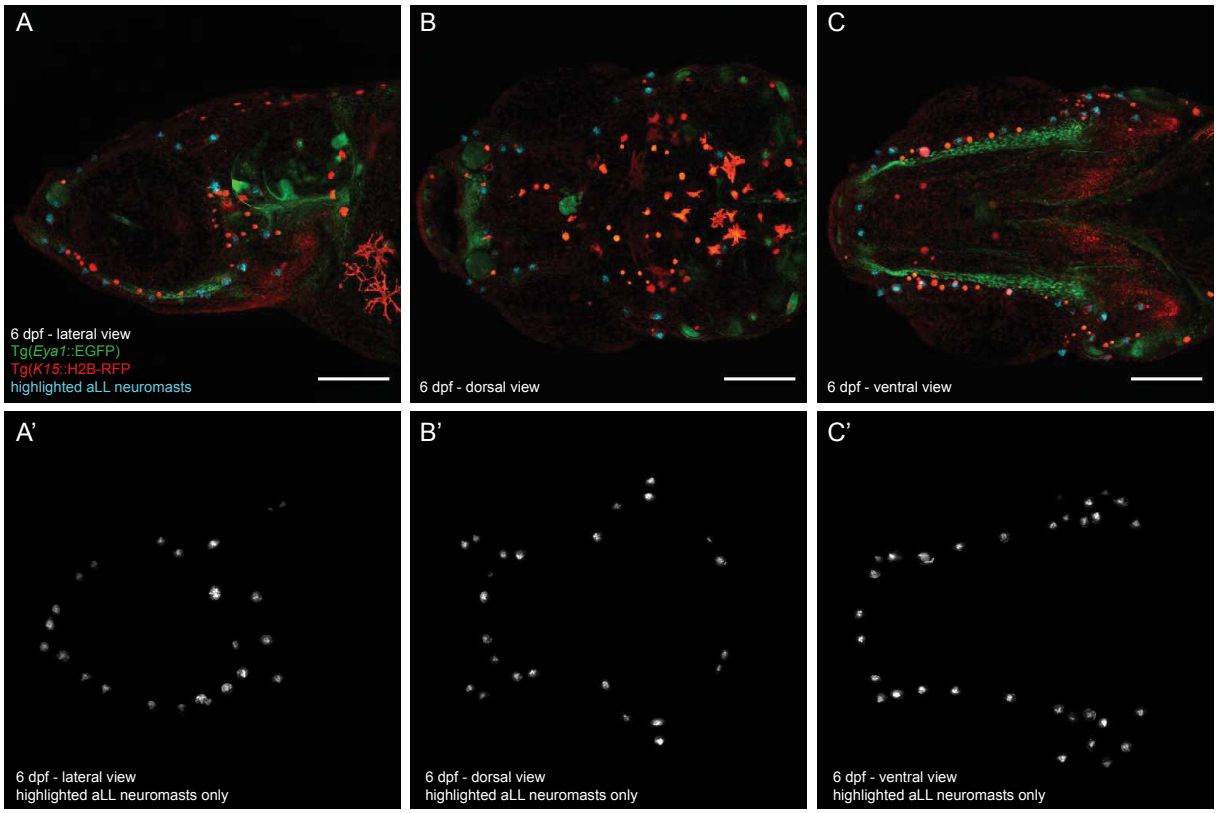

Figure 9: At 6 dpf embryonic development of the aLL is complete. A-C: Tg(*Eya1*:EGFP)/Tg(*K15*:H2B-RFP) at 6 dpf from a lateral, dorsal and ventral view. All aLL neuromasts have been formed and embryonic aLL development is complete. A'-C': Highlighted neuromasts extracted from A-C. Scale bars = 200 µm.

Whole-mount immunohistochemistry during aLL development revealed the formation of secondary neuromasts in the vol sub-line. Between primary neuromasts generated by a sensory ridge, smaller secondary neuromasts appeared (Fig. 10, white arrow). Formation of secondary aLL neuromasts in the vol sub-line is reminiscent of secondary neuromast formation in the pLL. The slight decrease of vol organ numbers in *cxcr4b*^{D625} mutants might even suggest that secondary neuromasts of the aLL and pLL are formed in similar ways. Secondary organ formation in the pLL relies on intact chemokine signaling via Cxcr4b (Seleit et al., 2017a). In its absence, secondary organs cannot be formed. Possibly, secondary neuromasts in the vol sub-line depend on intact chemokine signaling via Cxcr4b as well. Although formed differently, aLL sub-lines rc and vol display common traits with the pLL. rc sub-line formation is driven by chemokine signaling via Cxcr4b and in the vol sub-line secondary neuromasts are generated in a similar fashion as secondary pLL neuromasts.

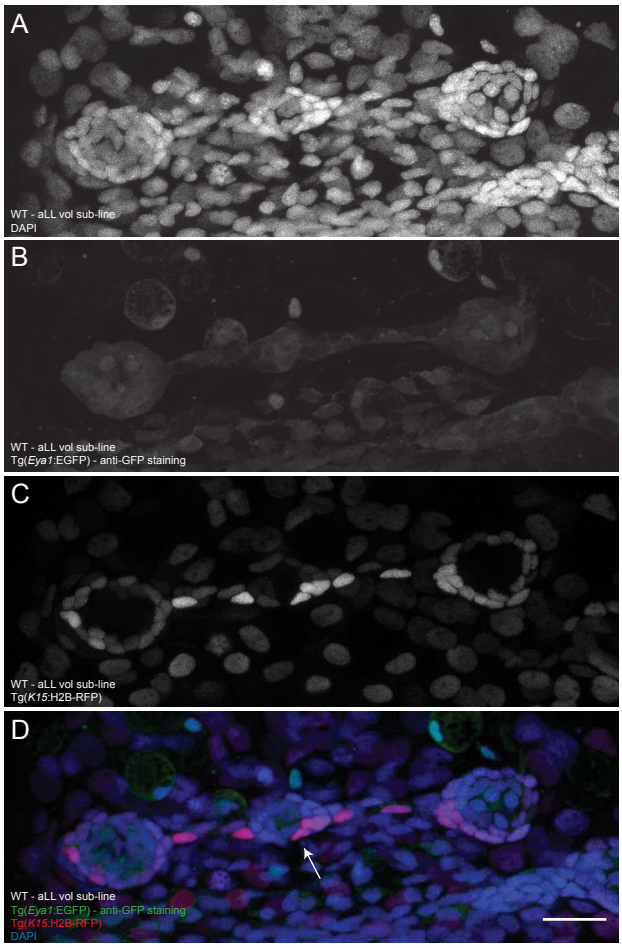

Figure 10: Formation of secondary neuromasts in the vol sub-line. Primary neuromasts in the vol sub-line are generated from a sensory ridge. In between primary neuromasts, secondary neuromasts are formed, similar to secondary pLL neuromasts. Images adapted from my master thesis. Scale bar = 20 µm.

2.1.4 rc neuromasts are formed by a migrating Cxcr4b-dependent primordium

Dependence on the chemokine receptor Cxcr4b suggests that development of the rc sub-line follows a similar rationale as pLL development. pLL formation has been thoroughly described before (Dona et al., 2013; Haas and Gilmour, 2006; Seleit et al., 2017a; Valentin et al., 2007). The pLL is formed by a migrating primordium that follows a trail of Cxcl12a ligand along the horizontal midline of the tail via the receptors Cxcr4b and Cxcr7. In order to examine if the same pathway is employed in rc sub-line formation, I performed an *in situ* hybridization (Seleit

et al., 2017a) against *Cxcl12a* at 3 dpf on wildtype fish. The previously described *Cxcl12a* trail on the tail (Haas and Gilmour, 2006; Seleit et al., 2017a) was used as a positive control (Fig. 11A). Indeed, *Cxcl12a* signal could be detected in the vicinity of the future rc neuromast position on the head (Fig. 11B, red arrows). This is in line with the hypothesis that rc neuromasts are formed by a primordium that relies on Cxcl12a and Cxcr4b for migration.

To further explore the possibility of a primordium-dependent rc sub-line formation, I performed time-lapse imaging of Tg(*Eya1*:EGFP) fish at 3 dpf from a frontal view (Fig. 11C-C''''). Tg(*Eya1*:EGFP) has been successfully used to visualize and follow pLL development in medaka (Seleit et al., 2017a). Therefore, I chose this line in the hope to visualize a possible rc sub-line primordium. Indeed, primordium-like structures could be detected at 3 dpf adjacent to the olfactory epithelium (Fig. 11C, blue and green dots, respectively). Since Tricaine, an anesthetic commonly used to immobilize fish, has only limited effect on young embryos, I injected 50 µg/µl *α-bungarotoxin* mRNA at the one-cell-stage to minimize movement of the fish during imaging (Lischik et al., 2019). α-bungarotoxin binds to and inhibits acetylcholine receptors and prevents neuro-muscular communication. Movement of the embryo was nevertheless not entirely prevented, and it shifted slightly. Therefore, as a reference, I marked the upper border of the left and right olfactory epithelium (Fig. 11C-C'''', yellow line). Over the course of the time-lapse imaging, the primordium-like structures (Fig. 11, blue and green dots, respectively) move dorsally in relation to the olfactory epithelium towards the final position of rc neuromasts, indicating migratory behavior. This, together with the *Cxcl12a in situ* hybridization and *Cxcr4b* mutant data, strongly indicate that the rc sub-line is formed by a migrating primordium (rc-primordium) that follows a Cxcl12a trail using the Cxcr4b receptor, comparable to the pLL primordium.

In the past, nerve connections have been used to infer neuromasts origin (Ishikawa, 1994; Schlosser, 2002a; Wada et al., 2013). Using the transgenic line Tg(*Eya1*:mCFP) (Seleit et al., 2017a) I visualized rc neuromast nerve connections to trace a possible origin (experiment was performed as part of my master thesis). Although being positioned on the dorsal side of the head, the rc neuromast (Fig. 11E', yellow arrow) surprisingly displays nerve connections projecting ventrally towards the AG/vol sub-line (Fig. 11E). This suggests that the rc sub-line originates ventrally and possibly shares a common origin with the AG/vol sub-lines. Interestingly, the AG and vol sub-lines are not or not as severely affected in the *cxcr4b*^{D625} mutant as the rc sub-line (Fig. 11F), likely due to the at least in part different, Cxcr4b-independent mode of development via sensory ridges.

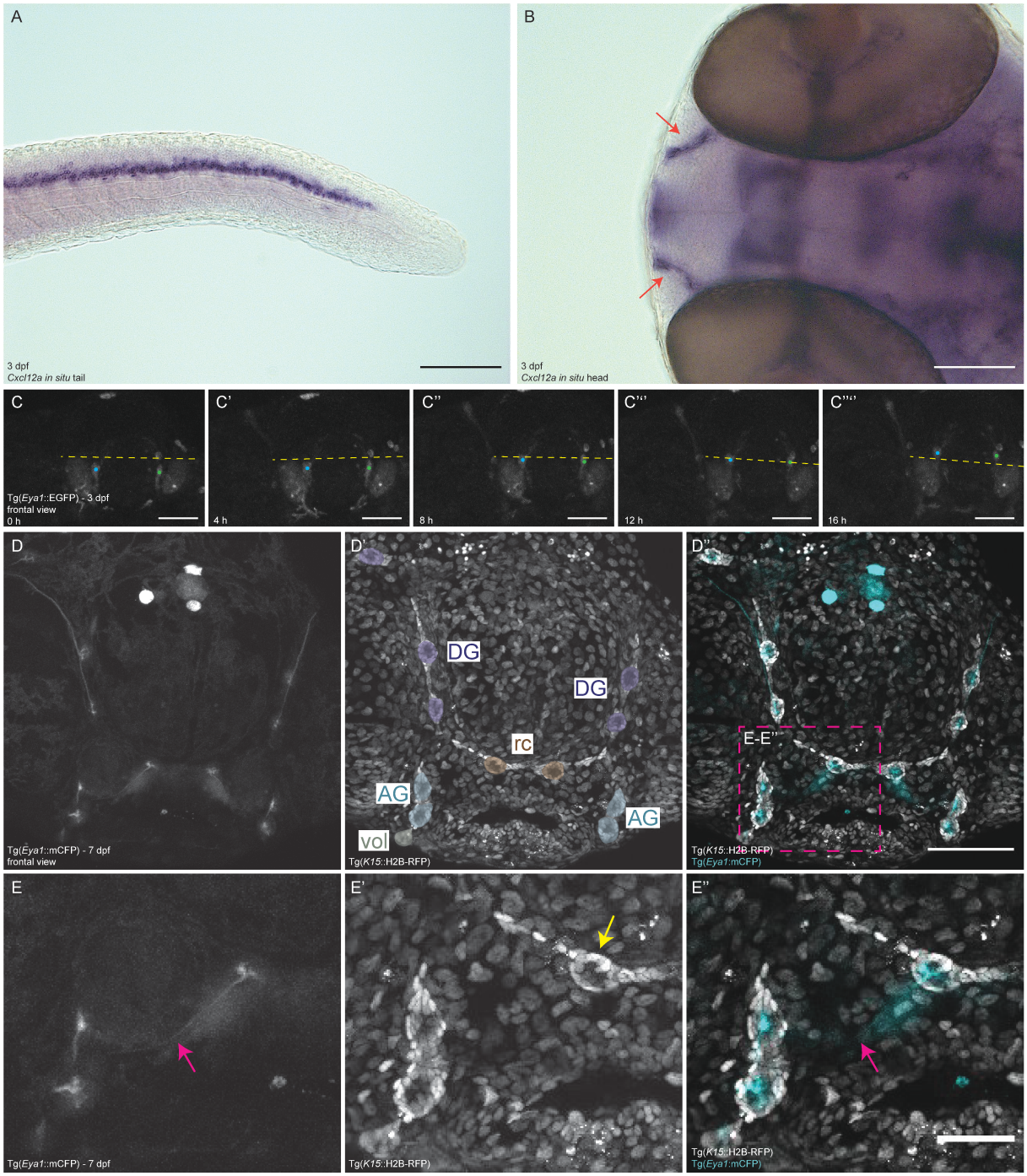

Figure 11: Development and origin of the rc sub-line. A-B: *Cxcl12a in situ* hybridization at 3 dpf. A: *Cxcl12a* signal at the horizontal midline of the tail can be detected. Scale bar = 100 µm . B: *Cxcr12a* signal on the head in the vicinity of future rc neuromast position. Scale bar = 100 µm. C-C'''': Time-lapse microscopy of Tg(*Eya1*:EGFP) with an interval of 2 h (only every other time point is shown). Primordium-like structures migrate dorsally (blue and green dot, respectively). Scale bar = 100 µm. D-D'': Frontal view of Tg(*Eya1*:EGFP) and Tg(*K15*:H2B-RFP) fish at 7 dpf. Scale bar = 100 µm. Images were adapted from my master thesis. E-E': Zoom in on rc (yellow arrow) and AG/vol neuromasts. Ventral nerve connection of rc neuromast (magenta arrow). Scale bar = 50 µm. Images were adapted from my master thesis.

2.1.5 Morphological challenging of aLL development

2.1.5.1 aLL pattern is robust against compromised epithelial integrity

As described above, most aLL sub-lines appear to be highly stereotypic under normal conditions. In the past, the pLL pattern has been shown to be susceptible towards genetic and morphological perturbation (Seleit et al., 2021). The pLL of *Keratin 15* (*K15*) mutants (*stuck-in-the-midline*, *siml* mutants) displays a pronounced pattern defect. Altered interactions between neuromasts and surrounding epithelium, results in many primary organs not being properly located at the ventral side but instead being "stuck" at the horizontal midline (Fig. 12B). This is not due to altered primordium migration, but to altered migration of primary neuromasts themselves (Seleit et al., 2021).Thus the typical alternating pattern (Fig. 12A) of primary and secondary neuromasts is disrupted (Seleit et al., 2021).

To assess the robustness of the aLL system in comparison to the pLL in this background, I quantified aLL organ numbers and pattern in *K15* mutants. Strikingly, most aLL sub-lines are unaltered in the mutant background. Only the DG (P=0.0027, two-tailed unpaired t-test) and vol (P=0.0327, two-tailed unpaired t-test) sub-lines show statistically significant differences when compared to wildtype numbers. However, median organ numbers are unchanged (Fig. 12E). The comparably mild phenotype in the aLL is in contrast to the severe pLL phenotype. This indicates, that aLL neuromast pattern and number does not depend on an intact epithelium to the same extent as the pLL. The pLL phenotype is due to the fact that pLL formation is driven by collective cell migration, both on the primordium and neuromast level that is heavily impacted by the epithelium (Seleit et al., 2021). In the aLL, most neuromasts are formed *in situ* by sensory ridges that themselves don't rely on migration but rather proliferate and extend over the head (Schlosser, 2002a). An intact epithelium that facilitates cell migration is therefore not required. Consequently, disturbed epithelial morphology in *K15* mutants does not heavily impact on aLL neuromast formation and position. Interestingly, the only aLL sub-line that is formed from a primordium, similar to the pLL, does not display a phenotype in *K15* mutants. I hypothesize that this is due to the relatively short distance that the rc-primordium has to travel. In summary, disturbance of epithelial integrity has a severe pattern defect on the pLL (Seleit et al., 2021), while aLL pattern displays no or only a minute phenotype. This indicates that the nature of interaction with the surrounding tissues is different in aLL and pLL development.

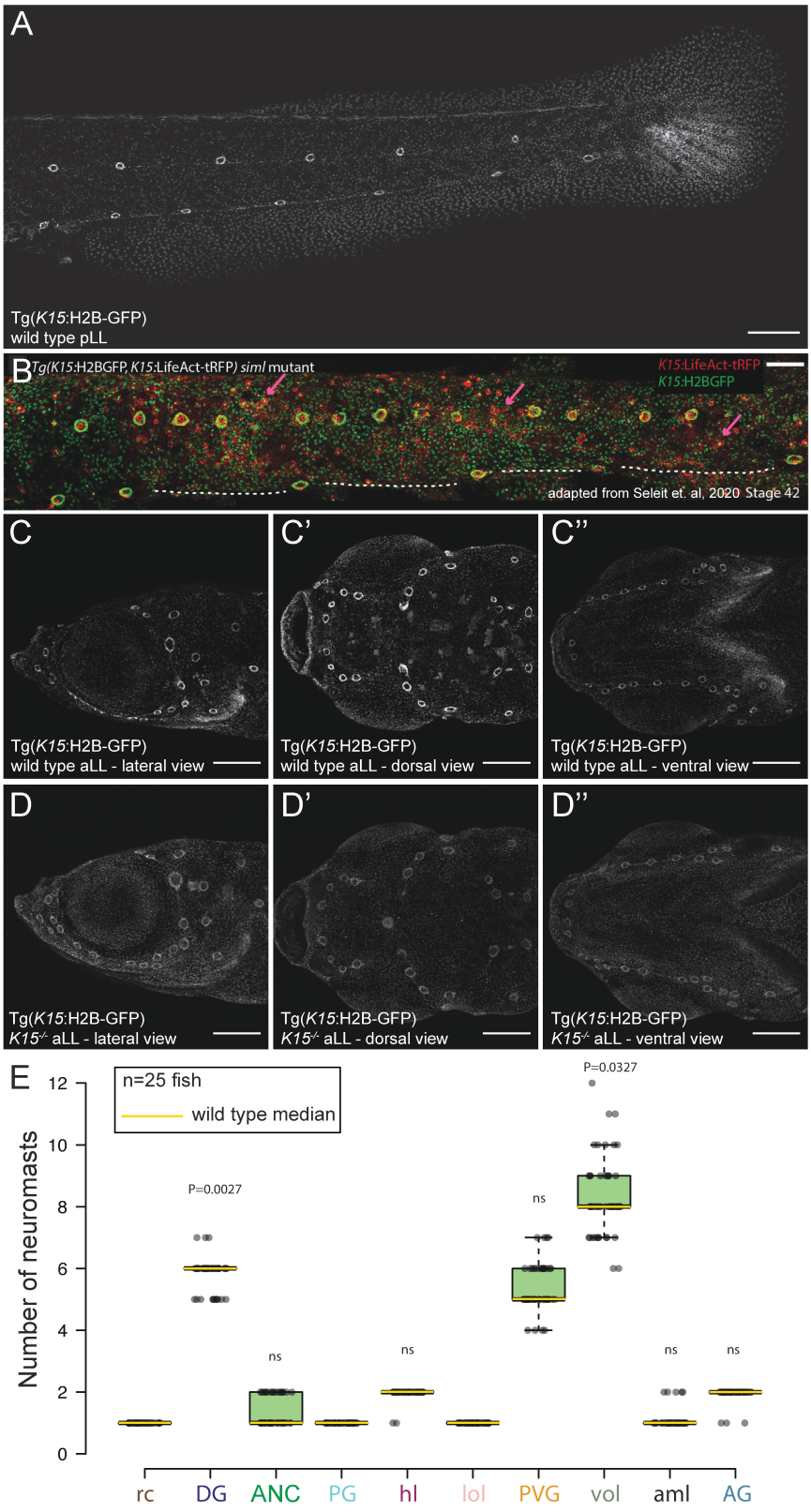

Figure 12: Minute aLL phenotype in *K15* mutants. A: Wildtype pLL pattern with alternating primary and secondary organs. Scale bar = 200 µm. B: *K15* mutant pLL pattern. Many primary organs are mislocalized at the horizontal midline. Image from Seleit et al. (2021). C-C'': Wildtype aLL pattern from a lateral, dorsal and ventral view. Scale bar = 200 µm. D-D'' aLL pattern in *K15* mutants from a lateral, dorsal and ventral view. All sub-lines can be identified, and no obvious phenotype can be detected. Scale bar = 200 µm. E: Quantification of aLL neuromast numbers. Statistically different organ numbers can only be detected for the sub-lines DG and vol.

2.1.5.2 Defects in eye size affect aLL neuromast number, but not identity

Interactions with the surrounding epithelium seem to have little or no effect on aLL development. To test if other morphological structures in the head impact on aLL development, I made use of the temperature sensitive *eyeless* (el) medaka mutant (Winkler et al., 2000). The el mutation affects the *rx3* locus and mutants display eye morphogenesis defects resulting in smaller or even absent eyes, leading to gross aberrations of head morphology. In some cases, *eyeless* mutants displayed a missing eye on one side and a normal eye on the contra-lateral side (Fig. 13C). These fish served as an internal control to exclude the possibility that a mutation in *rx3* itself affects aLL development, since the aLL pattern on the unaffected side was intact (Fig. 13D). For quantification of aLL pattern and neuromast number in *eyeless* mutants I only considered aLLs around smaller or absent eyes (Fig. 13D', E). In the wildtype, neuromasts are stereotypically connected by cells labelled in Tg(*K15*:lifeAct-tRFP) (Fig. 13A), similar to interneuromast cells in the pLL. Based on these connections, neuromasts can be unambiguously allocated to the ten aLL sub-lines. In *eyeless* mutants all aLL sub-lines are present, and neuromast identity seems unchanged as the relative position of organs is wildtype-like (Fig. 13D'). However, in contrast to the results from *K15* mutant fish, most aLL sub-lines display significantly different neuromast numbers compared to wildtype fish (Fig. 13E). This suggests that aLL tissues indeed interact with structures of the eye during aLL development and require input to build the system according to the surrounding. Out of all ten sub-lines, DG ($P<0.0001$, two-tailed unpaired t-test) and vol ($P<0.0001$, two-tailed unpaired t-test) exhibit the strongest defect in *eyeless* mutants. Both lines display a decrease of median organ numbers. Interestingly, DG and vol are the sub-lines that contain the most neuromasts and moreover, they are located directly adjacent to the eye. The sublines rc, PVG, and AG appear to be significantly different (with reduced organ numbers) from WT numbers, however median organ numbers are unchanged. Since I used a variety of *eyeless* mutant phenotypes ranging from decreased eye size to absent eyes, variability in organ number phenotypes can be expected. By focusing on the strongest *eyeless* mutant phenotypes, a clearer result might be obtained for these sub-lines. Organ numbers in the sub-lines aml and ANC seem increased compared to the wildtype. This is true both for sub-lines around affected, but also unaffected eyes. As previously mentioned, the ANC consists of two organs. The first organ that presumably stems from a sensory ridge generates the second neuromast. Since *eyeless* mutants are grown at higher temperatures to increase the severity of the *eyeless* mutant phenotype, it is possible that this process of additional neuromast formation is accelerated. A similar phenomenon might happen in the aml sub-line. Occasionally two aml organs were detected in wildtype fish, suggesting that additional organs are formed in the aml

sub-line at later stages. In fact, growing wildtype fish at higher temperatures results in a similar increase of neuromast numbers in ANC and aml.

Strikingly, the sub-lines PG, hl and lol are unaffected in the *eyeless* mutant. Possibly, this is due to low organ numbers in these sub-lines. Additionally, the results suggest that lines close to the original position of the aLL placode are less affected by defects of head morphology. This in turn indicates that placode specification is intact and the aLL pattern defect occurs at later stages of aLL development.

Taken together, these results show that similar to the pLL, aLL tissues interact with surrounding tissues during development. However, the nature of the interaction in pLL and aLL might be different. While the pLL relies on an intact epithelium for neuromast positioning, the aLL requires an intact eye or other underlying head structures to reach wildtype organ numbers.

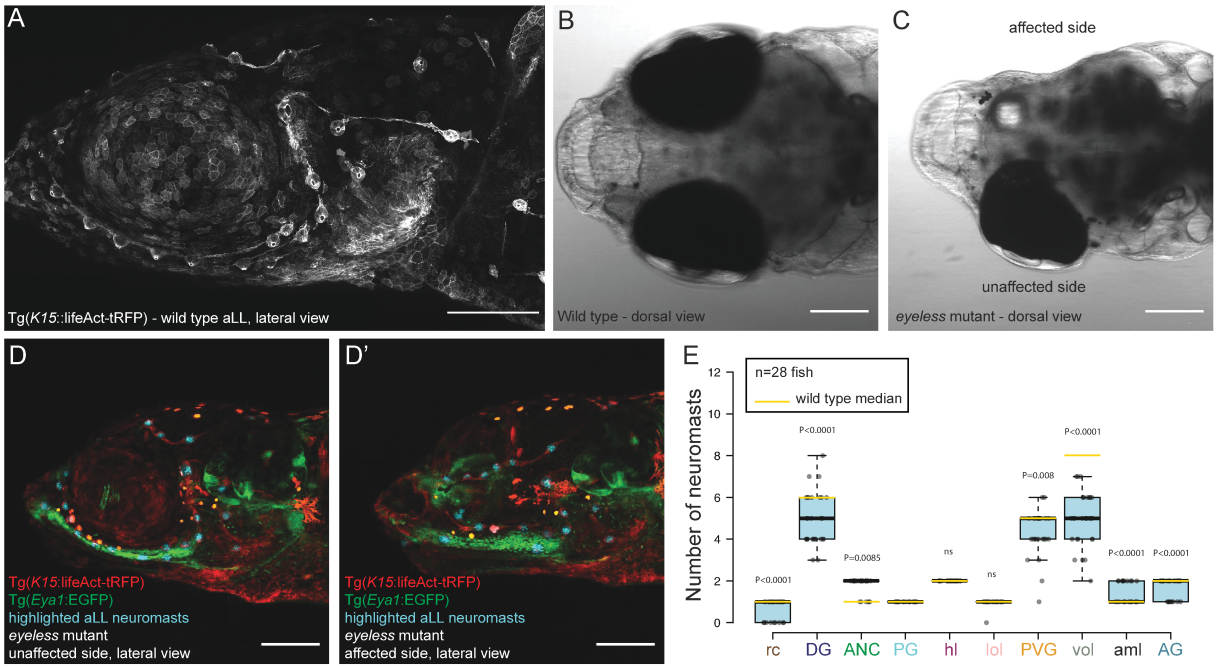

Figure 13: *eyeless* phenotype results in aLL pattern defect. A: Wildtype aLL pattern from a lateral view. Tg(*K15*:lifeAct-tRFP) shows cellular connections between aLL neuromasts that can be used to infer neuromast identity. B: Dorsal view on a wildtype head. C: Dorsal view on the head of an *eyeless* medaka mutant. The right eye of the fish is missing, while the left eye is wildtype-like. D: Lateral view on the aLL of the wildtype-like side of the *eyeless* medaka mutant shown in C. The pattern is wildtype-like. D': Lateral view on the aLL of the affected side of the *eyeless* medaka mutant shown in C. Neuromast identity is unaffected. Scale bars = 200 µm. E: Quantification of aLL neuromast numbers of *eyeless* medaka mutants displaying an eye phenotypes. The strongest effect can be seen in sub-lines DG and vol. Sub-lines PG, hl and lol are unaffected.

In order to examine the effect of an increase in eye size on aLL development, I used the recently published medaka line Tg(*rx2*:*caigf1r*), driving a constitutive active insulin-like growth factor 1 receptor (igf1r) under the *retinal homeobox gene 2* (*rx2*) promoter, which is active in eye stem and progenitor cells. As a result, retina growth is decoupled from body size, resulting in an increased eye size relative to body size (Becker et al., 2021) (Fig. 14A, A'). I quantified aLL organ numbers in fish displaying enlarged eyes (Fig. 14B). Interestingly, aLL organ numbers are not as severely

affected as in the *eyeless* mutant, yet they follow the same trend. Other than I expected, organ numbers in the vol sub-line are decreased (P<0.0001, two-tailed unpaired t-test). Organ numbers in the sub-lines rc (P=0.0244, two-tailed unpaired t-test) and DG (P<0.0001, two-tailed unpaired t-test) seem decreased as well, however, the median remains unchanged. The remaining sub-lines did not display significantly different organ numbers from the wildtype. Compared to the *eyeless* mutant, the aLL phenotype displayed by Tg(*rx2:caigf1r*) fish is relatively moderate. However, both fish lines resulted in a change of organ number with a trend towards decreased neuromast number, especially in the vol and DG sub-lines. This leads to the conclusion that aLL development, in particular the vol and DG sub-lines, require an intact eye. Regardless of the nature of the eye defect (increase or decrease in size), aLL numbers tend to be reduced in most aLL sub-line, suggesting that the system cannot adapt to changes in availability of space. More available space does not lead to increase in organ number. Instead, changed interaction with the surrounding tissues invariably leads to a reduction of organ numbers in most aLL sub-lines.

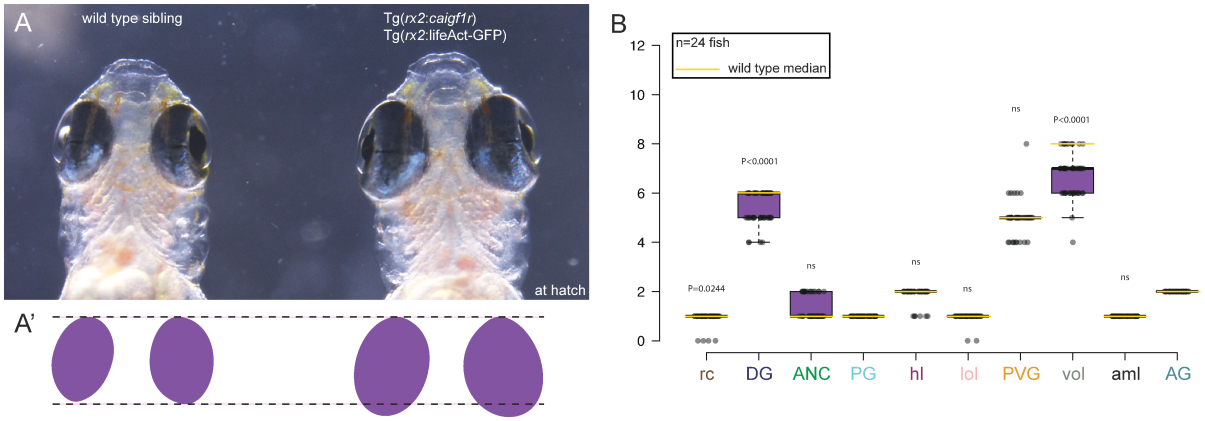

Figure 14: Increase in eye size leads to reduction of organ numbers in rc, DG and vol sub-lines. A: Wildtype sibling with normal sized eyes on the left and Tg(*rx2:caigf1r*) fish with increased eye size on the right. A': Comparison of eye area in wildtype sibling on the left and Tg(*rx2:caigf1r*) on the right. B: Quantification of aLL neuromast numbers in Tg(*rx2:caigf1r*) fish at hatch. Decrease of organ numbers can be observed in the sub-lines rc, DG and vol. Sub-lines ANC, PG, hl, lol, PVG, aml and AG are unaffected.

2.1.6 Differential reaction of aLL sub-line symmetry to higher temperature

Despite the previously described low degree of variability in certain sub-lines, the aLL displays a high degree of symmetry, where organ numbers of the distinct sub-lines equal organ numbers of corresponding sub-lines on the contralateral side (Fig. 15A). This symmetry is only broken in the vol (median: 88%) and PVG sub-lines. The PVG sub-line is characterized by high variability of symmetry, however median symmetry is 100%. Variability in organ number among the left

and right side of the same fish has previously been described for the medaka midline pLL (mpLL) (Seleit et al., 2017a). Comparison of PVG and vol symmetry with vpLL (median: 100%) and mpLL (median: 86%) symmetry via one-way ANOVA statistical analysis did not result in a significant difference, indicating that symmetry levels are comparable between PVG, vol, vpLL and mpLL. Although formed differently, PVG, vol, mpLL and vpLL share the same characteristic of variable organ numbers, resulting in lower levels of bilateral symmetry.

To challenge the robustness of aLL and pLL sub-line symmetry, I grew fish under high temperature conditions at 32°C. After embryogenesis I quantified aLL, vpLL and mpLL symmetry (Fig. 15B). Symmetry in most aLL sub-lines and both vpLL and mpLL was unchanged. Strikingly, symmetry in the PVG line was decreased substantially from a median of 100% to 80% symmetry, when compared to control conditions at 28°C (P=0.0301, two-tailed unpaired t-test). Quantification of organ numbers in the PVG sub-line revealed a slight increase at 32°C, which is not bilaterally coordinated (mean organ number at 28°C: 4.8; mean organ number at 32°C: 5.1), resulting in a decrease of symmetry.

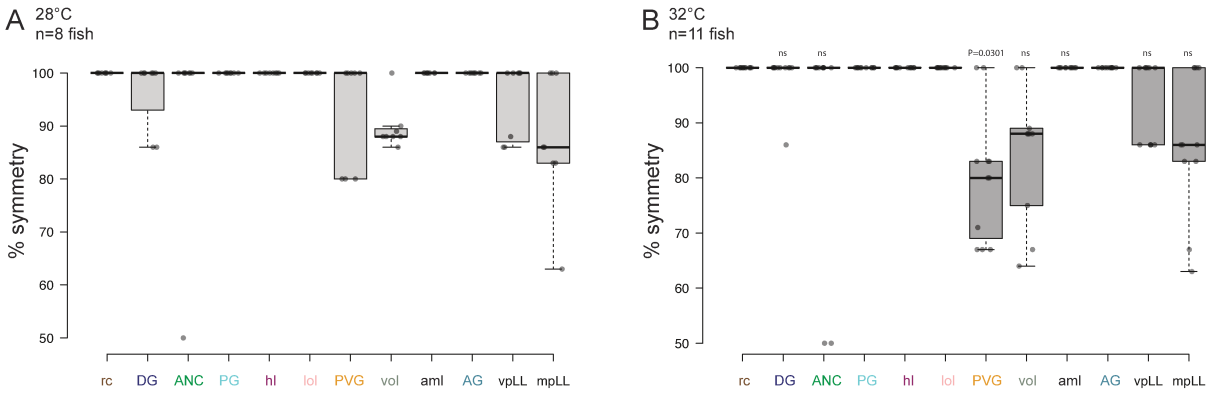

Figure 15: Temperature sensitivity of PVG sub-line. A: Quantification of aLL sub-line, vpLL and mpLL symmetry at 28°C. Most aLL sub-lines highly symmetric. The PVG sub-line displays a high degree of variability in symmetry. The vol sub-line only reaches 88% symmetry. PVG and vol sub-line symmetry is comparable with vpLL and mpLL symmetry according to one-way ANOVA statistical analysis. B: Quantification of aLL sub-line, vpLL and mpLL symmetry at 32°C. Most aLL sub-lines, vpLL and mpLL are unchanged. PVG displays a statistically significant decrease of symmetry.

These results suggest that PVG sub-line development and therefore neuromast numbers are temperature sensitive, in contrast to the remaining aLL sub-lines and pLL, which are unaffected by increased temperatures. This in turn suggests once again that different aLL sub-lines follow different developmental rationales, which might be linked back to distinct origins within the aLL placodes.

2.2 Part II: Post-embryonic organogenesis of neuromasts

2.2.1 Post-embryonic organs in the CNC are formed from neuromast stem cells

Previous results based on lineage tracing and ablation studies indicate that the P0-neuromast gives rise to the entire CNC (caudal neuromast cluster) (Seleit, Krämer et al., 2017b). Ablation of the P0-neuromast resulted in the absence of the CNC. Moreover Cre/LoxP based lineage tracing performed by Isabel Krämer in our lab revealed that only a subset of *K15*$^{+}$ stem cells in the P0-neuromast generate the majority of cells in the adult CNC. In order to examine the cellular events leading to the formation of the first post-embryonic organ (PE1-neuromast), I performed live-imaging of Tg(*K15*:H2B-RFP) fish at different stages of organogenesis. In line with previous results, I observed that the PE1-neuromast is formed by *K15*$^{+}$ stem cells that are located in the anterior part of the P0-neuromast. I defined five hallmark stages (stages I-V) to describe the process (Fig. 16). At stage I, the P0-neuromast has been formed, but post-embryonic organogenesis has not yet started (Fig. 16A, A'). At stage II, a subset of stem cells in the anterior part of the P0-neuromast is re-arranged and starts to separate from the organ (Fig. 16B, B'). Stage III is characterized by stem cells that have delaminated from the P0-neuromast and are moving away from their initial position (Fig. 16C, C'). At stage IV, the delaminated stem cells coalesce (Fig. 16D, D'). With stage V post-embryonic organogenesis has been completed, as the PE1-neuromast is fully formed with differentiated cells (Fig. 16E, E').

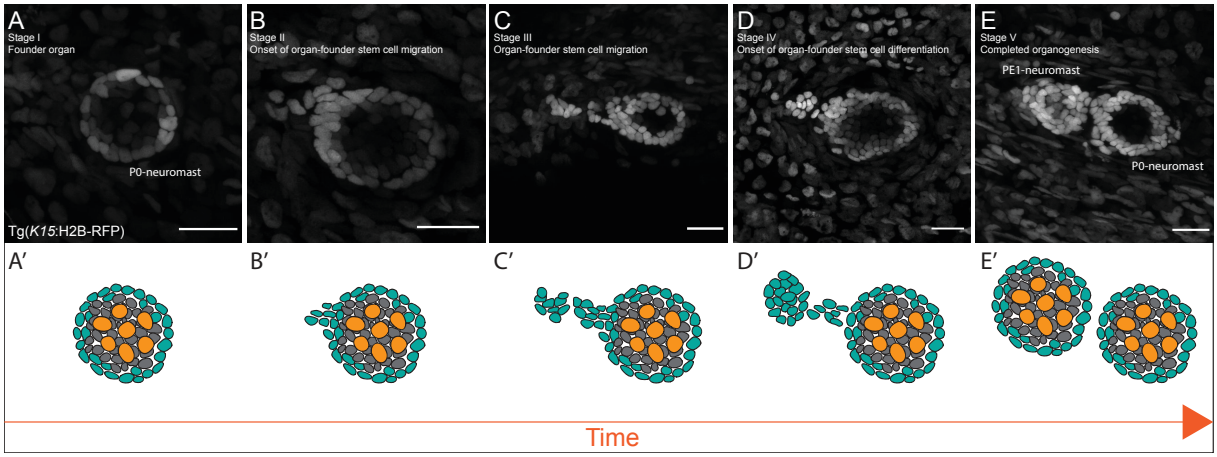

Figure 16: Stereotypic formation of the PE1-neuromast from the P0-founder neuromast. A, A': P0-neuromast prior to post-embryonic organogenesis at hatch (stage I). B, B': A subset of stem cells in the anterior part of the P0-neuromast are re-arranged and start to separate from the organ (stage II). C, C': Neuromast stem cells have detached from the P0-neuromast and moved in anterior direction (stage III). D, D': Detached neuromast stem cells coalesce anterior to the P0-neuromast (stage IV). E, E': The PE1-neuromast with differentiated cells (reduced *K15*:H2B-RFP signal) is formed anterior to the P0-neuromast (stage V). Scale bars = 20 µm.

The neuromast stem cells that generate the PE1-neuromast were termed organ-founder stem cells. Remarkably, post-embryonic organogenesis of the PE1-neuromast is highly stereotypic in terms of position. In 100% of cases (N>60 neuromast formation events, N>60 larvae) post-embryonic organogenesis occurred anterior to the P0-neuromast.

Despite the stereotypic position of the PE1-neuromast just anterior of the P0-neuromast, initiation of post-embryonic organogenesis can be variable in time. I quantified the distribution of developmental stages of PE1-neuromast formation from the end of embryonic development, when the fish hatch, until 8 dph, when most fish contained organs at stage III of post-embryonic organogenesis (Fig. 17). As a readout for initiation of organogenesis I used the transition from stage I to stage II of post-embryonic organogenesis. At the end of embryonic development (at hatch) most P0-neuromasts are in stage I. However, a number or organs have already initiated post-embryonic organogenesis at this point. Between 1 and 3 dph, most P0-neuromasts are in stage II, however, stage I organs can be observed until 5 dph. From 5 dph onwards, most P0-neuromasts are in stage III. From 8 dph onwards only stage III and later stages can be found. These results suggest that initiation of post-embryonic organogenesis is variable and occurs within a time window between hatch and 5 dph.

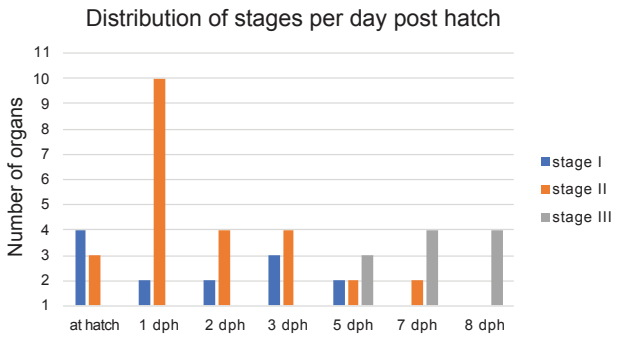

Figure 17: Variability in the onset of PE1-neuromast formation. Quantification of developmental stages of PE1-neuormast formation between hatch and 8 dph revealed that the onset of organogenesis (transition from stage I to stage II) can be variable from hatch until 7 dph. By 8 dph, all organs have entered stage III. n=35 CNCs.

2.2.2 Organ-founder stem cells undergo an EMT

Seeing cells moving away from the P0-neuromast, I wondered whether these cells actively migrate from the founder neuromast, or whether they are passively pushed or pulled out of the organ. To tackle this question, I followed a two-fold approach by examining the morphology of organ-founder stem cells prior and during post-embryonic organogenesis and investigating the expression of key EMT (epithelial-to-mesenchymal transition) molecules.

At stage I, neuromast stem cells are elongated with a typical epithelial basal and apical pole (Fig. 18A, A'). At the onset of stage II, organ-founder stem cells in the anterior part of the P0-neuromast undergo morphological changes and retract from the apical side of the PE1-neuromast (Fig. 18B, yellow arrow and orange highlight, B'). As post-embryonic organogenesis

proceeds, they extend lamellipodia-like protrusions in anterior direction (Fig. 18C, yellow arrow, C'). The observed changes in cell morphology suggest an active migratory behavior.

To further investigate whether organ-founder stem cells actively migrate out of the P0-neuromast, I performed whole-mount immunohistochemistry against E-Cadherin and N-Cadherin at stage III of post-embryonic organogenesis (Fig. 18D-D'''). E- and N-Cadherin are hallmark factors of an epithelial-to-mesenchymal transition (EMT). Typically, E-Cadherin is downregulated in cells undergoing an EMT, while N-Cadherin is upregulated (Gheldof and Berx, 2013; Kang and Massague, 2004; Thiery, 2002). Using antibodies against E- and N-Cadherin, I indeed observed a downregulation of E-Cadherin (Fig. 18E') and an upregulation of N-Cadherin (Fig. 18E'') specifically in migrating organ-founder stem cells. E-Cadherin continues to be expressed in stationary neuromast stem cells. N-Cadherin cannot be detected in stationary neuromast stem cells, but in support and hair cells, in line with its role in regulation of neural progenitor maintenance, differentiation and proliferation (Miyamoto et al., 2015). Taken together, these results strongly indicate that organ-founder stem cells undergo an EMT and actively migrate out of the P0-neuromast.

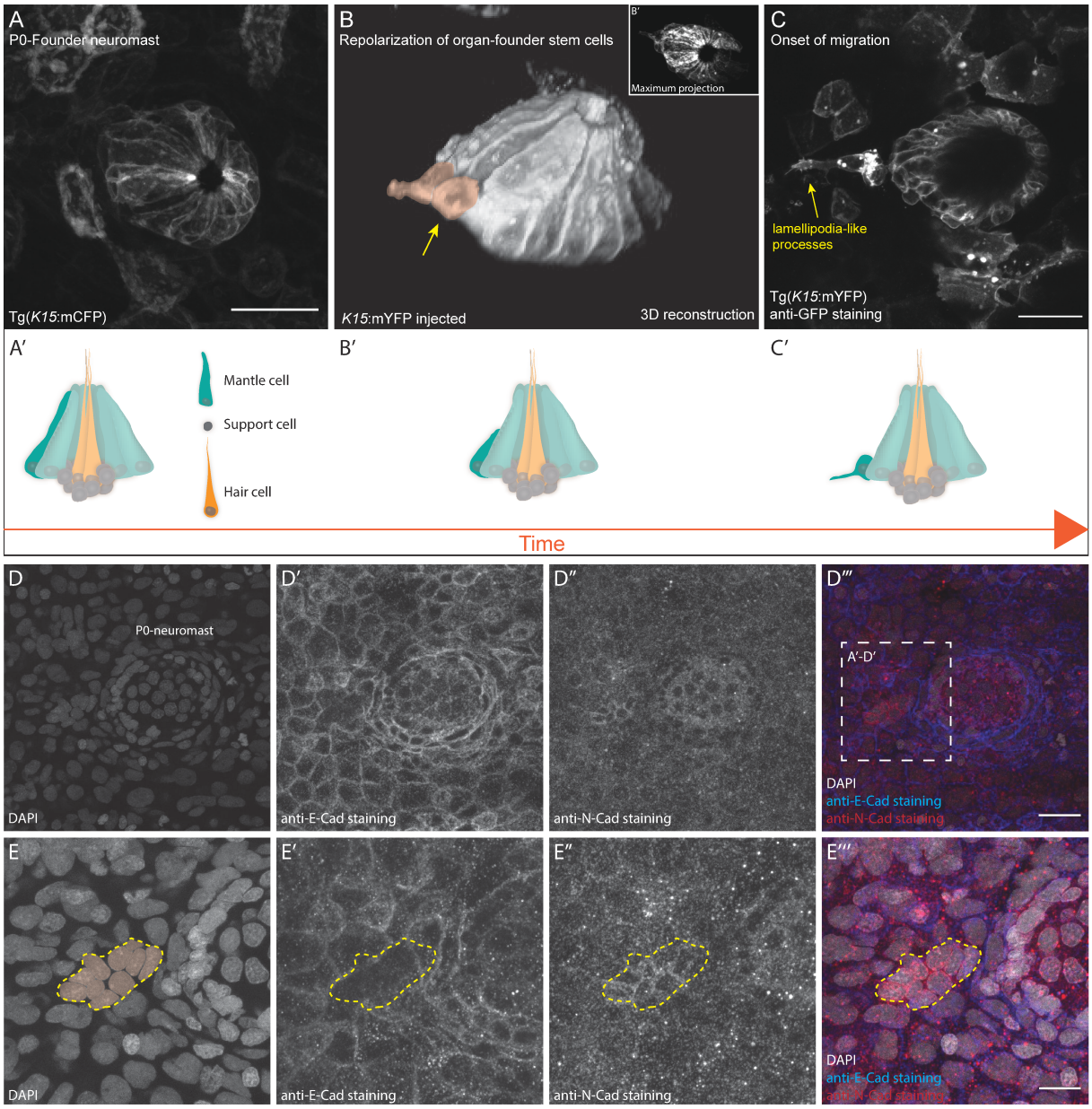

Figure 18: Organ-founder stem cells undergo active migration and EMT. A: P0-neuromast at stage I prior to post-embryonic organogenesis. A': Schematic and lateral view on a stage I P0-neuromast. B: Onset of stage II. Anterior organ-founder stem cells repolarize and retract from the apical side. B': Schematic and lateral view on organ-founder stem cell repolarization. C: Onset of cell migration. Organ-founder stem cells form lamellipodia-like processes in anterior direction. C': Schematic and lateral view on onset of organ-founder stem cell migration. D-D''': Whole-mount immunohistochemistry against E-Cadherin and N-Cadherin. P0-neuromast at stage III of organogenesis. Organ-founder stem cells have started to migrate in anterior direction. E-E''': Whole-mount immunohistochemistry against E-Cadherin and N-Cadherin. Zoom in on migrating organ-founder stem cells. Organ-founder stem cells (marked by yellow lines) downregulate E-Cadherin (E'), while N-Cadherin (E'') is upregulated. Scale bars = 20 µm.

2.2.3 Visualization of endogenous *snail* expression to monitor EMT during post-embryonic neuromast formation

Organ-founder stem cells undergo an EMT during post-embryonic PE1-neuromast formation. In order to dynamically monitor EMT within post-embryonic organogenesis I planned on following the expression of Snail transcription factors, key EMT regulators (Barrallo-Gimeno and Nieto, 2005). There are three *snail* genes present in medaka: *snail1a*, *snail1b* and *snail2* (Liedtke et al., 2011). I set out to endogenously tag each of the medaka *snail* genes using the CRISPR/Cas9 technology in combination with homology directed repair that was previously established (Gutierrez-Triana et al., 2018). The strategy I followed is illustrated below for the *snail2* gene (Fig. 19A-A''). I designed gRNAs in the first two exons of each *snail* gene and amplified specific homology flanks (between 300 and 500 bp) via PCR outside of the gRNA sites (Fig. 19A). Using Golden GATEway cloning (Kirchmaier et al., 2013), I assembled a DNA construct containing a GFP with a stop codon flanked by 5' and 3' homology flanks. Using biotinylated primers, I amplified the DNA donor that was eventually co-injected with Cas9 and *snail2* specific gRNAs (Fig. 19A'). I successfully tagged the *snail2* locus, which was confirmed by PCR using a GFP reverse primer and a forward primer binding outside of the 5' homology flank. The endogenous tag that I generated leads to a disruption of the *snail2* gene, since the GFP sequence contains a stop codon. The idea behind this was to use the tag as a transcriptional reporter in heterozygous conditions and as a knockout in homozygous conditions. Heterozygous fish are viable and have no detectable phenotype. Homozygous fish can be raised to adulthood, however, there is a high mortality rate. In depth analysis of possible phenotypes remains to be performed.

The expression pattern in the *snail2*-GFP tagged reporter line (Fig. 19B-E) resembles published *in situ* hybridization data (Liedtke et al., 2011), indicating that the line accurately recapitulates *snail2* expression. *Snail2*-GFP expression can be detected until adult stages.

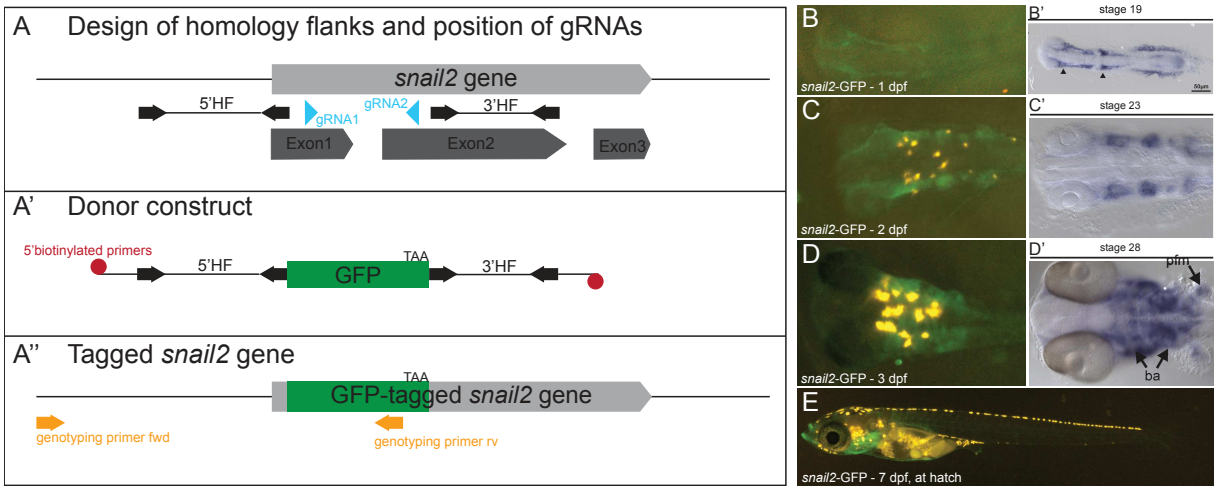

Figure 19: Generation of an endogenous *snail2*-GFP tag. A: Design of 5' and 3' homology flanks in the *snail2* locus and two gRNAs binding outside of the homology flanks used for homology directed repair. A': Final DNA-donor containing 5' and 3' homology regions flanking a GFP including a stop codon. The DNA-donor was generated using biotinylated primers to prevent polymerization. A'': Tagged *snail2*-gene, resulting in a truncated *snail2*-GFP. B: *Snail2*-GFP expression at 1 dpf. B': *snail2 in situ* hybridization data at stage 19 of medaka development. *Snail2* expression marks neural crest cells. C: *Snail2*-GFP expression at 2 dpf. C': *snail2 in situ* hybridization data at stage 23 of medaka development. *Snail2* labels head mesenchyme. D: *Snail2*-GFP expression at 2 dpf. D': *snail2 in situ* hybridization data at stage 28 of medaka development. *Snail2* is expressed in branchial arches and ventral mesenchyme. Images B', C' and D' were adapted from (Liedtke et al., 2011). E: *Snail2*-GFP expression at hatchling stage. The most prominent signal can be found in the gills.

Using this line, I examined *snail2*-GFP expression in neuromast stem cells during post-embryonic organogenesis. *Snail2*-GFP expression was visible in the epithelium and neuromast border cells (Fig. 20A'', white arrow). Border cell expression of *snail2*-GFP could be a remnant of the epithelial fate before recruitment (Seleit, Krämer et al., 2017b). Alternatively, this could also suggest a role for Snail2 in border cells. In migrating neuromast stem cells *snail2*-GFP expression could not be detected (Fig. 20A', yellow arrow), suggesting either a Snail2-independent EMT in organ-founder stem cells or undetectable expression levels. This line is therefore not suitable to monitor the EMT process in organ-founder stem cells.

In addition to the *snail2*-GFP tag that I generated, I examined a *snail1a*-venus functional tag that was generated by Carina Vibe in Alexander Aulehla's lab. Due to low *snail1a*-venus expression levels and in order to label neuromast stem cells, I performed whole-mount immunohistochemistry. Similar to the *snail2*-GFP tag, strong *snail1a*-venus expression can be detected in the epithelium and neuromast border cells (Fig. 20B'', white arrow). Again, distinguishing between border cell specific *snail1a* expression and remaining *snail1a*-venus from the epithelial fate prior to recruitment is not possible. As for *snail2*-GFP, *snail1a*-venus expression could not be detected in neuromast stem cells either (Fig. 20B'', yellow arrow).

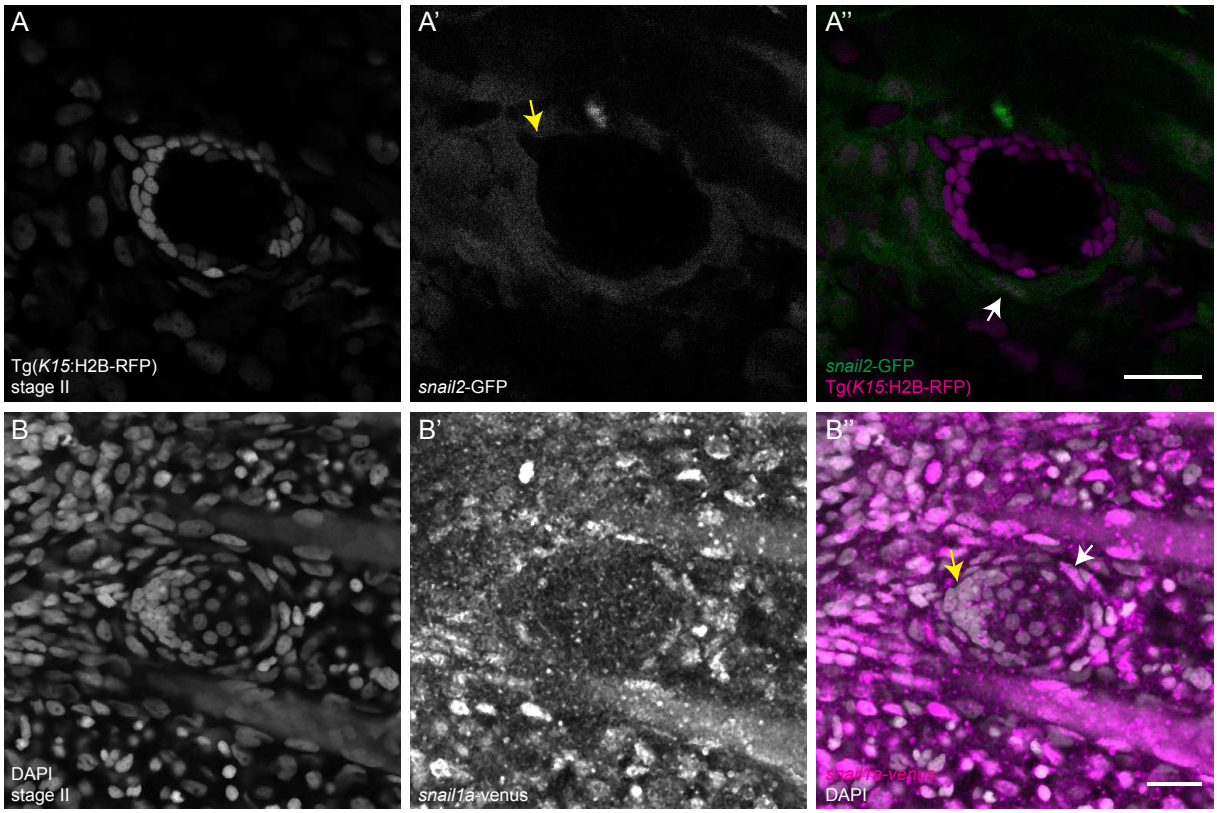

Figure 20: Endogenous *snail2* and *snail1a* expression cannot be detected in organ-founder stem cells. A-A'': *snail2*-GFP expression can be detected in epithelial and neuromast border cells (white arrow), not in organ-founder stem cells (yellow arrow). B-B'': *snail1a*-venus expression resembles *snail2*-GFP expression in epithelial and neuromast border cells (white arrow). *Snail1a*-venus is not detectable in organ founder stem cells (yellow arrow).

These results might suggest that neither Snail1a nor Snail2 are involved in the regulation of EMT in organ-founder stem cells. Possibly, Snail1b, which is a regulator of EMT in primordium cells during embryonic development of the pLL (Neelathi et al., 2018), regulates EMT during post-embryonic development as well. Alternatively, *snail1a*-venus and *snail2*-GFP might be expressed at a level that is not visible using microscopy. Single cell RNASeq could provide a solution to that problem and a possibility to further explore the expression profile of organ-founder stem cells.

2.2.4 Exit point of organ-founder stem cell migration is unchanged upon ectopic *snail* expression

Under normal conditions, EMT is induced only in anterior neuromast stem cells. Organ-founder stem cell migration and PE1-neuromast formation exclusively occur anteriorly. In order to test the robustness of the system I generated transgenic lines expressing the Snail transcription factors, key regulators of EMT, under the *K15* promoter. There are three *snail* genes in medaka: *snail1a*, *snail1b* and *snail2* (Liedtke et al., 2011). The underlying rationale was

to grant every *K15*$^{+}$ stem cell in the P0-neuromast the ability to migrate. Consequently, I expected ectopic stem cell migration and possibly neuromast formation. To visualize *snail* expression, I fused the respective CDS to H2A-cherry via a T2A site. I injected this construct together with *K15*:H2B-GFP to further visualize *K15*$^{+}$ cells to generate the transgenic lines Tg(*K15*:*snail1a*-T2A-H2A-cherry)/Tg(*K15*:H2B-GFP), Tg(*K15*:*snail1b*-T2A-H2A-cherry)/Tg(*K15*:H2B-GFP) and Tg(*K15*:*snail2*-T2A-H2A-cherry)/Tg(*K15*:H2B-GFP). All lines displayed comparable phenotypes, however, expression levels of Tg(*K15*:*snail1b*-T2A-H2A-cherry)/Tg(*K15*:H2B-GFP) were best suited for live-imaging. Therefore, analysis of post-embryonic organogenesis in the CNC was done on this transgenic line.

In order to assess the functionality of the DNA construct I quantified cellular shape. To increase n numbers and because phenotypes were obvious, I focused on secondary neuromasts on the tail for quantification of cell morphological phenotypes. Below, I quantified secondary pLL neuromast morphology with a focus on stem cells in wildtype (Tg(*K15*:mYFP)/Tg(K15:H2B-RFP)) (Fig. 21A-D'') and Tg(*K15*:*snail1b*-T2A-H2A-cherry)/Tg(*K15*:H2B-GFP)/Tg(*K15*:mYFP)) (Fig. 21E-H'') fish at 3 dph. Since *K15*:mYFP resulted in a massive bleed-through when imaging *K15*:*snail1b*-T2A-H2A-cherry, I performed whole mount immunohistochemistry visualizing H2A-cherry in the far-red channel. I focused on phenotypes in neuromast stem cells that are indicative of the functionality of the *K15*:*snail1b*-T2A-H2A-cherry construct. Therefore, I quantified the proportion of secondary neuromasts displaying an intact stem cell ring, stem cells protruding from the ring and stem cells that have detached from the stem cell ring. Using Tg(*K15*:mYFP) I was able to unambiguously determine the identity of cells as either neuromast stem cell or epithelial cell, due to cellular connections. In the wildtype, 48.6% of secondary neuromasts have an intact stem cell ring. In Tg(*K15*:*snail1b*-T2A-H2A-cherry)/Tg(*K15*:H2B-GFP)/Tg(*K15*:mYFP) fish this number is reduced to 20.3%. Strikingly, the proportion of secondary neuromasts displaying stem cells protruding from the stem cells ring is 76%, while only 42.9% of organs in the wildtype display this behavior. The number of stem cells per secondary neuromast showing protruding behavior is slightly increased from 1.6 in the wildtype to 2.2 in Tg(*K15*:*snail1b*-T2A-H2A-cherry)/Tg(*K15*:H2B-GFP)/Tg(*K15*:mYFP) fish. The proportion of secondary neuromasts with stem cells that have detached from the organ is comparable with 14.6% in the wildtype and 15.5% in Tg(*K15*:*snail1b*-T2A-H2A-cherry)/Tg(*K15*:H2B-GFP)/Tg(*K15*:mYFP) fish. However, the number of detached stem cells per neuromast is slightly increased from 1 to 1.3. The phenotype displayed by Tg(*K15*:*snail1b*-T2A-H2A-cherry)/Tg(*K15*:H2B-GFP)/Tg(*K15*:mYFP) fish is in line with the hypothesis that ectopic *snail* expression leads to ectopic acquisition of migratory behavior in neuromast stem

cells. Fish displaying phenotypes in secondary neuromasts were used to assess PE1-neuromast formation.

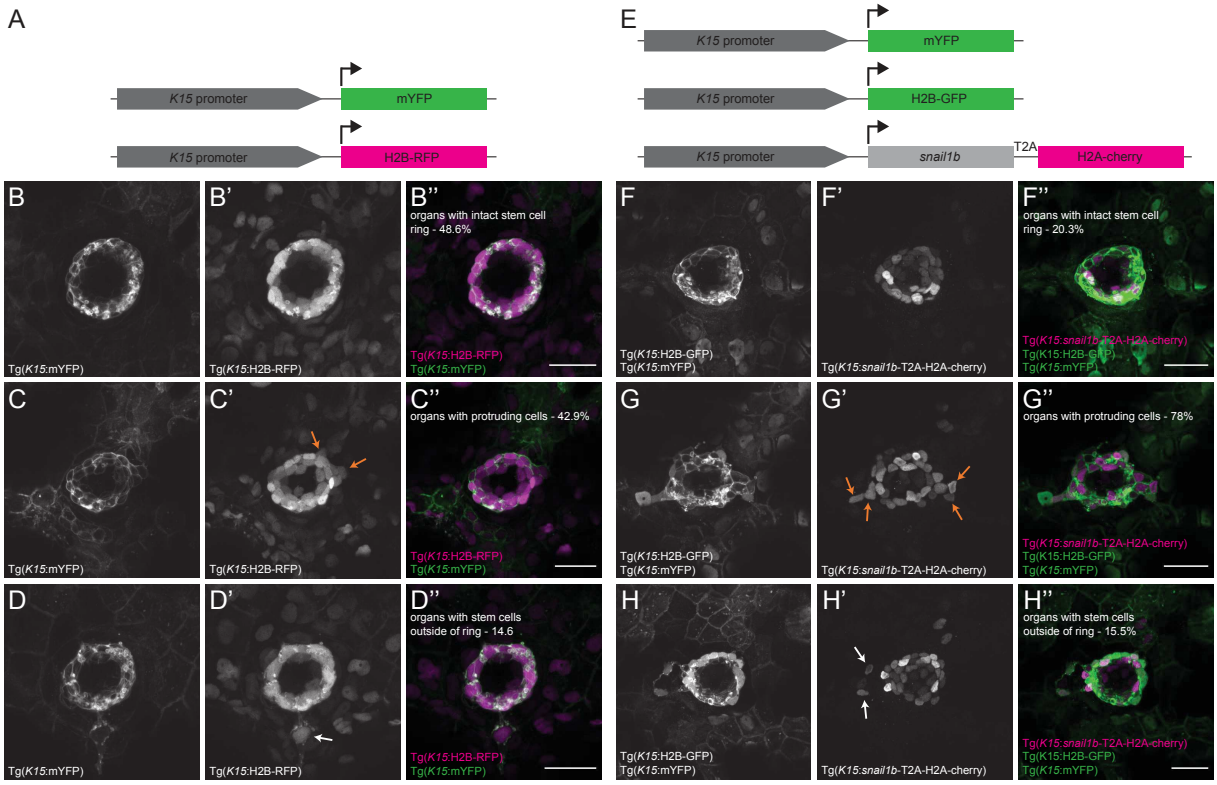

Figure 21: Ectopic *snail1b* expression affects neuromast morphology. A: Schematic depiction of transgenes expressed by wildtype fish used for quantification of neuromast morphology. B-B'': Majority of wildtype neuromasts (48.6%) displays intact stem cell ring. C-C'': 42.9% of secondary neuromasts exhibit stem cells protruding from the stem cell ring (orange arrows). The number of protruding stem cells per neuromast is 1.6. D-D'': In 14.6% of secondary organs neuromast stem cells have detached from the stem cell ring (white arrow). Identity was assigned based on cellular connections visualized by *K15*:mYFP. The number of detached stem cells per neuromast is 1. E: Schematic depiction of transgenes in fish ectopically expressing *snail1b*. F-F'': Only 20.3% of *K15*:*snail1b*-T2A-H2A-cherry expressing secondary neuromasts display an intact stem cell ring. G-G'': The proportion of secondary neuromasts with protruding stem cells (orange arrows) is increased to 78%. At the same time, the number of protruding stem cells per neuromast increased to 2.2. H-H'': In 15.5% of neuromasts detached stem cells can be observed (white arrows). The number of detached stem cells per neuromast is slightly increased to 1.3. Scale bars = 20 µm.

To assess PE1-neuromast formation in Tg(*K15*:*snail1b*-T2A-H2A-cherry)/Tg(*K15*:H2B-GFP) fish, I performed live-imaging at hatch, 1 wph and 2 wph. Strikingly, ectopic stem cell migration was never observed. Instead, neuromast stem cell migration and PE1-neuromast formation exclusively occurred anterior (n=15 CNCs in 11 fish) (Fig. 22A-B''). Interestingly, *K15*:*snail1b*-T2A-H2A-cherry expression appears to be heterogeneous, and organ-founder stem cells tend to display a stronger signal than stem cells remaining in the P0-neuromast. This heterogeneous expression might be due to heterogeneous activity of the *K15* promoter, as indicated by unpublished results from Jasmin Onistschenko (a Ph.D. student in the lab). *K15* tends to be upregulated in cells that are about to divide. Possibly, anterior stem cells undergo increased cell proliferation, the *K15* promoter is activated and therefore *K15*:*snail1b*-T2A-H2A-cherry

expression is higher in organ-founder stem cells. Alternatively, higher *snail1b* expression might drive cell migration and therefore bias stem cells in favor of an organ-founder stem cell fate.

Formation of the PE1-neuromasts tends to happen faster in the ectopic *snail1b* expression paradigm than in the wildtype (Fig. 22C). While only 8% of wildtype fish have generated the PE1-neuromast already at 1 wph, this ratio is increased to 33% in Tg(*K15*:*snail1b*-T2A-H2A-cherry)/Tg(*K15*:H2B-GFP) fish.

Together, this suggests that acquisition of migratory ability is not sufficient to induce ectopic stem cell migration. Possibly, the local environment is only permissive to cell migration at a certain position, anterior to the P0-neuromast. While the exit point of organ-founder stem cells seems fixed, the time point of migration can be variable, suggesting that the local microenvironment at the anterior side of the P0-neuromast is pre-patterned to allow the passage of neuromast stem cells.

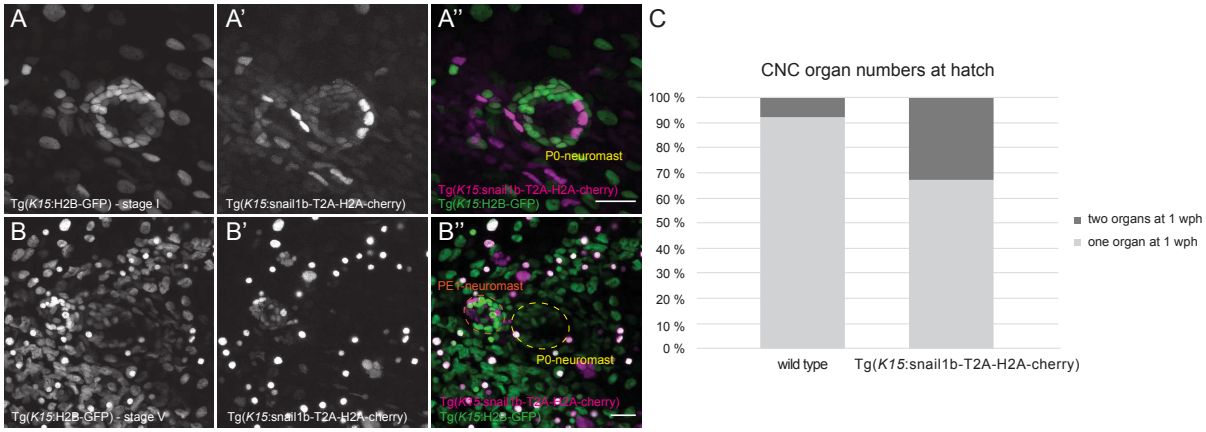

Figure 22: PE1-neuromast formation under ectopic *snail1b* expression conditions. A-A'': P0-neuromast of a Tg(*K15*:snail1b-T2A-H2A-cherry)/Tg(*K15*:H2B-GFP) fish at stage I. B-B'': P0- and PE1-neuromast at stage V of post-embryonic development in the same fish at 1 wph. The PE1-neuromast has been formed within 1 week. PE1-neuromast stem cells express higher levels of *K15*:*snail1b*-T2A-H2A-cherry than P0-neuromast stem cells. C: Quantification of organ numbers in the CNC at 1 wph in wildtype (N = 12 CNCs in 12 fish) and Tg(*K15*:snail1b-T2A-H2A-cherry)/Tg(*K15*:H2B-GFP) (N = 15 CNCs in 11 fish) fish. PE1-neuromast formation seems to be completed faster in *K15*:*snail1b* expressing fish than in wildtype fish. Scale bars = 20 µm.

2.2.5 Induction of organ-founder stem cell fate in anterior position

Organ-founder stem cell migration and eventually PE1-neuromast formation occur exclusively at the anterior side of the P0-neuromast. This begs the question of whether organ-founder stem cell fate is pre-specified or if all neuromast stem cells have the capacity to acquire organ-founder stem cell fate. Using a BrdU pulse of 6 h, I analyzed proliferation activity of stem cells within the P0-neuromast at late embryonic stages, when the P0-neuromast is deposited, until stage III,

when organ-founder stem cell migration takes place. Interestingly, this revealed a bias of cell proliferation towards the anterior part of the founder organ across all analyzed stages (Fig. 23). This is indicative of the first signs of asymmetry along the anterior-posterior axis of the P0-neuromast, possibly marking the onset of post-embryonic organogenesis. Moreover, the analysis revealed a proliferation peak at stage I and II, with 6 and 5.4 BrdU$^+$ cells per neuromast, respectively. At stage II, most BrdU$^+$ cells can be found in anterior positions (Fig. 23). I hypothesized that organ-founder stem cell fate is manifested around stage I/II. Therefore, to tackle the question of fate pre-specification vs. acquisition, I performed multi-photon laser ablation of prospective organ-founder stem cells at the anterior side of the P0-neuromast around stage I/ II of post-embryonic organogenesis and examined the reaction of the system (Fig. 24). For multi-photon laser ablation I used the transgenic line Tg(*K15*:H2B-GFP).

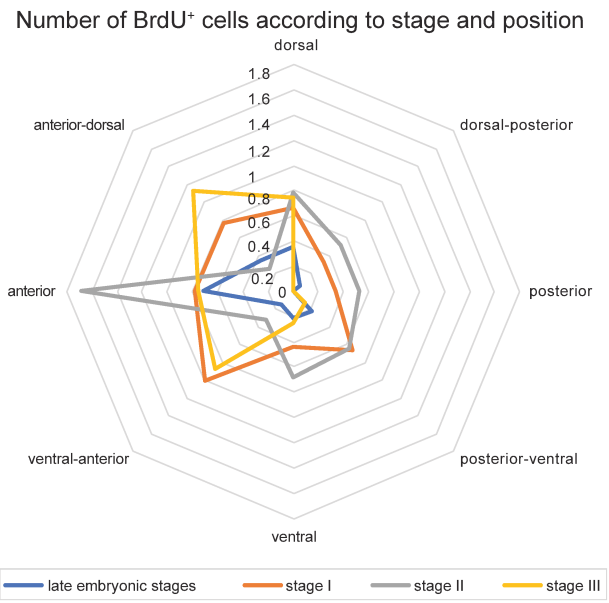

Figure 23: Proliferation bias at anterior position of the P0-neuromast. Analysis of proliferation activity at different stages and according to position within the P0-neuromast. There seems to be a bias towards proliferation in the anterior part of the P0-neuromast across all stages. A proliferation peak is reached at stage I and II.

Strikingly, the PE1-neuromast was formed nevertheless from ablated P0-neuromasts (n=8/9 fish). In 5/8 fish, the P0-founder neuromast appeared to be smaller compared to the newly formed PE1-neuromast and the non-ablated control neuromast on the contra-lateral side (Fig. 24A'', B, C). The fact that the PE1-neuromast was of regular size, suggests that cell number is not a critical factor in the decision how many organ-founder stem cells are specified and migrate out of the P0-neuromast. Instead, it seems like the number of organ-founder stem cells that leave the P0-neuromast is fixed regardless of the state of the P0-founder neuromast, suggesting that commitment to the organ-founder stem cell fate is irreversible. This is in line with results obtained from ablation experiments performed by Ali Seleit. Ablation of posterior P0-neuromast stem cells at stage II/III of organogenesis did not lead to a reversion of organ-founder stem cell fate to drive cells towards regeneration of the P0-neuromast. Instead, migrating neuromast stem cells continued migration and PE1-neuromast formation (Seleit, 2019). The results obtained in this thesis suggest that irreversibility of organ-founder stem cell fate occurs already before the onset of cell migration.

The system appears to be very robust towards ablation of prospective organ-founder stem cells by reconstituting organ-founder stem cells. To uncover the mechanism of how organ-founder stem cells are reconstituted, I performed time-lapse imaging immediately following multi-photon ablation. Interestingly, this revealed that the organ's first response upon cell ablation entails cell rearrangements. Non-ablated stem cells from other positions within the P0-neuromast reorganize, resulting in the closing of the injury gap and reconstruction of organ morphology (Fig. 24D-D'''').

By rearranging, neuromast stem cell positions are altered and cells previously located at dorsal or ventral positions now find themselves in anterior position. Thereby, the stem cells encounter a hitherto unfamiliar environment. 3 h post ablation the first cell divisions were observed in the posterior part of the organ (Fig. 24D''', D''''; green and orange dots). To exclude the possibility of organ-founder stem cell reconstitution by cell proliferation, I performed a 6 h BrdU pulse 3h after the ablation. In 7 out of 9 fish no BrdU incorporation into neuromast stem cells could be observed. This indicates that within the 6 h pulse neuromast stem cells did not undergo S-phase in preparation of cell division. Only in 2 ablated P0-neuromasts $BrdU^+$ cells could be detected. Interestingly, in contrast to the unablated situation (Fig. 23), $BrdU^+$ cells were exclusively found in the posterior half of the P0-neuromast. This suggests that organ-founder stem cells are not reconstituted via proliferation of remaining neuromast stem cells, but solely by stem cell rearrangement. The fact that these newly positioned anterior stem cells are able to generate the PE1-neuromast indicates that organ-founder stem cell fate can be induced in cells that were previously not destined to become organ-founder stem cells. Moreover, these results suggest that the local microenvironment, specifically the one anterior to the P0-neuromast, has inductive capacities turning neuromast stem cells into organ-founder stem cells. This in turn suggests that organ-founder stem cell fate is not pre-specified, but that given the right circumstances, other neuromast stem cells have the ability to become organ-founder stem cells.

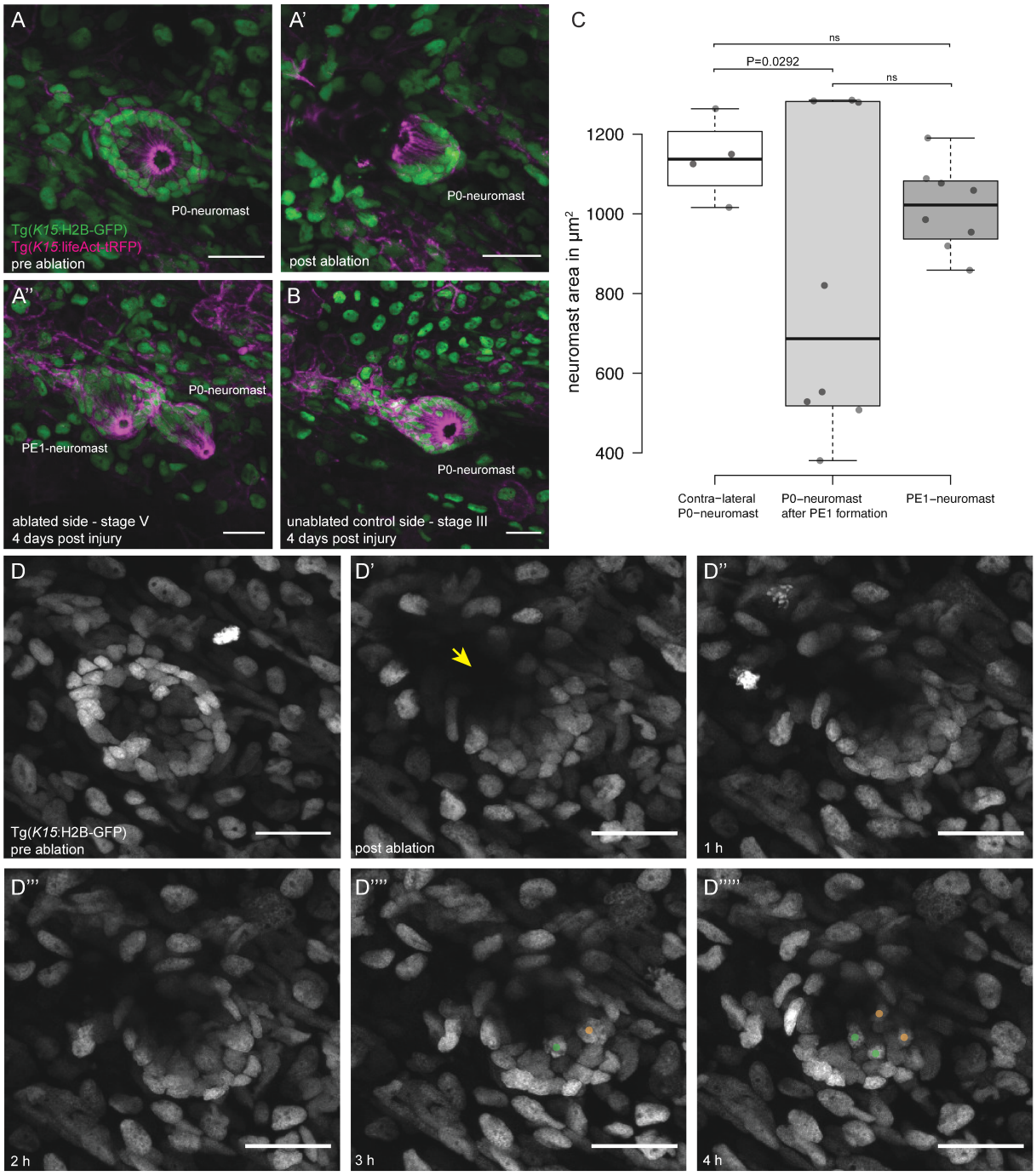

Figure 24: Organ-founder stem cell fate is induced at anterior position. A: P0-neuromast at stage II prior to ablation of prospective organ-founder stem cells. A': Same neuromast after ablation of prospective organ-founder stem cells at the anterior side of the organ. A'': The ablated P0-neuromast has generated the PE1-neuromast. The P0-neuromast appears to be smaller in size compared to the PE1-neuromast and the contra-lateral control P0-neuromast. B: P0-neuromast on the contra-lateral control side. The P0-neuromast is in stage III of post-embryonic organogenesis. C: Quantification of organ area of ablated fish. The graph shows the area of unablated P0-neuromasts, ablated P0-neuromasts after PE1-neuromast formation and PE1-neuromasts that were generated from ablated P0-neuromasts. Ablated P0-neuromasts display a high variability in organ size, with most being smaller than the newly generated PE1-neuromast. The newly formed PE1-neuromast reaches regular size in comparison to unablated control P0-neuromasts. D-D''''': Time-lapse imaging of stem cell behavior after prospective organ-founder stem cell ablation with an interval of 30 min. By rearrangement of the remaining stem cells the injury site (yellow arrow) is closed. Cell proliferation is rare within 9 h after ablation and was exclusively observed in the posterior part of the organ (green and orange dots). Scale bars = 20 µm.

2.2.6 Post-embryonic organogenesis in the medaka CNC is independent from the pLL nerve

Onset of post-embryonic organogenesis in the CNC is variable even within the two sides of the same fish. 50% of fish display different stages of post-embryonic organogenesis on the left and right side, with a maximum difference of one stage. This suggests that organogenesis is not regulated by a systemic signal, but rather local cues.

In the past it has been shown that post-embryonic neuromast formation on the caudal fin of zebrafish depends on the presence of the pLL nerve (Wada et al., 2013). Although initial phases of the process, like cell repolarization and elongation, take place, neuromast cells do not leave the founder neuromast and a new organ is not formed. The situation in the opercular aLL neuromasts in zebrafish seems different. It has been shown that innervation is dispensable for post-embryonic organ formation (Wada et al., 2010).

In order to examine if innervation is crucial for post-embryonic neuromast formation in the CNC of medaka, Ali Seleit (a former Ph.D. student) and I decided to perform nerve ablation experiments. Ali Seleit performed nerve ablations using Tg(*Eya1*:mCFP)/Tg(*K15*:H2B-RFP) fish at hatch, when the P0-neuromast was already fully formed. The fish were followed until stage II/ III. In all cases of successful nerve ablations, cells migrating from the P0-neuromast could be overserved despite a missing nerve connection (n=7 fish) (Seleit, 2019). To exclude prior patterning of the P0-neuromast by the pLL nerve before ablation I performed earlier ablations at 3-5 dpf, before formation of the P0-neuromast. In order to assess if post-embryonic organogenesis can be completed (presence of PE1-neuromast with differentiated cells), I followed the ablated fish until stage V of organogenesis. For ablation of the pLL nerve I used Tg(*Kremen1*:mYFP)/Tg(*Eya1*:EGFP) fish. While *Kremen1* labels sensory neurons (including the pLL nerve), *Eya1* labels differentiated neuromast hair cells (Seleit et al., 2017a), which can be used as a measure for completed organogenesis. I examined the ablated fish at 1 and 2 wph. At 1 wph, 8/11 fish were in stage II/III of organogenesis. The remaining 3/11 fish had already generated the PE1-neuromast, as indicated by the presence of differentiated hair cells. Out of the eight P0-neuromasts in stage II/III at 1wph, three fish died and were not imaged at 2 wph. Three of the fish generated the PE1-neuromast within 2 wph. Only two P0-neuromasts did not generate the PE1-neuromast within 2 wph. Possibly, the PE1-neuromast would have been generated at later time points, but due to animal experiment regulations imaging beyond stage 42 of medaka development was not possible. Fig. 25 shows a representative case, where pLL nerve ablation was performed at 3 dpf (Fig. 25A, A'), before the primordium (Fig. 25A, magenta arrow) had reached the caudal fin. At 2 wph post-embryonic organogenesis was assessed in this

fish. The contralateral PE1-neuromast on the unablated control side was formed normally. Differentiated hair cells can be detected using Tg(*Eya1*:EGFP) (Fig. 25B). On the ablated side the PE1-neuromast was formed as well, including differentiated hair cells (Fig. 25C). However, both the P0- and PE1-neuromast appear to contain significantly less hair cells, indicating that a functional nerve connection is either required for hair cell formation or maintenance, in line with results from zebrafish (Wada et al., 2013), amphibians (Jones and Singer, 1969; Speidel, 1948; Wright, 1947) and medaka (Seleit, 2019). Together, these results strongly indicate that unlike in the caudal fin of zebrafish, post-embryonic neuromast formation in the medaka CNC is independent of the pLL nerve.

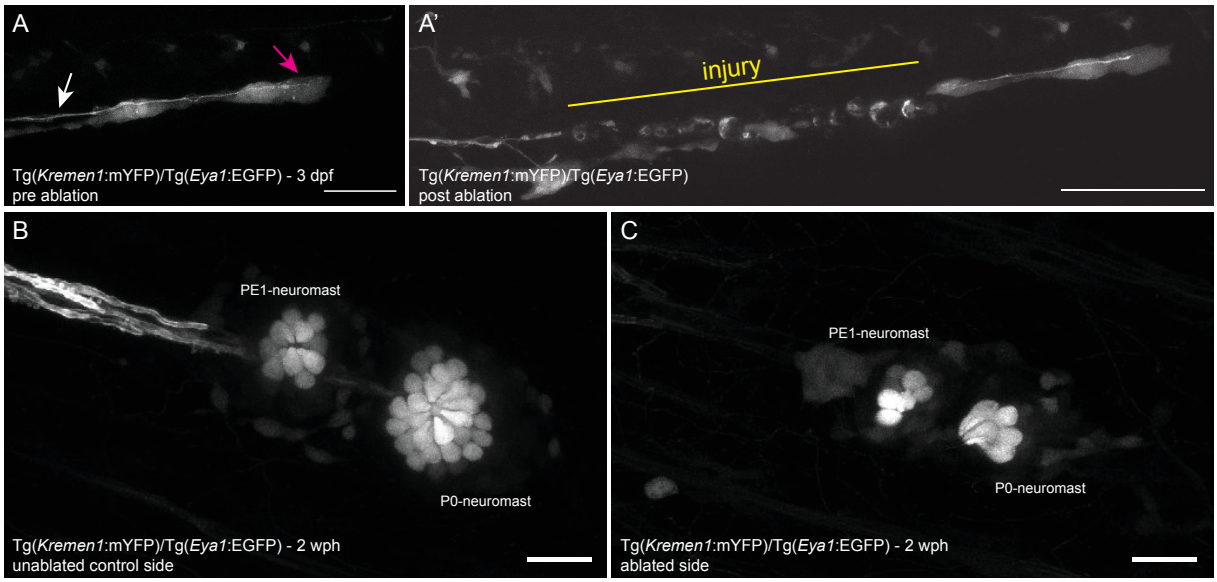

Figure 25: PE1-neuromast formation is independent of the pLL nerve. A: Tg(*Kremen1*:mYFP)/Tg(*Eya1*:EGFP) embryo at 3 dpf. *Kremen1*:mYFP labels the pLL nerve (white arrow) and *Eya1*:EGFP labels primordium (magenta arrow) and differentiated hair cells at later stages. A': Same fish after pLL nerve ablation using a multi-photon laser. Primordium migration was not disturbed, as the neuromast pattern was unaffected and wildtype-like. B: Unablated control side at 2 wph. The PE1-neuromast was successfully formed. Both P0- and PE1-neuromast are innervated. C: Ablated side at 2 wph. The PE1-neuromast was formed in absence of the pLL nerve. Both the P0- and PE1-neuromast seem to have less hair cells than neuromasts on the contralateral control side.

2.2.7 Chemokine signaling via Cxcr4b is involved in post-embryonic organogenesis

The fact that organ-founder stem cells undergo an EMT is reminiscent of the embryonic program of pLL development. The migratory property of the primordium is conveyed by cells in the leading edge undergoing an EMT. In these cells, EMT is induced by the ligand Cxcl12a via the chemokine receptor Cxcr4b (Neelathi et al., 2018). To examine if the same mechanism might be re-employed by organ-founder stem cells for post-embryonic organogenesis, I first

performed an *in situ* hybridization (Seleit et al., 2017a) to determine the presence of *Cxcl12a* mRNA at post-embryonic stages. Indeed, *Cxcl12a* expression could still be detected at the posterior end of the tail, near the position of the P0-neuromast (Fig. 26).

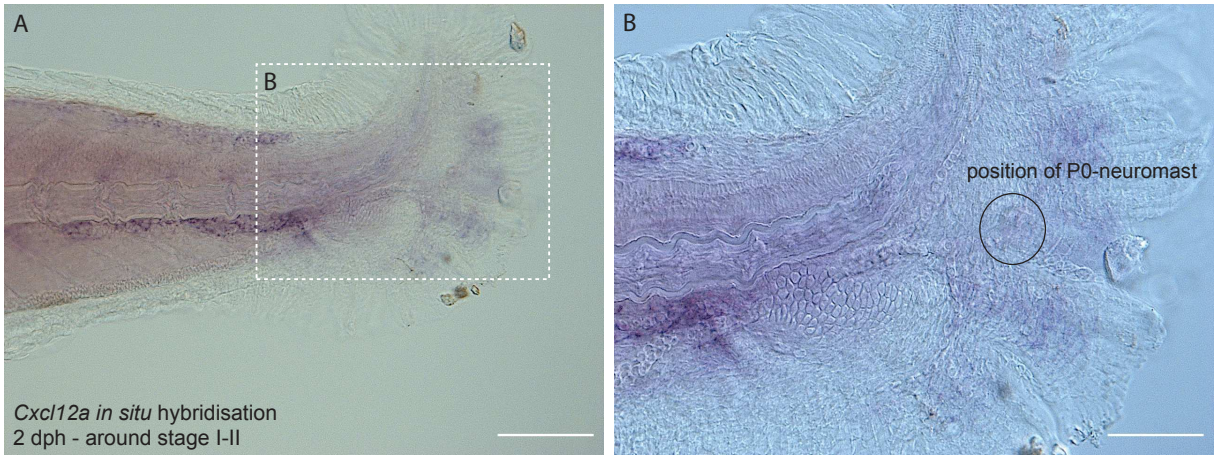

Figure 26: *Cxcl12a* expression in the vicinity of the P0-neuromast at the onset of post-embryonic organogenesis. A: Posterior part of the tail at 2 dph. *Cxcl12a* expression can be detected. Scale bar = 100 µm. B: *Cxcl12a* expression can be detected in the vicinity of the P0-neuromast. Scale bar = 50 µm.

To functionally test whether chemokine signaling via Cxcl12a and Cxcr4b is necessary for post-embryonic formation of the PE1-neuromast, I followed a two-fold approach using *cxcr4b*^{D625} mutants and a transgenic line mimicking a loss of Cxcr4b signaling. Since *cxcr4b*^{D625} mutants fail to generate the P0-neuromast due to disturbed primordium migration, post-embryonic organogenesis in the CNC cannot be assessed. For this reason, I generated a transgenic line expressing the Cxcr7 receptor under the *K15* promoter in combination with an H2B-GFP driven by the *K15* promoter as well for visualization of neuromast stem cells. Both Cxcr7 and Cxcr4b bind to and compete for the same ligand, Cxcl12a. Binding of Cxcl12a to Cxcr4b results in intracellular signaling, while binding of Cxcl12a to Cxcr7 does not (Dambly-Chaudiere et al., 2007; Valentin et al., 2007). By expressing Cxcr7 in neuromast stem cells, possible chemokine signaling via Cxcr4b should therefore be impaired. Although specific for neural stem cells in the mature neuromast, the *K15* promoter drives expression in the lateral line at earlier stages, after primary neuromasts were deposited by the primordium (Seleit et al., 2021). As expected for the over-expression of a functional Cxcr7, Tg(*K15*::*Cxcr7*) fish are often missing secondary embryonic neuromasts. All H2B-GFP^{+} fish showed defects in pLL development. In 24/28 pLLs variable numbers of secondary neuromasts failed to be formed in between the pairs of primary neuromasts (Fig. 27A). Wildtype pLLs displayed an average number of 6.1 secondary neuromasts (97 secondary neuromasts in 16 wildtype pLLs). In Tg(*K15*:Cxcr7) pLLs the average number of secondary neuromasts was reduced to 2.6 (72 secondary neuromasts in 28 pLLs). In 12/28 pLLs the pLL primordium failed to reach the tail, resulting in a truncated

pLL. Since *K15* mRNA is not detectable via *in situ* hybridization in the pLL primordium (Seleit et al., 2021), the primordium defect in Tg(*K15*:Cxcr7) fish is most likely due to insertional effects, driving Cxcr7 already in the pLL primordium. For analysis of the phenotype in post-embryonic organogenesis in the CNC, I used fish displaying defects in secondary pLL neuromasts, while the P0-neuromast was present (Fig. 27 B,B'). Five P0-neuromasts were followed from hatch until 2 wph. Only 1/6 (17%) P0-neuromasts reached stage V of PE1-neuromast formation, while 5/6 P0-neuromasts reached stage III/IV at 2 wph. At 2 wph, 4/7 (57%) PE1-neuromasts have been formed in the wildtype. Therefore, PE1-neuromast formation in Tg(*K15*:Cxcr7) seems slightly delayed, although organ-founder stem cell migration occurred in all cases.

As the fish grow, new neuromasts are added to the CNC. Comparing CNC organ numbers in adult fish, we observed a significantly lower CNC organ number in Tg(*K15*:Cxcr7) than wildtype fish (WT mean: 3.8 organs per CNC; Tg(*K15*:*Cxcr7*) mean: 2.2 organs per CNC). These results suggest that chemokine signaling via Cxcr4b/Cxcl12a/Cxcr7 is involved in PE1-neuromast formation. However, despite disturbance of chemokine signaling stem cell migration is not abolished.

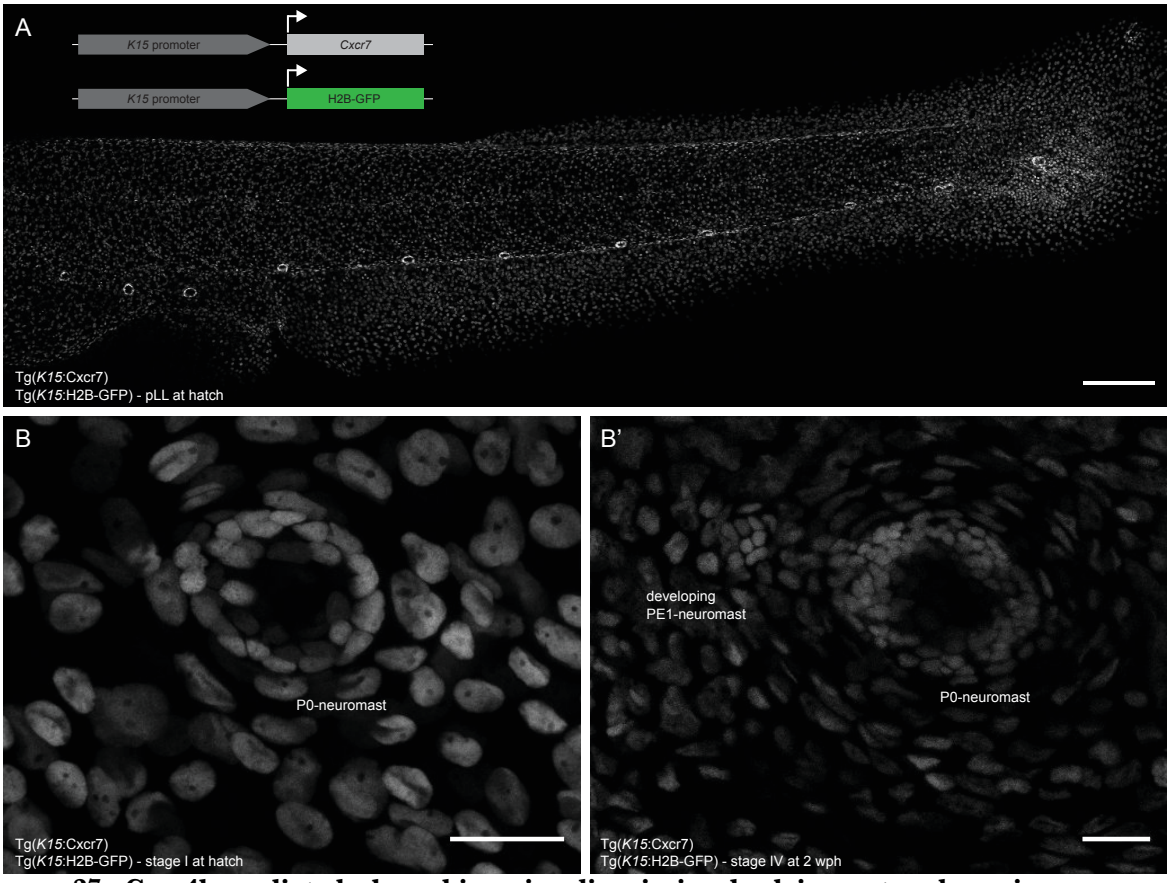

Figure 27: Cxcr4b-mediated chemokine signaling is involved in post-embryonic neuromast formation. A: Schematic depiction of constructs used to generate the stable line. pLL phenotype of Tg(*K15*:*Cxcr7*)/Tg(*K15*:H2B-GFP) fish. Secondary neuromasts are not formed properly. Scale bar = 100 µm. B: P0-neuromast of a Tg(*K15*:*Cxcr7*)/Tg(*K15*:H2B-GFP) at stage I of post-embryonic organogenesis. Scale bar = 20 µm. B': Same P0-neuromast at stage IV of post-embryonic organogenesis at 2 wph. Neuromast stem cells have migrated and coalesced, but not yet formed the PE1-neuromast. Scale bar = 20 µm.

In order to further investigate the influence of chemokine signaling via Cxc4b I made use of the previously generated *cxcr4b*^{D625} mutant line. Since *cxcr4b*^{D625} mutants are lacking most pLL neuromasts, including the P0-neuromast, analysis of PE1-neuromast formation in the CNC is not possible. I have shown in previous sections of this thesis that aLL formation occurs robustly in *cxcr4b*^{D625} mutant. Therefore, I searched for aLL neuromasts undergoing post-embryonic organogenesis in a similar fashion as in the CNC. Post-embryonic organogenesis via organ-founder stem cell migration occurs in the aLL sub-line ANC (Fig. 28A) and the same stages can be applied as for the CNC (Fig. 28B-B''). Formation of the ANC sub-line is unaffected in *cxcr4b*^{D625} mutants and therefore poses a suitable model system to study the loss of Cxcr4b on post-embryonic organogenesis via organ-founder stem cells. Interestingly, post-embryonic organogenesis in the ANC is not disturbed in the *cxcr4b*^{D625} mutant background (Fig. 28C-D). Organ-founder stem cells are able to migrate and generate the ANC PE1-neuromast within the wildtype timeframe. Quantification of ANC organ numbers in wildtype and *cxcr4b*^{D625} mutants at hatch did not reveal a significant difference.

Taken together, these results suggest, that in contrast to the CNC, chemokine signaling via Cxcr4b is dispensable for organ-founder stem cell migration and eventually PE1-neuromast formation in the ANC.

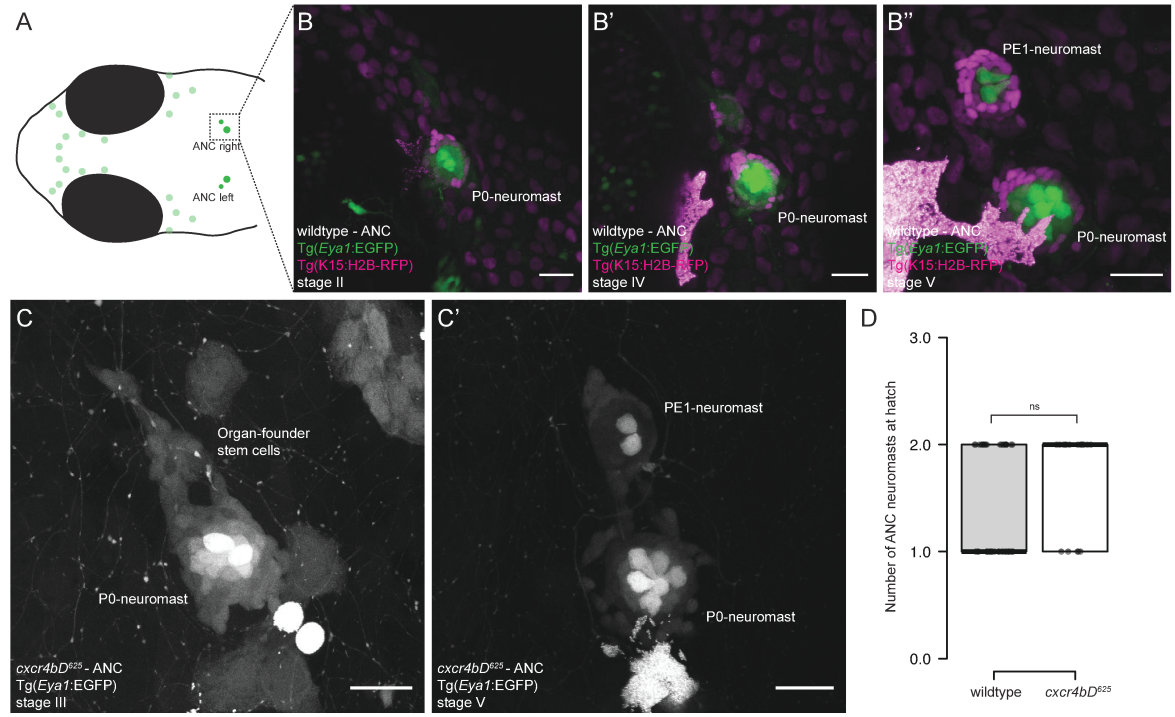

Figure 28: ANC PE1-neuromast formation occurs in the absence of Cxcr4b. A: Schematic description of ANC sub-line position. The ANC is positioned on the dorsal side of the head. Since the lateral line occurs bilaterally, every fish possesses two ANCs. B: ANC P0-neuromast at stage II of post-embryonic organogenesis in the wildtype. B': ANC P0-neuromast at stage IV of post-embryonic organogenesis in the wildtype. B'': Stage V of post-embryonic development in the wildtype – the ANC PE1-neuromast is fully formed. C: Stage III of the ANC P0-neuromast in the *cxcr4b*^{D625} mutant background. C: Same fish at stage V of post-embryonic development. The ANC PE1-neuromast has been successfully formed. Scale bars = 20 µm. D: Quantification of ANC organ number in wildtype and *cxcr4b*^{D625} mutants. There is no significant difference.

Post-embryonic organogenesis in the ANC can however only be an approximation of the situation in the CNC. It is possible that post-embryonic organogenesis in the aLL and pLL rely on different molecular mechanism, although the processes resemble each other on the morphogenetic level. In order to unambiguously determine the effect of a loss of Cxcr4b, genetic mosaic experiments should be carried out by transplanting wildtype cells into *cxcr4b*^{D625} mutants. Primordium migration can be rescued by only few wildtype cells (Haas and Gilmour, 2006; Seleit et al., 2017a). Thereby, it is possible to obtain *cxcr4b*^{D625} mutant fish containing a P0-neuromast with mostly mutant cells. I performed blastula transplantations of Tg(*K15*:H2B-GFP) cells into *cxcr4b*^{D625} mutants. However, I was unsuccessful in generating the desired fish (n transplanted fish > 50).

2.2.8 The vasculature is a possible determinant for direction of organ-founder stem cell migration

There is extensive evidence that the vasculature provides instructive signals (either secreted or mechanical) for organ morphogenesis and differentiation (reviewed in (Ramasamy et al., 2015), such as in the liver (Matsumoto et al., 2001), pancreas (Lammert et al., 2001; Yoshitomi and Zaret, 2004) and kidney (Serluca et al., 2002). Therefore, I was wondering whether the blood vessels around the P0-neuromast might influence the position of cell migration and post-embryonic organ formation in the lateral line of medaka. To investigate this I followed a transgenic line labelling endothelial cells in combination with neuromast stem cells: Tg(*Fli1*:EGFP/*K15*:H2B-RFP). Live-imaging of the same fish before and during organogenesis revealed a correlation between increased blood vessel/neuromast distance and onset of post-embryonic organogenesis (Fig. 29). Before the onset of organogenesis, the P0-neuromast is positioned on top of a blood vessel (Fig. 29A). Imaging of the very same fish at stage III of organogenesis revealed that blood vessel and P0-neuromast had been displaced, probably due to passive movements during caudal fin morphogenesis (Fig. 29A')'. Interestingly, organ-founder stem cells (Fig. 29A', yellow arrow) migrate towards the original position on top of the blood vessel junction. During post-embryonic growth, morphogenetic changes lead to the formation of the adult caudal fin (Huxley, 1859; von Baer, 1835). In the course of that, the immediate environment of the P0-neuromast is changed. In order to assess these changes, I quantified blood vessel/P0-neuromast distance at stage I (before the onset of post-embryonic organogenesis) and stage II/III, revealing a significant difference (P=0.0193, two-tailed unpaired t-test) (Fig. 29B). Onset of post-embryonic organogenesis therefore appears to correlate with an increased distance between blood vessels and P0-neuromast. Possibly, an

increase in distance between blood vessel and P0-neuromast results in the onset of organ-founder stem cell migration and hence post-embryonic organogenesis. Additionally, the vasculature might provide signals determining the migratory pathway of organ-founder stem cells.

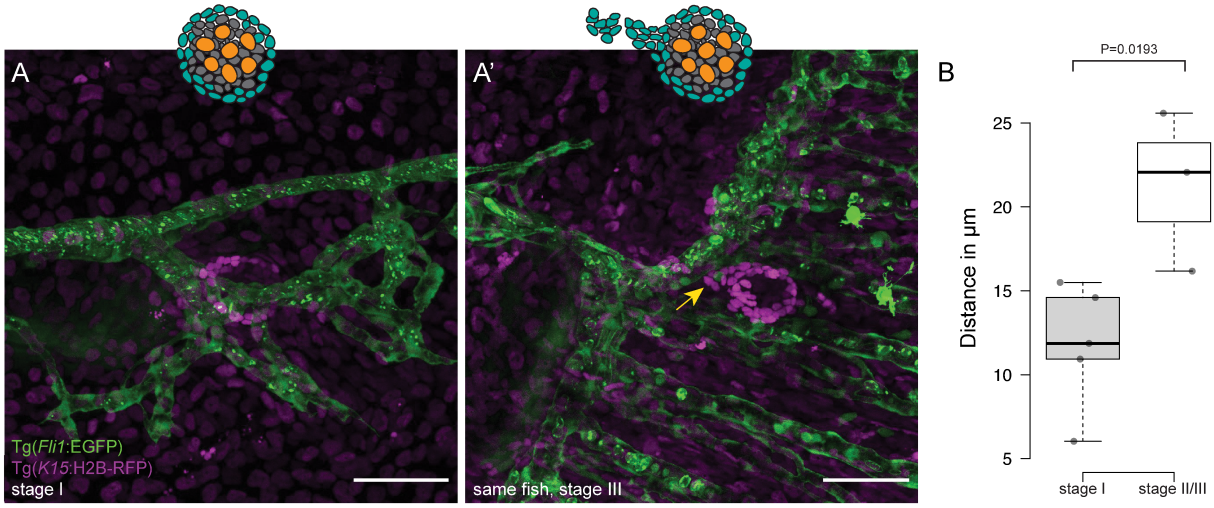

Figure 29: Correlation between increased blood vessel/neuromast distance and onset of post-embryonic organogenesis. A: Stage I of post-embryonic organogenesis. The P0-neuromast is stereotypically positioned above a blood vessel junction. A': Stage III of the same fish. The relative position of blood vessels and neuromast was changed. Organ-founder stem cells migrate anteriorly towards their original position. The P0-neuromast is surrounded by blood vessels on the anterior, dorsal and ventral side, not the posterior side. Scale bars = 50 µm. B: Quantification of blood vessel/neuromast distance in z at stage I (n = 5 P0-neuromasts) and stage II/III (n = 3 P0-neuromasts) of post-embryonic organogenesis. Two-tailed unpaired t-test revealed a significant difference (P=0.0193).

The P0-neuromast is surrounded by blood vessels on three sides: anterior, ventral and dorsal. However, cell migration occurs only in anterior direction (parallel to the fin rays) and never in dorsal or ventral direction. I hypothesize that the fin rays that enclose the P0-neuromast on the dorsal and ventral side (Fig. 30A, B) prevent cell migration by either restricting organ-founder stem cell mobility or blocking signals from reaching the stem cells. This hypothesis is supported by the fact that in adult fish the CNC is found in between the very same fin rays as the P0-neuromast in the beginning, meaning neuromast stem cells do not cross the fin ray boundary.

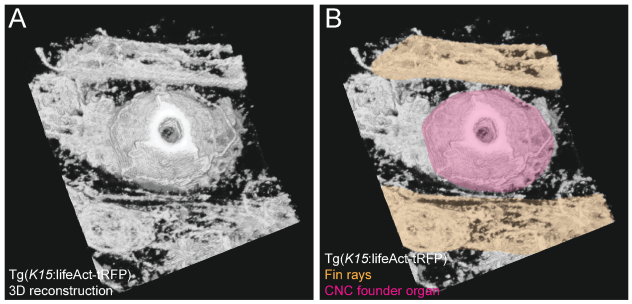

Figure 30: Fin rays as roadblocks for stem cell migration. A: 3D reconstruction of the P0-neuromast with surrounding fin rays on the dorsal and ventral side in Tg(*K15*:lifeAct-tRFP). B: Same image with fake-colored fin rays (orange) and P0-neuromast (magenta).

In order to further support the hypothesis that the vasculature provides directionality for post-embryonic organogenesis I performed laser ablation of blood vessels during embryonic stages.

However, this turned out to be experimentally challenging. Small injuries resulted in quick regeneration of the vasculature. Larger injuries did indeed result in aberrations of the blood vessel pattern, however, the P0-neuromast was often injured during the ablation procedure or was degenerated afterwards.

As an alternative, I made use of a genetic approach based on the CRISPR/Cas9 system. It has previously been reported that a loss of *vegfr1* can lead to an increase in blood vessel sprouting (Chappell et al., 2016; Krueger J, 2011). Conceptionally, I hypothesized that ectopic blood vessels would result in signals attracting organ-founder stem cells to ectopic positions.

Therefore, I designed guideRNAs against the *vegfr1* locus (Fig. 31A) and injected them together with Cas9 mRNA into the 1-cell stage of Tg(*Fli1*::EGFP) embryos. While screening the fish I solely focused on abnormal blood vessel phenotypes in the caudal fin. As expected, *vegfr1* crispants displayed abnormal blood vessel sprouting (Fig. 31C). This phenotype could later also be observed in stable F1 mutants. Among these fish I selected candidates with ectopic blood vessels in the vicinity (especially the posterior side) of the P0-neuromast at stage I of organogenesis (Fig. 31C). At stage III, organ-founder stem cell migration was assessed. In a wildtype fish, the blood vessels in the caudal fin are rather parallel running in and out of the fin rays (Fig. 31D). During stage III of post-embryonic organogenesis, the P0-neuormast borders on blood vessels at the anterior, dorsal and ventral side, while organ-founder stem cells migrate anteriorly (Fig. 31D'-D''').

In *vegfr1* crispants ectopic blood vessels are common, yet overall morphology of the caudal fin does not seem disturbed (Fig. 31E, E'). The position of ectopic blood vessels can be variable and moreover can change as the fish grows. I screened for fish displaying ectopic blood vessels at hatch and grew them for one week until stage III of post-embryonic organogenesis was reached. Although most crispants displayed ectopic blood vessels also at 1 wph, the presence of ectopic blood vessels at the posterior border of the P0-neuromast only occurred seldomly. In two cases with ectopic blood vessels posterior to the P0-neuromast posterior stem cell migration could be observed (Fig. 31E''-E''', highlighted in blue). Whether these migrating stem cells are able to generate a post-embryonic neuromast remains to be examined. Posterior organ-founder stem cell migration has never been observed in the wildtype background. Even though the number of ectopic migration events is low, the results suggests that blood vessels might indeed determine direction of organ-founder stem cells and ectopic blood vessels are sufficient to induce ectopic stem cell migration. The low n number of *vegfr1* crispants displaying ectopic blood vessels and organ-founder stem cell migration suggests that direction of organ-founder stem cell migration possibly does not only depend on the vasculature, but also other cues.

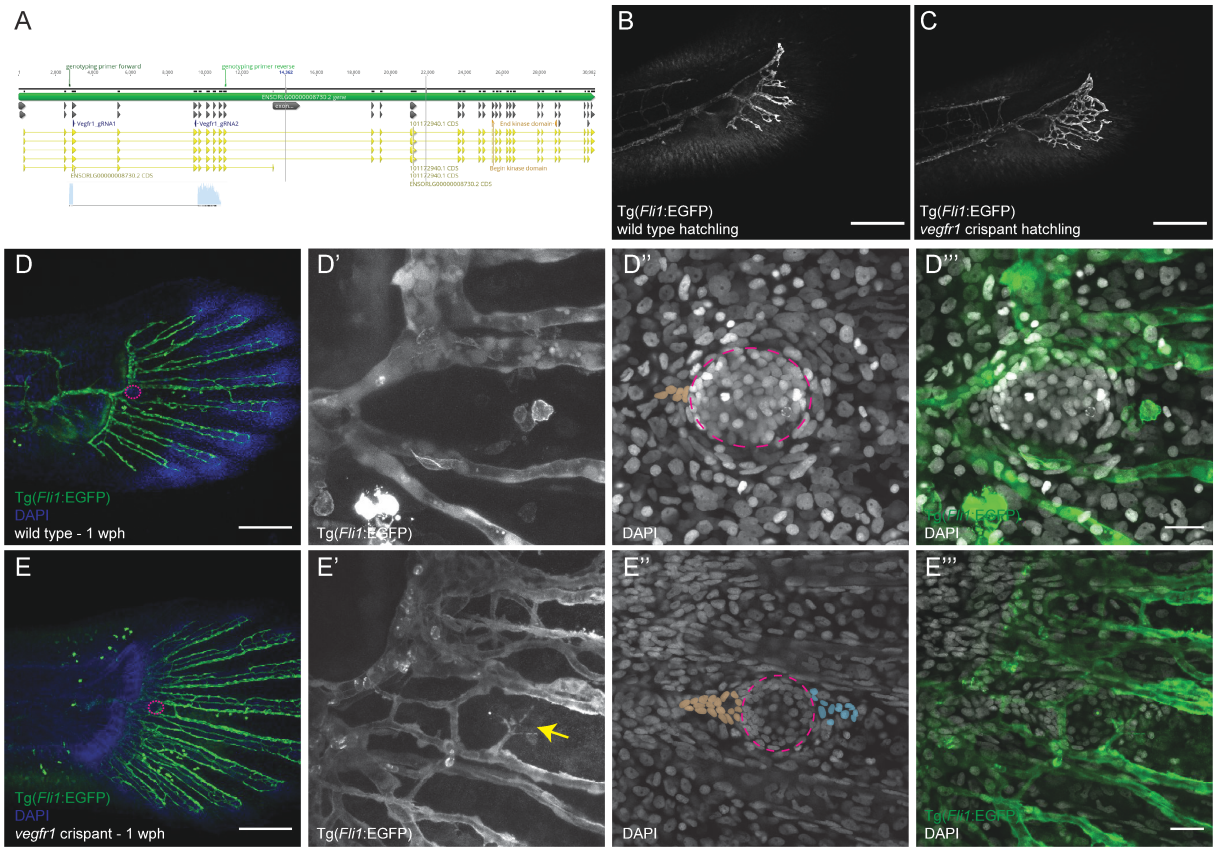

Figure 31: Ectopic blood vessels can induce ectopic stem cell migration. A: *Vegfr1* locus including gRNAs and sequencing read of a mutant allele found in crispants. B: Blood vessel pattern in the caudal fin in a wildtype fish. C: Ectopic blood vessel sprouting in the caudal fin of a *vegfr1* crispant. D: Overview image of the blood vessels in a wildtype caudal fin at 1 wph. Fin rays run parallel in and out of fin rays. D': Zoom in on blood vessels surrounding the P0-neuromast. D'': P0-neuromast displays organ-founder stem cell migration in anterior direction. D''': P0-neuromast borders on blood vessels at the anterior, dorsal and ventral side. E: Overview image of the blood vessel in a *vegfr1* crispant caudal fin at 1 wph. E': Zoom in on blood vessels surrounding the P0-neuromast. Additional blood vessel sprouting can be observed, and an ectopic blood vessel is present at the posterior side of the P0-neuromast (yellow arrow). E'': P0-neuromast of *vegfr1* crispant displays anterior and posterior stem cell migration. E''': P0-neuromast in *vegfr1* crispant is surrounded by blood vessels at the anterior, dorsal, ventral and posterior side. Scale bars (B, C, D, E) = 200 µm. Scale bars (D''', E''') = 50 µm.

As the fish grow, more and more neuromasts are formed in the CNC. Therefore, I examined the CNC neuromast pattern of adult wildtype fish and *vegfr1* crispants and mutants to analyze the cumulative effect of blood vessel aberrations on ectopic organ formation. In wildtype conditions all CNC neuromasts are positioned in between the middle fin rays, dorsal fin ray 1 and ventral fin ray 1, respectively (90% of CNCs) (Fig. 32A). In a minority of 10% of the observed cases (1/10 CNCs), ectopic neuromasts positioned between ventral fin ray 1 and ventral fin ray 2 were observed. In *vegfr1* crispants, ectopic neuromasts can be observed in 25% of cases, while this number is even increased to 33% in stable *vegfr1* mutants. In all cases CNC neuromasts can be observed in between the normal fin rays, however, in many cases ectopic neuromasts can be found between dorsal fin ray 1 and dorsal fin ray 2 (Fig. 32C) or ventral fin ray 1 and ventral fin ray 2. Possibly, ectopic blood vessels in *vegfr1* crispants and mutants resulted

in ectopic organ formation, further highlighting the involvement of the vasculature in post-embryonic organogenesis. How the vasculature might affect organ-founder stem cell migration and post-embryonic organogenesis remains to be elucidated.

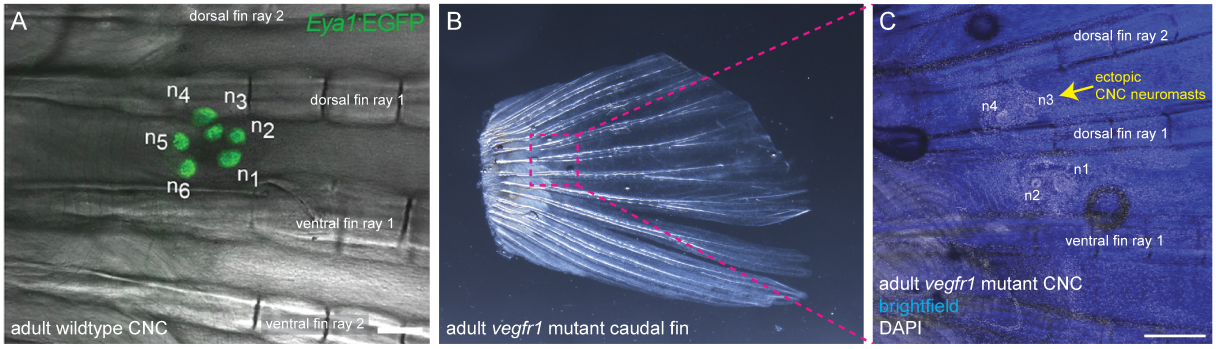

Figure 32: Ectopic CNC neuromasts in *vegfr1* mutants. A: Wildtype CNC. All neuromasts are found in between the middle fin rays (dorsal fin ray 1 and ventral fin ray 1). The image was adapted from (Seleit, Krämer et al., 2017b). B: Binocular image of *vegfr1* mutant caudal fin. The caudal fin does not exhibit morphological defects despite aberrant blood vessel pattern. B': CNC of *vegfr1* mutant. CNC neuromasts n1 and n2 are positioned correctly in between dorsal fin ray 1 and ventral fin ray 1. Neuromasts n3 and n4 are ectopically positioned in between dorsal fin ray1 and dorsal fin ray 2. Scale bar = 200 µm.

Interestingly, by examining the transgenic line Tg(*Egln3*:EGFP) I uncovered an upregulation of *Egln3*:GFP in migrating organ-founder stem cells (Fig. 33, white arrow). Egln3 is a key enzyme of the oxygen sensing pathway. In the presence of oxygen, Egln3 hydroxylates Hif1α and thereby targets it for degradation (Kaelin and Ratcliffe, 2008). Thus, Hif1α is not able to activate hypoxia-related gene transcription. In the absence of oxygen (hypoxic conditions), Hif1α translocates to the nucleus and activates hypoxia-related gene transcription. Among the upregulated genes is *Egln3* (Pescador et al., 2005). An upregulation of *Egln3*:EGFP therefore indicates hypoxic conditions in migrating organ-founder stem cells. Possibly, increase in blood vessel/neuromast distance results in hypoxic conditions in anterior neuromast stem cells and acts as a switch for organ-founder stem cell migration. Alternatively, upregulation of *Egln3*:EGFP in organ-founder stem cells could suggest that these cells are primed for hair cell differentiation. Support and especially hair cells are characterized by a strong expression of *Egln3*:EGFP (Fig. 33B, C)

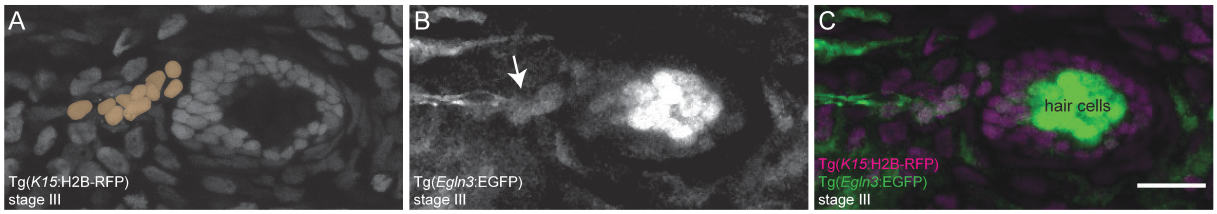

Figure 33: Hypoxic conditions in organ-founder stem cells. A: Organ-founder stem cells are highlighted in orange. B: Organ-founder stem cells upregulate *Egln3*:EGFP (white arrow), indicating hypoxic conditions. C: Overlay of both channels. Scale bar = 20 µm.

2.2.9 Post-embryonic organogenesis in the ANC and CNC might rely on similar mechanisms

In the CNC there is indication that the vasculature provides directionality cues for organ-founder stem cell migration. Since post-embryonic organogenesis in the ANC seems to follow similar developmental sequences, I examined the relative position of blood vessels and ANC P0-neuromast during organogenesis. Strikingly, organ-founder stem cell migration occurs along blood vessels (Fig. 34A, B, D), reinforcing the notion that the vasculature might provide directionality cues for stem cell migration. Additionally, stem cell migration occurs along a prominent tissue furrow (Fig. 34C, D). This suggests, similar to the fin rays in the CNC, that the surrounding tissue architecture confines stem cell migration. Thus, there might be a dual control of organ-founder stem cell migration by biochemical and mechanical signals emanating from the vasculature and the tissue architecture, respectively.

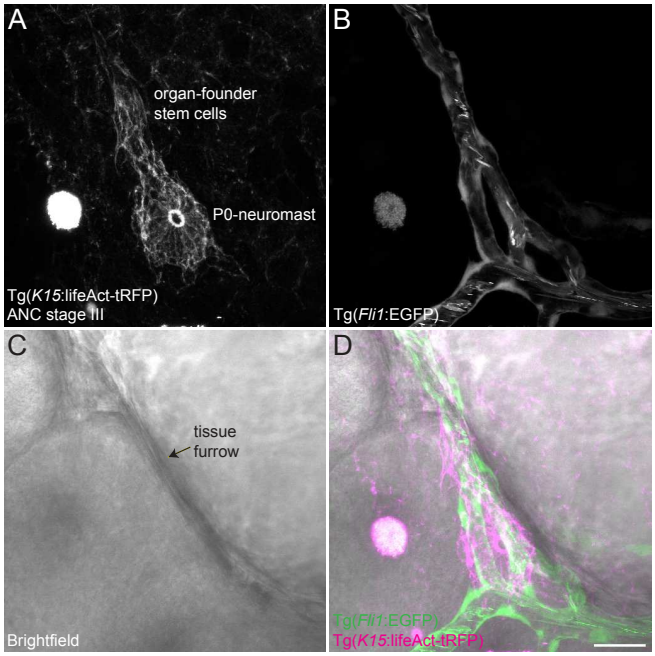

Figure 34: ANC organ-founder stem cell migration follows vasculature and tissue architecture. A: ANC P0-neuormast at stage III of post-embryonic organogenesis. Organ-founder stem cells are migrating in stereotypic direction. B: Blood vessel pattern underneath the ANC. C: Brightfield image of position of ANC. The ANC P0-neuromast is positioned on top of a tissue furrow. D: Organ-founder stem cells migrate along the blood vessels and tissue furrow. Scale bar = 20 μm.

3 Discussion

Organs are the functional units of multicellular organisms and their function is vital to ensure survival. In order to fulfil a specific function, organ integrity is crucial. Therefore, organ formation, homeostasis and regeneration need to be tightly controlled to prevent organ failure, which might jeopardize the survival of the organism.

Mammals are born with a fixed number of organs that are present in a species-specific manner. These organs are generated during embryonic development and grow in size only until early post-embryonic stages. Opposed to this, fish, amphibia and reptiles exhibit indeterminate growth. Their organs adapt to this by increasing in size and/or in number as the animal grows. In the lateral line, both mechanisms of adaptation to increased body size can be observed. The lateral line presents an excellent model system to study the formation of organs, both during embryonic and post-embryonic development.

Neuromasts can be generated in various ways. Among those are neuromast formation via a sensory ridge, a migrating primordium, interneuromast cells and cells from neighbouring neuromasts and migrating organ-founder stem cells. Despite the diverse morphogenetic and possibly genetic basis leading to the formation of a functional organ, there are certain principles that are common among the different ways of forming a neuromast. During embryonic development, aLL and pLL neuromasts originate from placodes that are specified at the anterior part of the neural plate (Schlosser, 2002a). Via sensory ridges and migrating primordia, lateral line tissues spread out from their region of origin and populate the fish body with neuromasts. During post-embryonic organogenesis in the ANC and CNC, organ-founder stem cells are induced, migrate out of the founder organ and generate a new neuromast at a new location. Common principles of neuromast formation are therefore induction of organ-forming tissues, displacement to other locations and formation of morphologically identical neuromasts at new positions. There is evidence that interactions between lateral line and surrounding tissues (biochemical and mechanical) are crucial for the processes of induction, displacement and organ formation. In this thesis I have shown that neuromast formation during embryonic development in the aLL and post-embryonic development in the CNC in medaka depends on interaction with the surrounding tissue.

3.1 Interaction between aLL tissues and surrounding environment

For embryonic pLL development, lateral line tissue/environment interactions have been suggested to be involved in primordium migration and neuromast positioning (Nogare et al., 2019; Seleit et al., 2021; Seleit et al., 2017a; Valentin et al., 2007). Regarding the aLL, most studies addressing interaction with surrounding tissues focus on placode specification and not later stages of aLL development (Baker and Bronner-Fraser, 2001; Schlosser, 2002a). Elegant transplantation experiments showed that ventral belly ectoderm can be induced to form lateral line placodes when put in the head region of neurula stage axolotls (Liedke, 1955). In line with this it has been reported that mesoderm and neural plate might be involved in the induction of lateral line placodes in amphibia and zebrafish (Harrison, 1945; Mangold, 1929; Nikaido et al., 2017).

At later stages of aLL development, interactions of placodes, sensory ridges and neuromasts with surrounding tissues have not been extensively studied so far (Iwasaki et al., 2020; Stone, 1928). Transplantation of post-otic posterior lateral line placodes on the head in salamanders resulted in the formation of sensory ridges instead of migratory primordia, suggesting that the posterior lateral line placode might be competent to respond to signals emanating from head structures, driving the formation of sensory ridges instead of migrating primordia (Stone, 1928). Alternatively, formation of sensory ridges might represent the default state of a lateral line placode, and only upon exposure to inductive signals is a migrating primordium formed. Transplantation of the pre-otic supraorbital placode (generating neuromasts above the eye) on the trunk resulted in the formation of neuromasts along the tail as well (Stone, 1928). While the placode followed the normal path, it did not form a migrating primordium, but rather a sensory ridge that elongated along the tail, suggesting that the supraorbital placode is able to follow directionality cues, but not able to process signals driving the formation of a migrating primordium. Interestingly, the sensory ridge did not reach the end of the tail, suggesting that neuromast number is fixed as an inherent characteristic of the supraorbital placode (Stone, 1928). Using the Tg(*rx2*:*caigf1r*) I addressed the question of fixed neuromast number in the aLL of medaka. Intuitively, increase in eye size might lead to an increased number of aLL neuromasts surrounding the eye. Yet, this is not observed in fish with enlarged eyes. Instead, neuromast numbers in lines surrounding the eye (vol and DG) are decreased. In line with results previously reported in salamanders (Stone, 1928), maximum neuromast number might be an intrinsic property of the placode in medaka and changes in sensory ridge/environment interaction can only lead to a decrease of organ number.

In zebrafish, mutants for the Wnt activator R-spondin2 lack specific neuromasts in the aLL, termed HM1 and HM2 (Iwasaki et al., 2020), which likely correspond to PVG neuromasts in medaka. Analysis of *R-spondin* mutants revealed that while the 'primordium' generating the HM1 and HM2 neuromasts was specified normally, proliferation and differentiation at later stages were abolished, resulting in the absence of HM1 and HM2. As a possible source for R-spondin and therefore regulation of proliferation and differentiation, the underlying hyoid mesenchyme was identified (Iwasaki et al., 2020). In line with this study that provides first mechanistic insights into how aLL sensory ridges/primordia interact with surrounding tissues during embryonic development in zebrafish, the results acquired in this thesis suggest, that aLL sub-lines in medaka depend on interactions with the surrounding tissue as well. Results on the *eyeless* mutant and Tg(*rx2*:*caigf1r*) suggest that regardless of a reduction or increase of eye size, neuromast numbers are reduced, especially in sub-lines directly adjacent to the eye, suggesting proliferation defects in sensory ridges generating these sub-lines. Possibly, sensory ridge proliferation is controlled by signals emanating from the eye itself, or from tissues surrounding the eye that are disturbed in the *eyeless* mutant and Tg(*rx2*:*caigf1r*) background. Moreover, using *cxcr4b*^{D625} mutants, I was able to show that the rc sub-line depends on the expression of *Cxcl12a* in the underlying tissue for the rc-primordium to migrate and subsequently generate the rc neuromast. Most likely, there are different signals/mechanisms guiding the specification and growth of the various placodes, sensory ridges and primordia. This is also supported by the differential reaction of the aLL and pLL to a loss of K15. Placodes and sensory ridges seem to be competent to process signals emanating from the surrounding tissues, suggesting that positional effects might at least in part dictate placode/sensory ridge output, as also indicated by the transplantation experiments described above as well (Stone, 1928).

3.2 Developmental robustness vs variability in aLL sub-lines

In undisturbed conditions, some aLL sub-lines are characterized by fixed organ numbers, resulting in perfect symmetry, while others display minute to substantial variability, leading to asymmetry. Whether this is due to genetic determinants, mechanical constraints or both is not known at the present. It has been suggested that symmetry is tightly associated with organ function (Moubayidin and Ostergaard, 2015). It would be interesting to see, if the differential degree of symmetry among lateral lines does in fact impact on the function of the organ system. Disturbance of aLL development in Tg(*rx2*:*caigf1r*) and especially *eyeless* mutant revealed that some aLL sub-lines are more robust than others in the context of increased or decreased eye size (PG, hl, lol). Interestingly, these sub-lines are characterized by low organ numbers and

moreover, positioning posterior to the eye, in the region of placode/sensory ridge specification. I hypothesize therefore, that developmental robustness correlates with both low organ numbers and organ position near the place of placode induction. It is conceivable that increased distance of primordium migration or sensory ridge elongation leads to the accumulation of variation within organ-forming tissues or in the interaction with the surrounding tissues, eventually leading to variability in organ number.

Upon exposure to higher temperatures, PVG sub-line symmetry decreases significantly. This is due to an increase in neuromast number, which is not coordinated among the left and the right side of the fish. Interestingly, asymmetry in what I believe is at least in part the PVG sub-line, correlates with asymmetry in the underlying bone in different cave fish species. Whether this difference is due to embryonic development or exclusively post-embryonic development is not clear however, since aLL neuromast number and position were quantified in adult fish (Gross et al., 2016). It has been shown that embryonic PVG sub-line development in zebrafish depends on the underlying hyoid mesenchyme (Iwasaki et al., 2020), which generates the opercular bones. Furthermore, there is evidence that increased temperatures accelerate bone and cartilage growth in mice (Al-Hilli and Wright, 1983; Serrat, 2014). Therefore, it is possible that growing fish at increased temperatures leads to altered development of the hyoid mesenchyme and other bone or cartilage structures and thereby affect neuromast number specifically in the PVG sub-line. Due to slight developmental variation, alterations might differ between the left and right side of the fish.

Sub-line variability under normal conditions might be an indicator for dependence on stimuli from surrounding tissues during embryonic development. Slight variations in the surrounding tissue lead to variable organ number, again reinforcing the notion that different sub-line sensory ridges or primordia respond to different stimuli and follow different developmental mechanisms. The phenomenon of translating tissue variations into variable organ numbers might be intensified in sub-lines with high neuromast numbers. As opposed to that, sub-lines that are characterized by robust symmetry might not rely on interactions with the surrounding tissue to the same extend, but rather follow intrinsically controlled mechanisms, like intrinsically fixed organ numbers in the supraorbital placode of salamanders (Stone, 1928).

The establishment of symmetry and breaking of symmetry have long interested researchers, (Grimes, 2019; Hollo, 2017; Hudson, 2000; Morgan, 1923; Thompson), however, the underlying mechanisms have not been fully understood yet. In this thesis I have shown that the anterior lateral line hast both symmetric and asymmetric modules. This places the lateral line among other model systems to elucidate the formation of symmetric and asymmetric patterns among the left and right side.

3.3 Relation between infraorbital aLL sub-lines and pLL

Cranial placodes (among others the lateral line placodes) are generated from a pan-placodal area adjacent to the anterior part of the neural plate (Schlosser, 2002a, 2007, 2010). It has been hypothesized that there is a multi-step induction model regulating the specification of different cranial placodes from the pan-placodal area (Schlosser, 2002a, b). The mechanisms regulating this process are not fully understood yet. It has been proposed that the otic and lateral line placodes are derived from the same pan-placodal area and are separated only at later stages (Schlosser, 2002a). It is therefore conceivable that induction of different lateral line placodes occurs successively in a multi-step model as well. The modular character of anterior lateral line placodes is supported by results on evolutionary modifications of the anterior lateral line pattern in amphibians, where different lateral line sub-lines have been lost or modified in different species (Schlosser, 2002b).

Assuming a model of successive specification of lateral line placodes, the question arises of whether some placodes are exposed to similar signals, thereby acquiring similar behavior and are possibly closer related to one another than to others. The results I obtained in this thesis indicate that the infraorbital aLL sub-line vol and its possible derivative, the rc sub-line share common characteristics with the pLL. Variability of neuromast organ number is comparable in the vol sub-line and pLL. Both vol and pLL generate secondary neuromasts seemingly in a Cxcr4b-dependent manner. Furthermore, I speculate that the most anterior part of the sensory ridge generating the vol and AG sub-lines is able to respond to Cxcl12a ligand expressed in the very anterior parts of the fish head, resulting in the formation of a primordium that migrates dorsally and generates the rc sub-line. Like in the pLL, primordium migration depends on chemokine signaling via Cxcr4b. Transplantation of the supraorbital pre-otic placode on the trunk of amphibians resulted in the formation of a sensory ridge instead of a migrating primordium (Stone, 1928). This indicates that the supraorbital placode is not able to respond to primordium-inducing signals emanating from the tail and instead generates a sensory ridge, seemingly the default state of lateral line placodes. Since the infraorbital placode might be competent to respond to Cxcl12a, it would be interesting to see if transplantation of the infraorbital placode to the tail generates a migrating primordium or a sensory ridge. However, transplantation of placodes is experimentally challenging in fish.

I hypothesize that the placode generating the infraorbital aLL sub-lines and the placode generating the pLL might be exposed to similar signals and thereby inherit similar characteristics. Possibly, they might even share a common origin, while other aLL placodes are already set aside. However, similar characteristics do not necessarily indicate a common lineage.

Additional experiments addressing the relation between aLL and pLL sub-lines need to be performed. By transplanting cells of a labelled donor into a host, the co-labelling frequency between aLL and pLL sub-lines could be quantified. Frequent co-labelling of infraorbital and pLL neuromasts would suggest common placodal origin. Alternatively, to uncover the multi-step induction of lateral line placodes, laser ablation at different areas and timepoints of placode specification could be performed. Lateral line pattern could be assessed after embryonic development and based on the presence or absence of different sub-lines, a map describing the relationship among different lateral line placodes could be drawn.

3.4 Tissue interactions induce heterogeneity among neuromast stem cells in post-embryonic organogenesis

During embryonic development, interactions with surrounding tissues seem to be instructive at different stages of lateral line development (Iwasaki et al., 2020; Nogare et al., 2019; Seleit et al., 2021; Seleit et al., 2017a; Valentin et al., 2007). Therefore, it seems conceivable that tissue interactions are an integral part of post-embryonic development as well. The results acquired in this thesis indicate that this process is at least in part driven by extrinsic cues, rather than exclusively neuromast intrinsic cues. It has been reported for numerous model systems, that cell behavior (e.g. proliferation, differentiation, quiescence, migration) is influenced by the surrounding microenvironment (both mechanical and biochemical signals) (Choi et al., 2018; de Lucas et al., 2018; Fiore et al., 2018). Only slight changes in the microenvironment can have drastic consequences for cell behavior.

The medaka CNC P0-neuromast displays radial symmetry before post-embryonic organogenesis. Onset of post-embryonic organogenesis is marked by breaking the radial symmetry due to cell proliferation, cellular rearrangement, formation of highly polarized cellular protrusions and eventually cell migration of neuromast stem cells exclusively at the anterior side. By ectopically expressing *snail1b* in all *K15*$^{+}$ neuromast stem cells, I was aiming at equalizing asymmetry within the P0-neuromast. However, position of cell migration and PE1-neuromast formation was unchanged, indicating that the local microenvironment restricts migratory behavior of neuromast stem cells - only the anterior side is permissive to organ-founder stem cell migration. I hypothesize that interaction between anterior neuromast stem cells and the local microenvironment is a crucial factor for post-embryonic organogenesis in the CNC of medaka. This is supported by the fact that ablation of prospective organ-founder stem cells is followed by cell rearrangements, which is sufficient to induce organ-founder stem cell fate in neuromast stem cells that are now positioned anteriorly. This indicates that organ-

founder stem cells are not pre-specified, as is the case for certain neural crest cells for example (Harris and Erickson, 2007; Reedy et al., 1998; Wilson et al., 2004), but that on the contrary, neuromast stem cells are equal and only upon exposure to inductive cues are they able to acquire organ-founder stem cell fate. Cell fate changes upon changes in tissue interactions have been studied in the development of ectodermal tissues. Lateral line placode fate can be induced in belly ectoderm upon transplantation onto head regions in axolotls (Liedke, 1955). The mammary mesenchyme can induce ectopic mammary buds in mid-ventral and dorsal epidermis regions (Cunha et al., 1995). Bird oral epithelium is able to generate tooth-like structures when mixed with mouse neural crest-derived mesenchyme (Mitsiadis et al., 2006; Mitsiadis et al., 2003). Even at post-embryonic stages cell fate changes have been observed after tissue recombination experiments in the mammary tissue: Mouse mammary epithelial cells were mixed with neural stem cells and transplanted into host mice. Neural stem cells contributed to mammary epithelial growth and were even observed to adopt mammary-specific functions such as milk protein synthesis (Booth et al., 2008). A system with inducible organ-founder stem cells in contrast to a pre-specified number of organ-founder stem cells allows for more dynamic reaction to the needs of the fish. As soon as microenvironmental conditions are right (migration-inducing signals, permissive environment), a new neuromast is formed and integrated into the pre-existing organ system.

Although it remains to be formally proven, anterior neuromast stem cells in the P0-neuromast seem to undergo polarity changes from a rather apico-basal to front-rear polarity. A major signaling pathway governing these changes is the PCP (planar cell polarity) pathway (Campanale et al., 2017; Davey and Moens, 2017). The PCP pathway can be induced by non-canonical Wnt signaling (Seifert and Mlodzik, 2007). Interestingly, post-embryonic organogenesis in the zebrafish caudal fin requires induction of Wnt signaling via R-spondin presented by the pLL nerve (Wada et al., 2013). It has been shown that R-spondin family members are able to induce PCP signaling (Ohkawara et al., 2011). Although post-embryonic organogenesis in the CNC of medaka is independent from a functional nerve connection, it is possible that similar to zebrafish, the process depends on the activation of non-canonical Wnt and PCP signaling. Possibly, activators of non-canonical Wnt and PCP signaling are presented to the P0-neuromast not via the pLL nerve, but other tissues at the anterior side of the founder organ.

3.5 Is cellular memory guiding organ-founder stem cell migration in CNC and ANC?

Induction of cell protrusions necessary for cell migration and cell migration itself are often regulated by distinct signals (Aman and Piotrowski, 2010; Blaser et al., 2005; Blaser et al., 2006). In the CNC there is a possibility that chemokine signaling via Cxcr4b plays a role in post-embryonic organogenesis, since I observed a slight developmental delay of PE1-neuromast formation and reduction of CNC organ number in adult fish of Tg(*K15*:*Cxcr7*/*K15*:H2B-GFP). The relative robustness of PE1-neuromast formation in the presence of Cxcr7 might be explained by the stochasticity in competition for the ligand Cxcl12a between Cxcr4b and Cxcr7. Possibly, organ-founder stem cells are continuously initiating cell migration. In the absence of Cxcr4b-mediated signaling due to the presence of Cxcr7, migration cannot be executed. However, as soon as Cxcr4b signaling can be initiated, due to stochastic differences in the ratio of Cxcr4b and Cxcr7, cell migration occurs. Alternatively, directional migration and not induction of migratory behavior itself might be affected by the presence of Cxcr7. Detailed analysis of *cxcr4b* mutant cell behavior in the pLL primordium of zebrafish revealed that migratory behavior was displayed by primordium cells, however, directional movement was abolished, leading to a lower net movement of the primordium as a whole (Haas and Gilmour, 2006). To unambiguously determine the influence of chemokine signaling via Cxcr4b in post-embryonic organogenesis in the CNC mosaic experiments using *cxcr4b*^{D625} mutants need to be performed.

In the ANC, organ-founder stem cell migration seems independent of chemokine signaling via Cxcr4b, since *cxcr4b*^{D625} mutants develop normally. Interestingly, embryonic pLL development relies on the Cxcl12a/Cxcr4b signaling axis (Haas and Gilmour, 2006; Seleit et al., 2017a; Valentin et al., 2007), while it is dispensable for the majority of embryonic aLL development, including the ANC P0-neuromast (Ghysen and Dambly-Chaudiere, 2007; Piotrowski and Baker, 2014; this thesis). During embryonic pLL development, the primordium expresses both Cxcr4b and Cxcr7 to generate a gradient of Cxcl12a ligand that is expressed at the horizontal myoseptum. Once the primordium reaches the caudal fin, migration comes to an end and the primordium transforms into the CNC P0-neuromast. It is possible, that the P0-neuromast retains the expression of Cxcr4b from the primordium, which is reused for later organ-founder stem cell migration. Cxcl12a might then also be able to induce an EMT, similar to the embryonic mechanism driving primodium migration (Neelathi et al., 2018). In the case of the ANC, directionality cues for sensory ridge elongation are unknown at the present. Interestingly, in both CNC and ANC post-embryonic organogenesis, the PE1-neuromast is formed along the

innervating nerve, indicating that post-embryonic neuromast formation occurs towards the position of origin of the primordium/sensory ridge, meaning positional cues that were used by the primordium or sensory ridge might very well be reutilized for organ-founder stem cell migration.

Despite the presumed differences in regulation of organ-founder stem cell migration, post-embryonic organogenesis in ANC and CNC seems to follow comparable rationales: In both cases are post-embryonic neuromasts formed by migrating neuromast stem cells. Furthermore, there seems to be a correlation of the position of blood vessels and organ-founder stem cell migration. Lastly, there is indication that the architecture of the surrounding tissue affects the position of the PE1-neuromast. This is in line with results on post-embryonic organogenesis in the aLL of zebrafish and cave fish. It has been reported that formation of a specific group of neuromast organs on the opercle in zebrafish (possibly corresponds to the lol sub-line) relies on the presence of opercle structures. In the absence of opercle structures, post-embryonic organogenesis does not happen (Wada et al., 2010). Adult cave fish display asymmetric facial bone fragmentations underlying aLL neuromasts. This correlates with asymmetry in neuromast numbers and position, which seems to be in part also caused during post-embryonic development (Gross et al., 2016).

3.6 Patterning of an exit point for organ-founder stem cells by the vasculature

Apart from supplying oxygen and metabolites, the vasculature has been recognized to play a crucial role in organogenesis, homeostasis and regeneration in a variety of tissues and model organisms (Karakatsani et al., 2019; Ramasamy et al., 2015; Tirziu and Simons, 2009). Signals emanating from the vasculature can be of both biochemical and mechanical nature.

During kidney development in zebrafish, bilateral pronephric primordia fuse and generate a glomerulus. This occurs via medial cell migration of pronephric primordium cells (Serluca and Fishman, 2001). Cell migration and glomerulus assembly has been shown to be regulated by blood flow. In the absence of blood flow, pronephric primordium cell migration is abolished and glomerulus assembly is disturbed, while podocyte differentiation and appearance occur normally. Initiation of blood flow seems to result in the stretch-sensitive expression of *matrix metalloproteinase-2*, which in turn might lead to remodeling of the extra cellular matrix, facilitating medial migration of pronephric primordium cells (Serluca et al., 2002).

Mouse liver development begins with the specification of hepatic cells within the endodermal epithelium. After proliferation, these newly specified hepatic cells migrate into the adjacent

septum transversum mesenchyme. While specification of hepatic cells occurs normally in the absence of endothelial cells, hepatic cell migration is eliminated, indicating a role of endothelial cell signaling in liver bud morphogenesis (Matsumoto et al., 2001).

The results presented in this thesis suggest that the vasculature provides instructive signals for organ-founder stem cell migration in the CNC as well, since ectopic blood vessels were sufficient to drive ectopic stem cell migration in rare cases. The nature of these vascular signals inducing cell migration is presently unknown. The low n number possibly speaks to the complexity of post-embryonic organogenesis, with several instructive cues emanating from different sources. Tampering with one signal might not necessarily result in a major change of tissue morphogenesis.

Since organ-founder stem cells migrate towards the blood vessels, it might also be conceivable that the vasculature provides cues stopping cell migration at a certain point. Migrating organ-founder stem cells upregulate *Egln3*:EGFP, indicating hypoxic conditions. Hypoxia might be used as a switch for initiating cell migration, similar to ovarian border cell migration in Drosophila (Djagaeva and Doronkin, 2010). As a response to hypoxia, vascular endothelial growth factor (vegf) is induced, promoting the growth of new vessels and thereby relief of hypoxia (Shweiki et al., 1992). Possibly, a similar mechanism acts in PE1-neuromast formation in the CNC: Increased distance to the blood vessels induces hypoxia, which in turn might induce cell migration. As the cells migrate towards the blood vessels, they upregulate vegf, which in turn promotes vascular remodeling to create a niche environment for the PE1-neuromast.

An alternative mechanism to stop cell migration might be provided by the chemokine ligand Cxcl12a. Primordial germ cell (PGC) migration depends on the Cxcl12a/Cxcr4b signaling axis (Doitsidou et al., 2002; Knaut et al., 2003). PGC migration is stopped at the prospective gonad by uniform *Cxcl12a* expression (Doitsidou et al., 2002). There is indication that organ-founder stem cell migration depends at least in part on chemokine signaling via Cxcl12a and Cxcr4b. Perhaps organ-founder stem cell migration is stopped in a similar way as PGC migration, by encountering an area with uniform *Cxcl12a* expression. Interestingly, it has been reported that neural progenitor cells in the adult subventricular zone home towards endothelial cells via a Cxcl12a/Cxcr4b dependent process. In that case Cxcl12a is expressed by the vascular plexus (Kokovay et al., 2010). This makes the vasculature an outstanding candidate for regulating Cxcl12a mediated organ-founder stem cell migration in the CNC of medaka.

3.7 Your inner fish is (hopefully) sleeping

Correct regulation of stem cell behavior is crucial for tissue integrity and deregulation can result in disease, such as cancer. One of the landmarks of cancer is uncontrolled proliferation of stem cells leading to the growth of tumors. In the course of disease progression, cancer stem cells can delaminate from a primary tumor and spread throughout the body to form metastases. The formation of metastases considerably worsens the prognosis. It is therefore imperative for both patient treatment and disease prevention to understand the regulation of cancer stem cell behavior, such as cancer stem cell proliferation and migration. However, the difficulty lies in finding a suitable model system to study these processes. Especially the problem of metastasis formation is difficult to address due to the unpredictability of when and where metastases will occur. It has been proposed that cancer stem cell programs recapitulate, at least in part, developmental programs (Kho et al., 2004). Understanding the regulation of stem cell behavior in physiological conditions might therefore aid in understanding the regulation of stem cell behavior in pathological conditions.

The process of post-embryonic organogenesis in the CNC of medaka shares similarities with the formation of metastases in cancer. Stem cells undergo an EMT, migrate away from an initial source, colonize a new position and proliferate to generate a new organ. Furthermore, there seems to be interaction with the vasculature, as described for many cancer types (Montana and Sontheimer, 2011; Ribatti et al., 1999; Singhal et al., 2021; Talmadge and Fidler, 2010). Yet, the nature of this interaction is so far only poorly understood. Although *in vitro* studies become more elaborate, the gold standard for understanding cell behavior is the *in vivo* situation. The CNC of the medaka lateral line might therefore present an ideal *in vivo* model system to study metastatic organogenesis under physiological conditions and thereby gain insights into the regulation of cancer metastasis.

In his book 'Your Inner Fish: A Journey into the 3.5-Billion-Year History of the Human Body' (Shubin, 2008), Neil Shubin describes the evolution of various anatomical structures and the many similarities they share between distant relatives like humans and fish. Similar to the notion that physiological and pathological processes share similar traits (Kho et al., 2004), I hypothesize that ancient physiological processes that are no longer required in animals with fixed body sizes, like adult humans, are still present, albeit suppressed, and can be hijacked during pathological conditions.

4 Conclusion

The results obtained in this thesis suggest that formation of the anterior lateral line is different from the posterior lateral line. While the posterior lateral line exclusively originates from a migrating primordium, the majority of anterior lateral line neuromasts are formed by sensory ridges. Only a subset of neuromasts (rc sub-line) is formed by a Cxcr4b-dependent primordium. Although the mode of development is different, common principles can be found in embryonic aLL and pLL development: Similar to pLL development, secondary neuromasts are formed in the vol sub-line in a similar fashion, there are chemokine responsive cells that generate a migrating primordium, giving rise to the rc sub-line and both aLL and pLL development relies on intact interactions with the surrounding tissues. However, the nature of these interactions seems different for aLL and pLL.

Furthermore, this work describes the process of post-embryonic neuromast formation in the CNC of medaka in detail and starts to elucidate the mechanistic basis. Post-embryonic organogenesis in the CNC occurs in a highly stereotypic manner via so-called organ-founder stem cells that migrate out of a founder organ and generate a new neuromast. The results acquired in this thesis indicate that stem cell behavior (acquisition of organ-founder stem cell fate and stem cell migration) is largely controlled by interaction with the surrounding microenvironment. Possibly, post-embryonic organogenesis in the CNC is a multifactor process that relies on various cues, resulting in the highly stereotypic character of this process.

Taken together, this thesis contributes to the expansion of knowledge on the embryonic development of the aLL and post-embryonic neuromast formation in the CNC. Furthermore, the results highlight the importance of tissue interactions in lateral line development.

5 Materials & Methods

5.1 Materials

5.1.1 Medaka fish lines

The medaka lines used and generated in this thesis are listed in the table below.

Table 1: Fish stocks used and generated in this thesis

Name	Stock number	Source
CR(Cxcr4b_2gRNAs)	8412, 8625, 8962, 9276	This thesis
CR(snail1a5'-EGFP-snail1a3')	8807, 9052, 9263,	This thesis
CR(snail2-5'-EGFP-snail2-3')	8841, 9038, 9240, 9703	This thesis
CR(Vegfr1_gRNA1and2)	9704, 9894	This thesis
CR(Vegfr1_gRNA3and4)	9705, 9706, 9895	This thesis
elB (eyeless mutants)	7882, 8805, 9451	(Winkler et al., 2000)
Sc(Eya1:EGFP)	7624, 7757, 8481, 9822	(Seleit et al., 2017a)
Sc(Eya1:mCFP)	7881, 8336, 8663, 9497,	(Seleit et al., 2021)
Sc(K15:Cxcr7_K15:H2B-GFP)	9514, 9702, 9835	This thesis
Sc(K15:lifeAct-tRFP)	7923, 7939, 9434,	(Seleit, Krämer et al., 2017b)
Sc(K15:mCFP)	8086, 8608,	This thesis
Sc(K15:mYFP)	7805, 8795, 9905	(Seleit et al., 2021)
Sc(Kremen1:mYFP)	7865, 8681, 9187	Katharina Lust
Sc(K15:snail1a-T2A-H2Acherry_K15:H2B-GFP)	9522, 10006	This thesis
Sc(K15:snail1b-T2A-H2Acherry_K15:H2B-GFP)	9523, 9687,9976	This thesis
Sc(K15:snail2-T2A-H2Acherry_K15:H2B-GFP)	9524, 9977	This thesis
Snail1a-Venus-3-6	9420, 9452	Alexander Aulehla
Wildtype Cab	7524, 7796, 8072, 8368, 8617, 8813, 9170, 9406, 9698	(Wittbrodt et al., 2002)
zFli-1:EGFP	8411,8680, 9313, 9721	Lázaro Centanin

5.1.2 Plasmids

The plasmids used and generated in this thesis are listed in the table below.

Table 2: Plasmids used and generated in this thesis

Name	Stock number	Source
I-SceI\keratin15::mYFP	4450	Lab stock/Lázaro Centanin
K15:H2B-GFP	4694	Lab stock/Ali Seleit
pBS\I-SceI\K15::BBW2.1 inv	5329	Lab stock/Lázaro Centanin
pBS\I-SceI\K15::Cxcr7	5830	This thesis
pBS\I-SceI\K15::snail1a-T2A-H2Acherry	5835	This thesis
pBS\I-SceI\K15::snail1b-T2A-H2Acherry	5836	This thesis
pBS\I-SceI\K15::snail2-T2A-H2Acherry	5837	This thesis
pCS2+ Inv X_Cas9	5197	Lab stock/Arturo Gutierrez
pGEMT easy\K15	5326	This thesis
pGEMTeasy\snail1a	5847	This thesis
pGEMTeasy\snail1b	5848	This thesis
pGEMTeasy\snail2	5849	This thesis
pGGDest(Snail1a5'HF-kozEGFPwCR13_polyA-Snail1a3'HF)	5632	This thesis
pGGDest(Snail25'HF-kozEGFPwCR13_polyA-Snail23'HF)	5633	This thesis
Pmtb-t7-alpha-bungarotoxin	5173	(Swinburne et al., 2015)
sgRNA backbone (T7)- DR274	3632	Lab stock/Manuel Stemmer

5.1.3 Primers

Table 3: Primers used in this thesis

Name	Purpose	Sequence
Cxcr7 CDS fwd	cloning	CTCCCCTTTCCGGTCATTGC

Cxcr7 CDS rv	cloning	ACCAGAGTCAAACTAAATCACTTT TGA
GFP rv	genotyping	TCGATGTTGTGGCGGATCTTGAA G
H2A-cherry rv (NotI overhang)	cloning	(GCGGCCGC)TGCATTCTAGTTGTG GTTTGTCCA
K15 CDS fwd	probe generation	GGAGGTGGTCTTGGTTCTGG
K15 CDS rv	probe generation	CCTCGTACTGCTCACGGATC
K15:Cxcr7 fwd	sequencing	AGAGTGACGCTTCAGCCTTT
K15:Cxcr7 rv	sequencing	TGAGTTTGCACGCAACTTCC
M13 fwd	sequencing	TGTAAAACGACGGCCAGT
M13 rv	sequencing	CAGGAAACAGCTATGACC
PCR donor generation fwd (biotinylated)	generation of PCR donor	CGAGCGCAGCGAGTCAGTGAG
PRC donor generation rv (biotinylated)	generation of PCR donor	CATGTAATACGACTCACTATAG
Snail1a 5'HF fwd	cloning	GCCGGTCTCAGTATCAAACTCCCC AATTGCGCAC
Snail1a 5'HF rv	cloning	GCCGGTCTCAAGGTCGTGCGTAAA AACAACCCGT
Snail1a 3'HF fwd	cloning	GCCGGTCTCAACTACCTGCCCACC TCTGAATCAG
Snail1a 3'HF rv	cloning	GCCGGTCTCACTTAGCAGTCATTG TTGCTGGGAC
Snail2 5'HF fwd	cloning	GCCGGTCTCAGTATCGCCCAACCA TGATTGCATT
Snail2 5'HF rv	cloning	GCCGGTCTCAAGGTCTGCGCTCT TGGAAACAGTG
Snail2 3'HF fwd	cloning	GCCGGTCTCAACTACGACACCTCC TCCAAAGACC
Snail2 3'HF rv	cloning	GCCGGTCTCACTTACACGGTCTGG AGAAAGCCTT
Snail2-GFP fwd	genotyping	AGGGAACGTGAGGCTTTCTG

Snail1a fwd (with SalI overhang)	cloning	(GTCGAC)TTCTGGGATTCTCCAGGACGC
Snail1a rv (partial T2A overhang)	cloning	(CCTCCACGTCACCGCATGTTAGAAGACTTCCTCTGCCCTC)TCCCACTGAGGTGGAGCAG
Snail1b fwd (with SalI overhang)	cloning	(GTCGAC)GTCTTCCAACATTTACGCACG
Snail1b rv (partial T2A overhang)	cloning	(CCTCCACGTCACCGCATGTTAGAAGACTTCCTCTGCCCTC)CGCTGAGGCACAGCAGGA
Snail2 fwd (with SalI overhang)	cloning	(GTCGAC)GTTTGTTCTTTACGCAGCGAA
Snail2 rv (partial T2A overhang)	cloning	(CCTCCACGTCACCGCATGTTAGAAGACTTCCTCTGCCCTC)TCCGTGTGCTACACAACAACC
Vegfr1 gRNA1 fwd	genotyping	AAGCCCTCTTATCTAAAGCG
Vegfr1 gRNA1 rv	genotyping	GATAAACAAAAGCGTGGAGG
Vegfr1 gRNA2 and3 fwd	genotyping	ATCAGCATGTGATTCTCTCC
Vegfr1 gRNA2and3 rv	genotyping	GAAGTGTGGAGAAGGAACTC
Vegfr1 gRNA4 fwd	genotyping	TAATGTCTGGAATGGACGTG
Vegfr1 gRNA4 rv	genotyping	CCCGTTGTTGTGAATTTACC

5.1.4 sgRNAs

Table 4: sgRNAs used in this thesis

gRNA	Sequence
Cxcr4b gRNA1 (cloned by Ali Seleit)	GTGAAAACCTGGTACTTCGGAGG
Cxcr4b gRNA2 (cloned by Ali Seleit)	CAAGTGGATTTCTATCACCGAGG
Snail1a gRNA1	CCGTGCGTAAAAACAACCCG
Snail1a gRNA2	CTCGGCAACAGGATACCTCT
Snail1b gRNA1	AATGTTGGAAGACGCGCCGA
Snail1b gRNA2	ACCACCCTCTTCTATGCCAC
Snail2 gRNA1	CGGGACTTTTGATTACGGAA
Snail2 gRNA2	GGAGAAGTCACTGGGGAC

Vegfr1 gRNA1	ACGTGGCTGAATCCCGTTGT
Vegfr1 gRNA2	AGGCCGACGTCGTAGTAAGT
Vegfr1 gRNA3	GCGGCACAGAGCCCGGATCT
Vegfr1 gRNA4	TGATGCAGGCATCCGCTTT

5.1.5 Chemicals and reagents

Table 5: Chemicals and reagents used in this thesis

Description	Source of Supply
2- propanol	Sigma-Aldrich
4-Di-2-ASP	Sigma-Aldrich
Acetone	Sigma-Aldrich
Adenosine triphosphate (ATP)	Thermo Fisher Scientific
Agar	Gibco
Agarose	Fisher BioReagents
Ampicillin (50 µg/ml working conc.)	Roth
Bacto-Trypton	Gibco
BCIP (5-bromo-4-chloro-3-indolyl phosphate)	Roche
Blocking reagent	Roche
Borax anhydrous	Fluka
Bovine Serum Albumin (BSA, 10 mg/ml)	NEB
BrdU (5-Bromo-2-deoxyuridine)	Sigma-Aldrich
Calcium chloride ($CaCl_2$)	AppliChem
Calcium chloride dihydrate ($CaCl_2$*$2H_2O$)	AppliChem
DAPI (4', 6-Diamidino-2-Phenyindole)	Roth
Deoxyadenosine triphosphate (dATP)	Thermo Fisher Scientific
Deoxynucleotide triphosphates (dNTPs)	Sigma-Aldrich
Dig-UTP	Roche
Disodium hydrogen phosphate dihydrate (Na_2HPO_4*$2H_2O$)	Sigma-Aldrich
Dimethyl sulfoxide (DMSO)	Roth
Dithiothreitol (DTT)	Thermo Fisher Scientific
GeneRuler DANN Ladder Mix	Thermo Fisher Scientific
DANN Purple loading dye	Thermo Fisher Scientific

Ethanol (EtOH)	Merck
Ethidium bromide (EtBr)	Sigma-Aldrich
Ethyl 3-aminobenzoate methane-sulfonate salt	Fluka
Ethylenediaminetetraacetic acid (EDTA)	Sigma-Aldrich
Formamide	Sigma-Aldrich
Glacial acetic acid	Merck
Glucose	Sigma-Aldrich
Glycerol	Sigma-Aldrich
Heparin	Gibco
Hydrogen chloride (HCl)	Merck
Hydrogen peroxide H_2O_2	Sigma-Aldrich
Kanamycin (100 μg/ml)	Roth
LB-Broth Lennox	Sigma-Aldrich
Low melt agarose	Roth
One Shot® Mach1™-T1R Chemically Competent *E. coli*	Thermo Fisher Scientific
Magnesium chloride ($MgCl_2$)	AppliChem
Magnesium sulfate heptahydrate	Merck
Methanol (MeOH)	Roth
Natural Goat Serum (NGS)	Sigma-Aldrich
NBT (4-nitro blue tetrazolium chloride)	Roche
Paraformaldehyde (PFA)	Roth
Polyethylene glycol – 4000 (PEG-4000)	Thermo Fisher Scientific
Potassium acetate (Kac)	AppliChem
Potassium chloride (KCl)	AppliChem
Potassium dihydrogen phosphate (KH_2PO_4)	Merck
Potassium hydroxide (KOH)	Merck
Red sea salt	Red Sea
RNase free water	Sigma-Aldrich
RNA Loading Dye 2x	Thermo Fisher Scientific
Sheep serum	Sigma-Aldrich
Sodium chloride (NaCl)	Sigma-Aldrich
Sodium citrate	Sigma-Aldrich
Sodium dodecyl sulphate sodium salt (SDS)	Serva
Sodium hydrogen carbonate ($NaHCO_3$)	Merck

Sodium hydroxide (NaOH)	Sigma-Aldrich
Tricaine (MS-222)	Sigma-Aldrich
Tris-hydrochloride (Tris-HCl)	Sigma-Aldrich
Tween20	Sigma-Aldrich
X-Gal	Thermo Fisher Scientific
Yeast extract	Roth

5.1.6 Media and solutions

Table 6: Media and solutions used in this thesis

Description	Ingredients	Composition
Blocking buffer (IHC)	1x PTW	10%
	BSA	1%
	DMSO	1%
	NGS	4%
Embryo rearing medium (ERM, 1x)	Sodium chloride	17 mM
	Potassium chloride	0.4 mM
	Calcium chloride dihydrate	0.27 mM
	Magnesium sulphate heptahydrate	0.66 mM
Hatch Medium Medaka (10x)	10x ERM	1l
	Methylene blue	1 ml
Hybridization Mix	Formamide	50%
	20x SSC	5x
	Heparin	50 µg/ml
	Torula-RNA	5 mg/ml
	Tween-20	0.1%
LB medium	Bacto-Tryptone	10 g/l
	Yeast extract	5 g/l
	Sodium chloride	5 g/l
LB plates	Bacto-Tryptone	10 b/l
	Yeast extract	5 g/l
	Sodium chloride	10 g/l
	Agar	15 g/l
Oligo annealing buffer	Tris-HCl, pH 7.5	10 mM

	NaCl	8.3 mM
P1	Glucose	50 mM
	Tris-HCl	50 mM
	EDTA	10 mM
	pH 8, stored at 4°C	
P2	Sodium hydroxide	0.2 N
	SDS	1%
P3	Potassium acetate	5 M
PTW	Sodium chloride	1.2 M
	Sodium hydrogen phosphate	0.35 M
	Potassium dihydrogen phosphate	25 mM
	Tween-20	0.1%
	pH 7.4	
SSC (20x)	Sodium chloride	3 M
	Sodium citrate	0.3 M
SSCT (4x)	SSC	4x
	Tween-20	0.1%
Staining buffer (in situ)	Tris-HCl (pH 9.5)	100 mM
	Sodium chloride	100 mM
	Magnesium chloride	50 mM
	Tween-20	0.1%
TAE (50x)	Tris base	242 g/l
	Glacial acetic acid	5.71%
	EDTA	50 mM
	pH 8.5	
TB (1x)	Bacto-Tryptone	12 g/l
	Yeast extract	24 g/l
	Glycerin	0.4%
	Potassium dihydrogen phosphate	2.13 g/l
	Potassium hydrogen phosphate	12.54 g/l
TE (1x)	Tris-HCl	10 mM
	EDTA	1 mM
	pH 8	
TNT (1x)	Tris-HCl pH 7.5	0.1 M

	NaCl	0.15 M
	Tween-20	0.1%
Tricaine (20x)	Ethyl 3-aminobenzoate methane-sulfonate salt	4 g/l
	Sodium hydrogen phosphate	10 g/l
	H_2O	up to 1 l
	pH 7-7.5	
Yamamoto (10x)	Sodium chloride	7.5 g/ml
	Potassium chloride	0.2 g/ml
	Calcium chloride dihydrate	0.2 g/ml
	Sodium hydrogen carbonate	0.02 g/ml
	pH 7.3	

5.1.7 Enzymes and buffers

Table 7: Enzymes and buffers used in this thesis

	Description	Source of Supply
Enzymes	DNaseI	Thermo Fisher Scientific
	Hatching enzyme	homemade
	I-SceI Meganuclease	NEB
	Proteinase K	Roche
	Q5 High-Fidelity DNA Polymerase	NEB
	Restriction enzymes	NEB/Thermo Fisher Scientific
	Sp6 Polymerase	Roche
	T7 Polymerase	Roche
	T4 DNA ligase	Thermo Fisher Scientific
	Taq DNA Polymerase	homemade/NEB
Buffers	10x I-SceI Buffer	NEB
	5x Q5 Reaction Buffer	NEB
	Restriction enzyme buffers	NEB/Thermo Fisher Scientific
	10x T4 DANN Ligase buffer	Thermo Fisher Scientific

5.1.8 Antibodies and conjugates

Table 8: Antibodies and conjugates used in this thesis

Antibody/conjugate	Host	Concentration	Source of Supply
α-BrdU	rat	1/200	Abcam, ab6326
α-GFP	rabbit	1/500	Invitrogen, A11122
	chicken	1/500	Life Technologies, A10262
α-E-Cadherin	mouse	1/500	BD Biosciences, 610181
α-N-Cadherin	rabbit	1/250	abcam, ab76011
α-mCherry	rabbit	1/500	abcam, ab167453
α-dsRed	mouse	1/500	BD Pharmingen, 51-8115GR
α-Dig-AP Fab fragments		1/2000	Roche, REF 11093274910
α-Dig-Fab POD		1/50	Roche, REF 11207733910
α-Fluo-Fab POD		1/50	Roche, REF 11426346910
α--rabbit-488	goat	1/500	Life Technologies, A-11034
α-mouse-546	goat	1/500	Life Technologies, A-11030
α-mouse-488	goat	1/500	Life Technologies, A-11029
α-rabbit-647	goat	1/500	Thermo LifeTech, A21245
α-mouse-647	donkey	1/500	Jackson/Dianova, 715-605-151
α-chicken-488	donkey	1/500	Jackson/Dianova, 703-545-155
α-rabbit-549	goat	1/500	Jackson, 112-505-144
α-rat-488	goat	1/750	Jackson, 112-485-143
α-rat-647	donkey	1/500	Jackson, 712-605-153

5.1.9 Kits

Table 9: Kits used in this thesis

Kit	Source of Supply
innuPREP Gel Extraction Kit	Analytic Jena
MEGAShortScript T7 Kit	Ambion

mMessage mMachine® Sp6 Trannscription	Thermo Fisher Scientific
mMessage mMachine ® T7 Transcription	Thermo Fisher Scientific
Monarch® DNA Gel Extraction Kit	NEB
Monarch® PCR & DNA Cleanup Kit	NEB
Plasmid Midi Kit	Qiagen
Rneasy Mini Kit	Qiagen
TSA™ Plus Cyanine 3 System	PerkinElmer
TSA™ Plus Cyanine 5 System	PerkinElmer
TSA™ Plus Fluorescein System	PerkinElmer

5.1.10 Consumables

Table 10: Consumables used in this thesis

Description	Source of Supply
Cell saver tips 200 µl	Roth
Cover slips	Roth
Dishes for microscopy	MatTek
Falcon tubes	Sarstedt
Filter paper	Whatman
Filter tips	Starlab
Folded filters	Roth
Glass beads	Roth
Injection molds	homemade
Injection needles GC100F-10	Harvard Apparatus
Latex gloves	Sempermed
Microloader tips	Eppendorf
Miniprep tubes	Sarstedt
Nitrile gloves	Starlab
Parafilm® M	Bemis
Pasteur pipettes	Sarstedt
PCR stripes	Sarstedt
PCR tubes	Kisker
Pestles	Eppendorf
Petri dishes	Greiner

Pipette tips	Kisker
Reaction tubes	Sarstedt
Sandpaper	Bauhaus
Scalpel blades	Roth
Transplantation molds	homemade
Well plates (6-well, 12-well)	Roth, Corning

5.1.11 Equipment

Table 11: Equipment used in this thesis

Description	Source of Supply
Bakterial Shaker INNOVA 44	New Brunswick
C1000 Touch™ Thermal Cycler	Bio-Rad
Centrifuge	Eppendorf
DeNovix DS-11 spectrophotometer	DeNovix
DM5000 B microscope	Leica
Electrophoresis chamber	PeqLab Biotechnologie GmbH
Forceps	Dumont
Freezer	Liebherr
Fridge	Liebherr
Fish incubators	Haraeus instruments and RuMed
Incubators (32°C, 37°C, 60°C)	Binder
InjectMan N12	Eppendorf
Leica TCS SP5	Leica
Leica TCS SPE	Leica
Microwave	Severin
Milli-Q water filtration station	Merck
Mini-centrifuge	neoLab
Mixing block	Bioer
Needle puller P30	Sutter Instrument Co USA
Nikon SMZ18 stereomicroscope	Nikon
Olympus SZX7	Olympus
pH-meter	Sartorius
PipetteBoy macro	Brand

Pipettes (2µl, 10 µl)	Eppendorf
Pipettes (20 µl, 100 µl, 1 ml)	Gilson
Power supply (gel electrophoresis)	Bio-Rad
Rotating arm	homemade
Scale	Sartorius
Stereomicroscope Zeiss Stemi 2000	Zeiss
UV-Gel Documentation System	Intas
UV table	Vilber Lourmat
Vortex	Scientific Industries, Inc.
Water bath	GFL
Zeiss Axio Imager M1	Zeiss

5.1.12 Applications/Software

Table 12: Software used in this thesis

Software	Source
Adobe Illustrator	Adobe
CCTop	(Stemmer et al., 2015)
Chimera	(Goddard et al., 2018)
Endnote	Clarivate Analytics
Fiji	(Schindelin et al., 2012)
FileMaker Pro	FileMaker, Inc.
Geneious	Biomatters Limited
Microsoft Office	Microsoft

5.2 Methods

5.2.1 Fish husbandry

In this thesis Medaka (*Oryzias latipes*) fish were used. The animals were kept according to Tierschutzgesetz 111, Abs. 1, Nr 1 (Haltungserlaubnis AZ35–9185.64 and AZ35–9185.64/BH KIT) and European Union animal welfare guidelines. The fish were maintained in closed recirculating systems at 28°C and 18°C, respectively on a 14 h light/10 h dark cycle.

5.2.2 Microinjection

Medaka embryos were collected at the one-cell stage and separated using forceps. The eggs were placed into injection molds that were prepared from 1.5% agarose in H_2O. Injection was performed with a glass needle at the one- or two-cell stage. According to the purpose of injection (transgenesis or mutagenesis) different injection mixes were prepared. Transgenesis was performed using the Meganuclease (I-SceI). For mutagenesis the CRISPR/Cas9 tool was used.

Table 13: Meganuclease and CRISPR/Cas9 injection mixes

Meganuclease injection mix	CRISPR/Cas9 injection mix
I-SceI (1 µl)	Cas9 mRNA (150 ng/µl)
I-SceI buffer (1.25 µl)	sgRNAs (15 ng/µl each)
DNA (10 ng/µl)	RNase free H_2O ad 10 µl
Yamamoto buffer (12.5 µl)	
H_2O ad 25 µl	

5.2.3 Hatching of fish

To hatch embryos, they were rolled on sandpaper and incubated in a drop of homemade hatching enzyme for 40 min at 28°C. Afterwards they were washed three times in 1x ERM.

5.2.4 4-Di-2-ASP staining

For staining of neuromast hair cells, fish were incubated in 1/1000 4-Di-2-ASP/1x ERM for 30 min – 2 h. Quantification of neuromast numbers was done using the GFP filter in a binocular.

5.2.5 Lateral line symmetry

Lateral line symmetry was quantified as a measure of organ number comparing the left and right side of aLL and pLL sub-lines. Sub-lines on the left and right side were compared and matching neuromast number was scored as a match. Unequal neuromast number was scored as a mismatch. A value of symmetry was calculated using following formula: 1/number of neuromast organs in a line * number of matching pairs.

5.2.6 Mounting

Living fish were tranquilized in Tricaine for 5-10 min and mounted in 0.6% low-melting agarose in matek dishes. After imaging, the fish recovered in 1x ERM.
Fixed fish were mounted in between cover slips and covered in glycerol.

5.2.7 Imaging

Imaging was performed using confocal laser-scanning microscopy at the Leica SP5 II and Leica TCS SPE. Time-lapse imaging was accomplished using a Microscope Slide Temperature Controller (Biotronix).

5.2.8 Multi-photon laser ablation

Embryos and fish were mounted as described above. Cell ablation was performed at the Leica SP5 using area or point ablation with the multi-photon laser at 40-65% power.

5.2.9 Fixation of fish

Fish were tranquilized for 15 min and fixed in 4%PFA/PTW overnight at 4°C. On the next day 4%PFA/PTW was replaced by 100% EtOH (for immunostaining) or 100% MeOH (for in situ) after washing with 1x PTW for storage at -20°C.

5.2.10 Whole-mount immunostaining

Embryos and fish were fixed as described above. For immunostaining, the samples were washed in 1x PTW, followed by water. To permeabilize the samples, they were treated with Acetone for 10-12 min at -20°C. Afterwards, the samples were blocked in blocking buffer (see media and solutions) for at least 2 h. Following the blocking step, the samples were incubated with primary

antibodies in blocking buffer overnight at 4°C. On the next day, the samples were washed six times in 1x PTW, before being incubated with secondary antibodies and DAPI for 2h in blocking buffer.

5.2.11 mRNA synthesis

mRNA for injection was prepared following the instructions provided by mMessage mMachine® Sp6 Transcription. The reaction was incubated overnight at 37°C. After DNaseI digestion, the mRNA was purified using the RNeasy Mini Kit. RNA quality was assessed using a DeNovix DS-11 spectrophotometer and performing agarose gel electrophoresis.

5.2.12 Probe synthesis for in situ hybridization

For in situ hybridization probes were synthesized from linearized plasmids using T7 and Sp6 promoters. After preparation of the mix (see below) the samples were incubated overnight at 37°C. After DNaseI digestion, the probes were purified using the RNeasy Mini Kit. Probe quality was secured using a DeNovix DS-11 spectrophotometer and performing agarose gel electrophoresis. 150 µl Hybridization Mix was added to the probes for storage at -20°C.

Table 14: *In vitro* transcription

Linearized template	1 µg
100 mM DTT	2 µl
NTP-Mix	1.3 µl
10 mM Dig-UTP/Fluorescein-UTP	0.7 µl
RiboLock	0.5 µl
10x Transcription buffer	2 µl
RNase free H2O	ad 18 µl
RNA-Polymerase (T7/Sp6)	2 µl

5.2.13 *In situ* hybridization

Fixed samples stored in 100% MeOH are rehydrated for 5 min in 75% MeOH/PTW, 5 min in 50% MeOH/PTW and 5 min in 25% MeOH/PTW. Afterwards, the samples are washed 2x 5 min in PTW and bleached if necessary, in 3% H_2O_2 + 0.5% KOH. To permeabilize the samples they are treated with Proteinase K (1/2000 in PTW) according to the stage from 5-12 min. After rinsing in PTW, the samples are fixed in 4% PFA/PTW for 20 min to stop Proteinase

K activity. Afterwards the samples are washed 5x 5 min in PTW. The samples are blocked in Hybridization Mix in a water batch at 65°C for 1-2 h. The samples are incubated with the probe (6-8 µl probe in 200 µl Hybridization Mix, denatured at 80°C for 10 min) overnight at 4°C. On the next day, the samples are washed 2x 30 min in 50% formamide/2x SSCT, 15 min in 2x SSCT and 2x 30 min in 0.2x SSCT at 65°C. Afterwards the samples are blocked in 5% sheep serum/PTW for 1-2 h at room temperature and incubated with α-Dig-AP Fab fragments (1/2000 in 5% sheep serum/PTW) overnight at 4°C. On the next day the samples were washed 6x 10 min in PTW. In situ detection was performed using NBT (337.5 µg/ml) and BCIP (175 µg/ml) in staining buffer after the samples were equilibrated 2x 5 min in staining buffer. The samples were stained up to 48 h in the dark. To stop the staining reaction the samples were fixed in 4%PFA/PTW for 20 min at room temperature. Imaging was performed at a Leica DM5000 B microscope.

5.2.14 Fluorescent *in situ* hybridization

Fixed samples were rehydrated and permeabilized and incubated with the probe as described above. After washing with 2x SSCT for 15 min and 2x 30 min with 0.2x SSCT at 65°C the samples were washed 3x 5 min in TNT. Blocking was done using 2% blocking reagent in TNT for 2 h at room temperature. The samples were incubated with α-Dig-Fab POD (1/50 in 2% blocking reagent in TNT) or α-Fluo-Fab POD (1/50 in 2% blocking reagent in TNT), respectively overnight at 4°C. On the next day, the samples were washed 5x 10 min in TNT and rinsed in 100 µl TSA Amplification Diluent (PerkinElmer Kit). The detection substrate (Fluorescein Fluorophore Tyramide/Cy3 Fluorophore Thyramide/Cy5 Fluorophore Tyramide) was added 1/50 in Amplification Diluent and incubated for 45 min in the dark. Afterwards the samples were washed 4x 10 min in TNT and were ready for imaging in case of a single probe fluorescent *in situ* hybridization.

In case of a double fluorescent *in situ* hybridization, the samples were incubated in 1% H_2O_2/TNT without shaking for 20 min in the dark to stop residual enzyme activity. After washing 4x 5 min and 1x 20 min in TNT, the samples were blocked in 2% blocking reagent in TNT for 1 h at room temperature. The samples were incubated with α-Dig-Fab POD (1/50 in 2% blocking reagent in TNT) or α-Fluo-Fab POD (1/50 in 2% blocking reagent in TNT), respectively together with DAPI (1/500) overnight at 4°C. On the next day detection was performed as described above. After washing the samples 3x 10 min in TNT, the samples were ready for imaging.

5.2.15 Genotyping

For genotyping of embryos or hatchlings they were killed in Tricaine. For genotyping of adult fish fin clips were performed. For gDNA extraction the genetic material was incubated at 95°C in 100 µl 50 mM NaOH for 30 min. Afterwards 25 µl 50 mM Tris-HCl pH8 was added. 1 µl of this was used for genotyping PCR. Analysis of the PCR reaction was done via agarose gel electrophoresis and sequencing in some cases.

Table 15: PCR reaction mix

5x Q5 Reaction Buffer	10 µl
2.5 mM dNTPs	4 µl
Primer forward	1 µl
Primer reverse	1 µl
Q5 High-Fidelity DNA Polymerase	0.5 µl
H_2O	ad 50 µl

5.2.16 Image processing

Image processing was performed with Fiji and Chimera. Figures were prepared using Adobe Illustrator.

5.2.17 DNA ligation

DNA ligation was performed using a 1:3 ratio of backbone to insert. For backbone concentration 20-50 ng was chosen. The insert was adjusted according to following calculation: (vector concentration*insert length/vector length)*3=insert concentration

Table 16: Ligation

	Ligation	Control
H_2O	ad 10 µl	ad 10 µl
10x T4 DANN Ligase buffer	1 µl	1 µl
T4 DNA ligase	1 µl	1 µl
Backbone	20-50 ng	20-50 ng
Insert	1:3 ratio	-
PEG	1 µl	1 µl

5.2.18 GoldenGATEway cloning

GoldenGATEway cloning was performed according to Kirchmaier et al. (2013) to generate the DNA donor construct for endogenous tagging of the *snail2* gene with GFP. Using primers listed above (see table 3), I amplified 5' and 3' homology flanks via PCR from wildtype gDNA. The PCR primers contained specific BsaI restriction sites that were later used in the GoldenGATEway assembly. As a source for the GFP sequence, a GoldenGATEway entry vector 3 containing a GFP with a stop codon was used (plasmid number #4608). GoldenGATEway assembly was done using amplified PCR products, the entry vector containing the GFP sequence and the destination vector (#3900). Using BsaI as a restriction enzyme resulted in specific overhangs, dictating the order of ligated sequences within the destination vector. The final construct contained a 3 bp 5' homology flank, followed by a GFP containing a stop codon and a 318 bp 3' homology flank. Generation of a DNA donor for injection was done via PCR and biotinylated primers (see table 3), preventing oligomerization of the DNA donor.

Table 17: Injection mix for endogenous tagging of *snail2*

CRISPR/Cas9 injection mix with DNA donor
Cas9 mRNA (150 ng/µl)
sgRNAs (15 ng/µl each)
DNA donor (5 ng/µl)
RNase free H_2O ad 10 µl

5.2.19 Transformation of One Shot® Mach1™-T1^R Chemically Competent *E. coli*

1-5 µl of Ligation was added to 50 µl of One Shot® Mach1™-T1^R Chemically Competent *E. coli*. Following an incubation step on ice for 20 min, the bacteria were heat shocked at 42°C for 50 sec. Afterwards, the bacteria were placed on ice for 2 min before adding 200 µl of TB broth. The bacteria were incubated in the shaker at 37°C for 1 h and plated on antibiotics containing LB plates. The plates were put in the 37°C incubator overnight. On the next day, mini cultures were inoculated and incubated at least 5 h before plasmid DNA extraction.

5.2.20 Extraction of plasmid DNA

Plasmid DNA from mini cultures was extracted as follows. 2 ml of the culture were centrifuged for 2 min at 14000 rpm and the supernatant was discarded. The pellet was resuspended using 250 µl P1 resuspension buffer in combination with shaking. Afterwards 250 µl P2 lysis buffer and 250 µl P3 neutralization buffer was added. The samples were inverted 5x after addition of each buffer. The samples were centrifuged for 10 min at full speed at 4°C. 600 µl of the supernatant was mixed with 600 µl 2- propanol by vortexing. The samples were centrifuged again for 10 min at full speed. The supernatant was discarded afterwards. 400 µl 70% EtOH was added to the samples and they were centrifuged for 5 min at full speed. Afterwards the EtOH was removed without disturbing the pellet. The pellet was dissolved in 30 µl H_2O. For further analysis restriction digests and sequencing were performed.
For injection, plasmid DNA was extracted using the Plasmid Midi Kit from Qiagen.

5.2.21 Preparation of sgRNAs

sgRNA sites were chosen using the CCTop tool and corresponding oligonucleotides ordered. Oligos were annealed in the PCR cycler. 1 µl of each oligo (100 µM) was added to18 µl H_2O and 20 µl annealing buffer. After oligo annealing the mix is diluted 1:33 (new concentration: 0.075 pmol/µl). 1 µl of this was ligated into the sgRNA backbone (T7)- DR274 (previously linearized by BsaI-HF digest). The ligation takes place at room temperature for 10 min and was transformed into One Shot® Mach1™-T1R Chemically Competent *E. coli*. After extraction the plasmids were digested with DraI-FD and purified using agarose gel electrophoresis and gel extraction of the 300 bp fragment. The sgRNAs were transcribed using the MEGAShortScript T7 Kit. After TurboDNase treatment and RNA cleanup, the sgRNAs were stored at -20 or -80°C.

Table 18: Oligo annealing program

95°C	5 min
Ramp down to 70°C (0.1°C/sec)	Hold at 70°C for 10 min
Ramp down to 65°C (0.1°C/sec)	Hold at 65°C for 10 min
Ramp down to 60°C (0.1°C/sec)	Hold at 60°C for 10 min
Ramp down to 10°C (0.1°C/sec)	

Table 19: Digest to obtain sgRNA template

10x FastDigest Green Buffer	6 µl
DNA	10 µg
DraI-FD	3 µl
H_2O	ad 60 µl

5.2.22 BrdU incorporation and staining

Fish at different stages were treated with 0.04 g BrdU in 50 ml 1x ERM for 6 h. The fish were fixed immediately after the BrdU treatment as described above. For the staining fish were washed 3x 5 min in 1x PTW and post-fixed for 30 min using 4% PFA/PTW. The fish were washed again as described above. Antigen retrieval was performed by incubating the fish in 1.7 N HCl (42.5 ml 2N HCl, 5 ml 10x PBS, 2.5 ml 10% Triton-X. After washing the fish as described above pH recovery was done by incubating the fish in Borax/PTW (4 ml of saturated borax solution in 6 ml 1x PTW) for 15 min. After washing the fish, they were blocked for at least 2 h with 10% NGS. The primary antibody was applied in 1% NGS overnight at 4°C. On the next day, the samples were washed 6x 5 min in 1xPTW and incubated with the secondary antibody in 1% NGS for at least 2 h at 37°C.

5.2.23 Agarose gel electrophoresis

For agarose gel electrophoresis 1%-1.5% agarose gels were prepared. Samples were mixed with loading dye and loaded into the gels. Gel electrophoresis was performed at 100-140 V. For imaging, the gel was incubated in EtBr for some minutes and visualized in a UV-Gel Documentation System.

5.2.24 Gel extraction

Gel slices were cut from the gel using a scalpel. Gel extraction was performed following the instructions provided with the respective kit: innuPREP Gel Extraction Kit and Monarch® DNA Gel Extraction Kit. Efficiency was determined using a DeNovix DS-11 spectrophotometer.

5.2.25 PCR cleanup

PCR cleanups were performed according to the instructions provided by the Monarch® PCR & DNA Cleanup Kit. Efficiency was determined using a DeNovix DS-11 spectrophotometer.

5.2.26 Restriction digest

Restriction digests were performed at 37°C for a duration of 1 h – overnight. Efficiency of restriction digests was examined using agarose gel electrophoresis. For restriction digests enzymes and buffers from NEB/Thermo Fisher Scientific were used.

Table 20: Ingredients for restriction digestion

Plasmid DNA	8 µg for cloning, 2 µl for test digest
Restriction digest buffer	1/10 dilution
Restriction enzyme	0.5-1 µl
H_2O	ad 30 µl for cloning, ad 10 µl for test digest

Acknowledgements

First and foremost, I would like to thank Lázaro. I am so grateful that you not only gave me the opportunity to do a Ph.D. in your lab, but you believed in me, even when I didn't. Although you were always there for support and advice (both scientifically and otherwise), you let me follow my own path. I cannot overstate the impact this had on me. During the time of my Ph.D. I grew immensely, both scientifically and personally, and this is largely due to your support. I will always look back fondly to my time in your lab and I hope I made a lasting impression as well.

Secondly, I would like to thank my TAC members Carmen, Steffen and Jochen. I am very grateful for your feedback during my TAC meetings. Together with Lázaro you helped me become the scientist I am now.

Furthermore, I need to thank the entire 5th floor including the fish team for creating an amazing working atmosphere - I feel very blessed to have been a part of such a community. I would like to especially thank Girish for a helpful discussion on the temperature experiment and Tina, whom I shared numerous conversations with. Your encouraging words helped me through many days!

Special thanks goes also to all former and current Centaniños. You all made my Ph.D. a great experience that I would not want to have missed! Throughout my time in the lab, I met many amazing colleagues that eventually became friends. When I started in the lab, Julian, Isa and especially Ali supervised and taught me a lot. Julian tried (and failed) to cure me of my naivety, by constantly bamboozling me. Unfortunately, and to my shame, I fell for it most of the times. Ali has been extremely supportive from the beginning. His passion for science inspired me immensely and I am truly grateful to call him a friend. I would also like to thank Claudia. Apart from your magical cloning hands I am grateful for the countless great conversations we had about the serious, but also funny sides of life. Furthermore, I would like to thank Jasmin, who truly became a friend over the course of my time in the lab. I would not have enjoyed my Ph.D. as much without you. I would also like to thank Javi for always offering a helping hand and Rebecca for her support in the aLL project and our shared passion for history. You all made the time I spent in the lab very enjoyable and memorable.

Even if their time in the lab was rather short, I would also like to thank Silvia for sharing my passion for funny dialect words, Leonie for many good conversations and confidence boosters, and Tugçe for her patience with cloning of the snail constructs.

I would also like to thank my friends outside of the lab. I am very grateful to you for balancing and grounding me.
Last, but not least, I need to thank my family, without whom I would not be the person I am. I am truly grateful for your unwavering love and support throughout my life.

References

Al-Hilli, F., Wright, E.A., 1983. The effects of changes in the environmental temperature on the growth of tail bones in the mouse. Br J Exp Pathol 64, 34-42.

Aman, A., Piotrowski, T., 2008. Wnt/beta-catenin and Fgf signaling control collective cell migration by restricting chemokine receptor expression. Dev Cell 15, 749-761.

Aman, A., Piotrowski, T., 2010. Cell migration during morphogenesis. Dev Biol 341, 20-33.

Ansai, S., Kinoshita, M., 2014. Targeted mutagenesis using CRISPR/Cas system in medaka. Biol Open 3, 362-371.

Baker, C.V., Bronner-Fraser, M., 2001. Vertebrate cranial placodes I. Embryonic induction. Dev Biol 232, 1-61.

Balfour, F.M., A Monograph on the Development of Elasmobranch Fishes.

Barrallo-Gimeno, A., Nieto, M.A., 2005. The Snail genes as inducers of cell movement and survival: implications in development and cancer. Development 132, 3151-3161.

Becker, C., Lust, K., Wittbrodt, J., 2021. Igf signaling couples retina growth with body growth by modulating progenitor cell division. Development 148.

Blaser, H., Eisenbeiss, S., Neumann, M., Reichman-Fried, M., Thisse, B., Thisse, C., Raz, E., 2005. Transition from non-motile behaviour to directed migration during early PGC development in zebrafish. J Cell Sci 118, 4027-4038.

Blaser, H., Reichman-Fried, M., Castanon, I., Dumstrei, K., Marlow, F.L., Kawakami, K., Solnica-Krezel, L., Heisenberg, C.P., Raz, E., 2006. Migration of zebrafish primordial germ cells: a role for myosin contraction and cytoplasmic flow. Dev Cell 11, 613-627.

Booth, B.W., Mack, D.L., Androutsellis-Theotokis, A., McKay, R.D., Boulanger, C.A., Smith, G.H., 2008. The mammary microenvironment alters the differentiation repertoire of neural stem cells. Proc Natl Acad Sci U S A 105, 14891-14896.

Campanale, J.P., Sun, T.Y., Montell, D.J., 2017. Development and dynamics of cell polarity at a glance. J Cell Sci 130, 1201-1207.

Centanin, L., Ander, J.J., Hoeckendorf, B., Lust, K., Kellner, T., Kraemer, I., Urbany, C., Hasel, E., Harris, W.A., Simons, B.D., Wittbrodt, J., 2014. Exclusive multipotency and preferential asymmetric divisions in post-embryonic neural stem cells of the fish retina. Development 141, 3472-3482.

Chacon-Martinez, C.A., Koester, J., Wickstrom, S.A., 2018. Signaling in the stem cell niche: regulating cell fate, function and plasticity. Development 145.

Chappell, J.C., Cluceru, J.G., Nesmith, J.E., Mouillesseaux, K.P., Bradley, V.B., Hartland, C.M., Hashambhoy-Ramsay, Y.L., Walpole, J., Peirce, S.M., Mac Gabhann, F., Bautch, V.L., 2016. Flt-1 (VEGFR-1) coordinates discrete stages of blood vessel formation. Cardiovasc Res 111, 84-93.

Choi, B., Kim, D., Han, I., Lee, S.H., 2018. Microenvironmental Regulation of Stem Cell Behavior Through Biochemical and Biophysical Stimulation. Adv Exp Med Biol 1064, 147-160.

Cunha, G.R., Young, P., Christov, K., Guzman, R., Nandi, S., Talamantes, F., Thordarson, G., 1995. Mammary phenotypic expression induced in epidermal cells by embryonic mammary mesenchyme. Acta Anat (Basel) 152, 195-204.

Dalle Nogare, D., Chitnis, A.B., 2017. A framework for understanding morphogenesis and migration of the zebrafish posterior Lateral Line primordium. Mech Dev 148, 69-78.

Dambly-Chaudiere, C., Cubedo, N., Ghysen, A., 2007. Control of cell migration in the development of the posterior lateral line: antagonistic interactions between the chemokine receptors CXCR4 and CXCR7/RDC1. BMC Dev Biol 7, 23.

Davey, C.F., Moens, C.B., 2017. Planar cell polarity in moving cells: think globally, act locally. Development 144, 187-200.

de Lucas, B., Perez, L.M., Galvez, B.G., 2018. Importance and regulation of adult stem cell migration. J Cell Mol Med 22, 746-754.

Dijkgraaf, S., 1963. The functioning and significance of the lateral-line organs. Biol Rev Camb Philos Soc 38, 51-105.

Djagaeva, I., Doronkin, S., 2010. Hypoxia response pathway in border cell migration. Cell Adh Migr 4, 391-395.

Doitsidou, M., Reichman-Fried, M., Stebler, J., Koprunner, M., Dorries, J., Meyer, D., Esguerra, C.V., Leung, T., Raz, E., 2002. Guidance of primordial germ cell migration by the chemokine SDF-1. Cell 111, 647-659.

Dona, E., Barry, J.D., Valentin, G., Quirin, C., Khmelinskii, A., Kunze, A., Durdu, S., Newton, L.R., Fernandez-Minan, A., Huber, W., Knop, M., Gilmour, D., 2013. Directional tissue migration through a self-generated chemokine gradient. Nature 503, 285-289.

Fiore, A., Ribeiro, P.F., Bruni-Cardoso, A., 2018. Sleeping Beauty and the Microenvironment Enchantment: Microenvironmental Regulation of the Proliferation-Quiescence Decision in Normal Tissues and in Cancer Development. Front Cell Dev Biol 6, 59.

Gheldof, A., Berx, G., 2013. Cadherins and epithelial-to-mesenchymal transition. Prog Mol Biol Transl Sci 116, 317-336.

Ghysen, A., Dambly-Chaudiere, C., 2007. The lateral line microcosmos. Genes Dev 21, 2118-2130.

Gillis, J.A., Modrell, M.S., Northcutt, R.G., Catania, K.C., Luer, C.A., Baker, C.V., 2012. Electrosensory ampullary organs are derived from lateral line placodes in cartilaginous fishes. Development 139, 3142-3146.

Goddard, T.D., Huang, C.C., Meng, E.C., Pettersen, E.F., Couch, G.S., Morris, J.H., Ferrin, T.E., 2018. UCSF ChimeraX: Meeting modern challenges in visualization and analysis. Protein Sci 27, 14-25.

Grabher, C., Wittbrodt, J., 2007. Meganuclease and transposon mediated transgenesis in medaka. Genome Biol 8 Suppl 1, S10.

Graf, T., Stadtfeld, M., 2008. Heterogeneity of embryonic and adult stem cells. Cell Stem Cell 3, 480-483.

Grimes, D.T., 2019. Making and breaking symmetry in development, growth and disease. Development 146.

Gross, J.B., Gangidine, A., Powers, A.K., 2016. Asymmetric Facial Bone Fragmentation Mirrors Asymmetric Distribution of Cranial Neuromasts in Blind Mexican Cavefish. Symmetry (Basel) 8.

Gutierrez-Triana, J.A., Tavhelidse, T., Thumberger, T., Thomas, I., Wittbrodt, B., Kellner, T., Anlas, K., Tsingos, E., Wittbrodt, J., 2018. Efficient single-copy HDR by 5' modified long dsDNA donors. Elife 7.

Haas, P., Gilmour, D., 2006. Chemokine signaling mediates self-organizing tissue migration in the zebrafish lateral line. Dev Cell 10, 673-680.

Harris, M.L., Erickson, C.A., 2007. Lineage specification in neural crest cell pathfinding. Dev Dyn 236, 1-19.

Harrison, R.G., 1904. Experimentelle Untersuchung über die Entwicklung der Sinnesorgane der Seitenlinie bei den Amphibien. Arch. Mikrosk. Anat. EntwMech 63.

Harrison, R.G., 1945. Relations of symmetry in thet developing embryo. Trans. Conn. Acad. Arts. Sci. 36: 277-330.

Hofer, B., 1908. Studien über die Hautsinnesorgane der Fische. I. Die Funktion der Seitenorgane bei den Fischen. Ber Kgl Bayer Biol Versuchsstation München 1: 115-164.

Hollo, G., 2017. Demystification of animal symmetry: symmetry is a response to mechanical forces. Biol Direct 12, 11.

Hudson, A., 2000. Development of Symmetry in Plants. Annu Rev Plant Physiol Plant Mol Biol 51, 349-370.

Huxley, T.H., 1859. Observations on the Development of some parts of the Skeleton of Fishes. Transactions of The Microscopical Society & Journal 7, 33-46.

Ishikawa, Y., 1994. Innervation of lateral line system in the medaka, Oryzias latipes. The Fish Biology Journal Medaka 6, 17-24.

Iwasaki, M., Yokoi, H., Suzuki, T., Kawakami, K., Wada, H., 2020. Development of the anterior lateral line system through local tissue-tissue interactions in the zebrafish head. Dev Dyn.

Jones, D.P., Singer, M., 1969. Neurotrophic dependence of the lateral-line sensory organs of the newt, Triturus viridescens. J Exp Zool 171, 433-442.

Kaelin, W.G., Jr., Ratcliffe, P.J., 2008. Oxygen sensing by metazoans: the central role of the HIF hydroxylase pathway. Mol Cell 30, 393-402.

Kang, Y., Massague, J., 2004. Epithelial-mesenchymal transitions: twist in development and metastasis. Cell 118, 277-279.

Karakatsani, A., Shah, B., Ruiz de Almodovar, C., 2019. Blood Vessels as Regulators of Neural Stem Cell Properties. Front Mol Neurosci 12, 85.

Kho, A.T., Zhao, Q., Cai, Z., Butte, A.J., Kim, J.Y., Pomeroy, S.L., Rowitch, D.H., Kohane, I.S., 2004. Conserved mechanisms across development and tumorigenesis revealed by a mouse development perspective of human cancers. Genes Dev 18, 629-640.

Kirchmaier, S., Lust, K., Wittbrodt, J., 2013. Golden GATEway cloning--a combinatorial approach to generate fusion and recombination constructs. PLoS One 8, e76117.

Knaut, H., Werz, C., Geisler, R., Nusslein-Volhard, C., Tubingen Screen, C., 2003. A zebrafish homologue of the chemokine receptor Cxcr4 is a germ-cell guidance receptor. Nature 421, 279-282.

Kokovay, E., Goderie, S., Wang, Y., Lotz, S., Lin, G., Sun, Y., Roysam, B., Shen, Q., Temple, S., 2010. Adult SVZ lineage cells home to and leave the vascular niche via differential responses to SDF1/CXCR4 signaling. Cell Stem Cell 7, 163-173.

Krueger J, L.D., Scholz K, Zimmer A, Shi Y, Klein C, Siekmann A, Schulte-Merker S, Cudmore M, Ahmed A, le Noble F, 2011. Flt1 acts as a negative regulator of tip cell formation and branching morphogenesis in the zebrafish embryo. Development 138(10):2111-20.

Lammert, E., Cleaver, O., Melton, D., 2001. Induction of pancreatic differentiation by signals from blood vessels. Science 294, 564-567.

Ledent, V., 2002. Postembryonic development of the posterior lateral line in zebrafish. Development 129, 597-604.

Leydig, F., 1850. Über die Schleimkanäle der Knochenfische. Archiv f. Anat., Phys. u. wiss. Med.

Liedke, K.B., 1955. Studies on lens induction in Amblystoma punctatum. J. Exp. Zool. 130, 353-379.

Liedtke, D., Erhard, I., Schartl, M., 2011. snail gene expression in the medaka, Oryzias latipes. Gene Expr Patterns 11, 181-189.

Lischik, C.Q., Adelmann, L., Wittbrodt, J., 2019. Enhanced in vivo-imaging in medaka by optimized anaesthesia, fluorescent protein selection and removal of pigmentation. PLoS One 14, e0212956.

Litsiou, A., Hanson, S., Streit, A., 2005. A balance of FGF, BMP and WNT signalling positions the future placode territory in the head. Development 132, 4051-4062.

Lush, M.E., Diaz, D.C., Koenecke, N., Baek, S., Boldt, H., St Peter, M.K., Gaitan-Escudero, T., Romero-Carvajal, A., Busch-Nentwich, E.M., Perera, A.G., Hall, K.E., Peak, A., Haug, J.S., Piotrowski, T., 2019. scRNA-Seq reveals distinct stem cell populations that drive hair cell regeneration after loss of Fgf and Notch signaling. Elife 8.

Mangold, O., 1929. Wilhelm Roux Arch Entwickl Mech Org 117, 586-696.

Manokawinchoke, J., Pavasant, P., Limjeerajarus, C.N., Limjeerajarus, N., Osathanon, T., Egusa, H., 2021. Mechanical loading and the control of stem cell behavior. Arch Oral Biol 125, 105092.

Matsumoto, K., Yoshitomi, H., Rossant, J., Zaret, K.S., 2001. Liver organogenesis promoted by endothelial cells prior to vascular function. Science 294, 559-563.

Mitsiadis, T.A., Caton, J., Cobourne, M., 2006. Waking-up the sleeping beauty: recovery of the ancestral bird odontogenic program. J Exp Zool B Mol Dev Evol 306, 227-233.

Mitsiadis, T.A., Cheraud, Y., Sharpe, P., Fontaine-Perus, J., 2003. Development of teeth in chick embryos after mouse neural crest transplantations. Proc Natl Acad Sci U S A 100, 6541-6545.

Miyamoto, Y., Sakane, F., Hashimoto, K., 2015. N-cadherin-based adherens junction regulates the maintenance, proliferation, and differentiation of neural progenitor cells during development. Cell Adh Migr 9, 183-192.

Montana, V., Sontheimer, H., 2011. Bradykinin promotes the chemotactic invasion of primary brain tumors. J Neurosci 31, 4858-4867.

Moody, S.A., LaMantia, A.S., 2015. Transcriptional regulation of cranial sensory placode development. Curr Top Dev Biol 111, 301-350.

Morgan, T.H., 1923. The Development of Asymmetry in the Fiddler Crab. The American Naturalist 57, No 650, 269-273.

Morrison, S.J., Spradling, A.C., 2008. Stem cells and niches: mechanisms that promote stem cell maintenance throughout life. Cell 132, 598-611.

Moubayidin, L., Ostergaard, L., 2015. Symmetry matters. New Phytol 207, 985-990.

Naumann, U., Cameroni, E., Pruenster, M., Mahabaleshwar, H., Raz, E., Zerwes, H.G., Rot, A., Thelen, M., 2010. CXCR7 functions as a scavenger for CXCL12 and CXCL11. PLoS One 5, e9175.

Nechiporuk, A., Raible, D.W., 2008. FGF-dependent mechanosensory organ patterning in zebrafish. Science 320, 1774-1777.

Neelathi, U.M., Dalle Nogare, D., Chitnis, A.B., 2018. Cxcl12a induces snail1b expression to initiate collective migration and sequential Fgf-dependent neuromast formation in the zebrafish posterior lateral line primordium. Development 145.

Nikaido, M., Navajas Acedo, J., Hatta, K., Piotrowski, T., 2017. Retinoic acid is required and Fgf, Wnt, and Bmp signaling inhibit posterior lateral line placode induction in zebrafish. Dev Biol 431, 215-225.

Nogare, D.D., Natesh, N., Chitnis, A., 2019. A sheath of motile cells supports collective migration in of the Zebrafish posterior lateral line primordium under the skin. 783043.

Northcutt, R.G., 1996. THE ORIGIN OF CRANIATES: NEURAL CREST, NEUROGENIC PLACODES, AND HOMEOBOX GENES. Israel Journal of Zoology 42, S273-S313.

Northcutt, R.G., Catania, K.C., Criley, B.B., 1994. Development of lateral line organs in the axolotl. J Comp Neurol 340, 480-514.

Nunez, V.A., Sarrazin, A.F., Cubedo, N., Allende, M.L., Dambly-Chaudiere, C., Ghysen, A., 2009. Postembryonic development of the posterior lateral line in the zebrafish. Evol Dev 11, 391-404.

Ohkawara, B., Glinka, A., Niehrs, C., 2011. Rspo3 binds syndecan 4 and induces Wnt/PCP signaling via clathrin-mediated endocytosis to promote morphogenesis. Dev Cell 20, 303-314.

Okuyama, T., Isoe, Y., Hoki, M., Suehiro, Y., Yamagishi, G., Naruse, K., Kinoshita, M., Kamei, Y., Shimizu, A., Kubo, T., Takeuchi, H., 2013. Controlled Cre/loxP site-specific recombination in the developing brain in medaka fish, Oryzias latipes. PLoS One 8, e66597.

Pescador, N., Cuevas, Y., Naranjo, S., Alcaide, M., Villar, D., Landazuri, M.O., Del Peso, L., 2005. Identification of a functional hypoxia-responsive element that regulates the expression of the egl nine homologue 3 (egln3/phd3) gene. Biochem J 390, 189-197.

Pieper, M., Eagleson, G.W., Wosniok, W., Schlosser, G., 2011. Origin and segregation of cranial placodes in Xenopus laevis. Dev Biol 360, 257-275.

Piotrowski, T., Baker, C.V., 2014. The development of lateral line placodes: taking a broader view. Dev Biol 389, 68-81.

Ramasamy, S.K., Kusumbe, A.P., Adams, R.H., 2015. Regulation of tissue morphogenesis by endothelial cell-derived signals. Trends Cell Biol 25, 148-157.

Reedy, M.V., Faraco, C.D., Erickson, C.A., 1998. The delayed entry of thoracic neural crest cells into the dorsolateral path is a consequence of the late emigration of melanogenic neural crest cells from the neural tube. Dev Biol 200, 234-246.

Ribatti, D., Vacca, A., Dammacco, F., 1999. The role of the vascular phase in solid tumor growth: a historical review. Neoplasia 1, 293-302.

Sapede, D., Gompel, N., Dambly-Chaudiere, C., Ghysen, A., 2002. Cell migration in the postembryonic development of the fish lateral line. Development 129, 605-615.

Schindelin, J., Arganda-Carreras, I., Frise, E., Kaynig, V., Longair, M., Pietzsch, T., Preibisch, S., Rueden, C., Saalfeld, S., Schmid, B., Tinevez, J.Y., White, D.J., Hartenstein, V., Eliceiri, K., Tomancak, P., Cardona, A., 2012. Fiji: an open-source platform for biological-image analysis. Nat Methods 9, 676-682.

Schlosser, G., 2002a. Development and evolution of lateral line placodes in amphibians I. Development. Zoology (Jena) 105, 119-146.

Schlosser, G., 2002b. Development and evolution of lateral line placodes in amphibians. - II. Evolutionary diversification. Zoology (Jena) 105, 177-193.

Schlosser, G., 2006. Induction and specification of cranial placodes. Dev Biol 294, 303-351.

Schlosser, G., 2007. How old genes make a new head: redeployment of Six and Eya genes during the evolution of vertebrate cranial placodes. Integr Comp Biol 47, 343-359.

Schlosser, G., 2010. Making senses development of vertebrate cranial placodes. Int Rev Cell Mol Biol 283, 129-234.

Schulze, F.E., 1870. Über die Sinnesorgane der Seitenlinie bei Fischen und Amphibien. Archif für mikroskopische Anatomie 6, 62-88.

Seifert, J.R., Mlodzik, M., 2007. Frizzled/PCP signalling: a conserved mechanism regulating cell polarity and directed motility. Nat Rev Genet 8, 126-138.

Seleit, A., 2019. On the Development and Evolution of the Lateral Line. Heidelberg University, https://archiv.ub.uni-heidelberg.de/volltextserver/26891/.

Seleit, A., Gross, K., Onistschenko, J., Hoang, O.P., Theelke, J., Centanin, L., 2021. Local tissue interactions govern pLL patterning in medaka. Dev Biol 481, 1-13.

Seleit, A., Kramer, I., Ambrosio, E., Dross, N., Engel, U., Centanin, L., 2017a. Sequential organogenesis sets two parallel sensory lines in medaka. Development 144, 687-697.

Seleit, A., Kramer, I., Riebesehl, B.F., Ambrosio, E.M., Stolper, J.S., Lischik, C.Q., Dross, N., Centanin, L., 2017b. Neural stem cells induce the formation of their physical niche during organogenesis. Elife 6.

Serluca, F.C., Drummond, I.A., Fishman, M.C., 2002. Endothelial signaling in kidney morphogenesis: a role for hemodynamic forces. Curr Biol 12, 492-497.

Serluca, F.C., Fishman, M.C., 2001. Pre-pattern in the pronephric kidney field of zebrafish. Development 128, 2233-2241.

Serrat, M.A., 2014. Environmental temperature impact on bone and cartilage growth. Compr Physiol 4, 621-655.

Shubin, N., 2008. Your inner fish : a journey into the 3.5 billion- year history of the human body. Allen Lane, London.

Shweiki, D., Itin, A., Soffer, D., Keshet, E., 1992. Vascular endothelial growth factor induced by hypoxia may mediate hypoxia-initiated angiogenesis. Nature 359, 843-845.

Singhal, M., Gengenbacher, N., Abdul Pari, A.A., Kamiyama, M., Hai, L., Kuhn, B.J., Kallenberg, D.M., Kulkarni, S.R., Camilli, C., Preuss, S.F., Leuchs, B., Mogler, C., Espinet, E., Besemfelder, E., Heide, D., Heikenwalder, M., Sprick, M.R., Trumpp, A., Krijgsveld, J., Schlesner, M., Hu, J., Moss, S.E., Greenwood, J., Augustin, H.G., 2021. Temporal multi-omics identifies LRG1 as a vascular niche instructor of metastasis. Sci Transl Med 13, eabe6805.

Speidel, C.C., 1948. Correlated studies of sense organs and nerves of the lateral-line in living frog tadpoles; the trophic influence of specific nerve supply as revealed by prolonged observations of denervated and reinnervated organs. Am J Anat 82, 277-320.

Stemmer, M., Thumberger, T., Del Sol Keyer, M., Wittbrodt, J., Mateo, J.L., 2015. CCTop: An Intuitive, Flexible and Reliable CRISPR/Cas9 Target Prediction Tool. PLoS One 10, e0124633.

Stone, L.S., 1928. Experiments on the transplantation of placodes of the cranial ganglia in the amphibian embryo. III. Preauditory and postauditory placodal materials interchanged. Journal of Comparative Neurology 47, 117-154.

Stone, L.S., 1933. The development of lateral-line sense organs in amphibians observed in living and vital-stained preparations. Journal of Comparative Neurology 57, 507-540.

Swinburne, I.A., Mosaliganti, K.R., Green, A.A., Megason, S.G., 2015. Improved Long-Term Imaging of Embryos with Genetically Encoded alpha-Bungarotoxin. PLoS One 10, e0134005.

Talmadge, J.E., Fidler, I.J., 2010. AACR centennial series: the biology of cancer metastasis: historical perspective. Cancer Res 70, 5649-5669.

Thiery, J.P., 2002. Epithelial-mesenchymal transitions in tumour progression. Nat Rev Cancer 2, 442-454.

Thompson, D.A.W., On Growth and Form. [With illustrations.].

Tirziu, D., Simons, M., 2009. Endothelium as master regulator of organ development and growth. Vascul Pharmacol 50, 1-7.

Tsingos, E., Hockendorf, B., Sutterlin, T., Kirchmaier, S., Grabe, N., Centanin, L., Wittbrodt, J., 2019. Retinal stem cells modulate proliferative parameters to coordinate post-embryonic morphogenesis in the eye of fish. Elife 8.

Valentin, G., Haas, P., Gilmour, D., 2007. The chemokine SDF1a coordinates tissue migration through the spatially restricted activation of Cxcr7 and Cxcr4b. Curr Biol 17, 1026-1031.

Vining, K.H., Mooney, D.J., 2017. Mechanical forces direct stem cell behaviour in development and regeneration. Nat Rev Mol Cell Biol 18, 728-742.

von Baer, C.E., 1835. Untersuchungen über die Entwicklungsgeschichte der Fische. F. Ch, W. Vogel.

Wada, H., Dambly-Chaudiere, C., Kawakami, K., Ghysen, A., 2013. Innervation is required for sense organ development in the lateral line system of adult zebrafish. Proc Natl Acad Sci U S A 110, 5659-5664.

Wada, H., Ghysen, A., Satou, C., Higashijima, S., Kawakami, K., Hamaguchi, S., Sakaizumi, M., 2010. Dermal morphogenesis controls lateral line patterning during postembryonic development of teleost fish. Dev Biol 340, 583-594.

Wilson, Y.M., Richards, K.L., Ford-Perriss, M.L., Panthier, J.J., Murphy, M., 2004. Neural crest cell lineage segregation in the mouse neural tube. Development 131, 6153-6162.

Winklbauer, R., Hausen, P., 1983. Development of the lateral line system in Xenopus laevis. I. Normal development and cell movement in the supraorbital system. J Embryol Exp Morphol 76, 265-281.

Winkler, S., Loosli, F., Henrich, T., Wakamatsu, Y., Wittbrodt, J., 2000. The conditional medaka mutation eyeless uncouples patterning and morphogenesis of the eye. Development 127, 1911-1919.

Wittbrodt, J., Shima, A., Schartl, M., 2002. Medaka--a model organism from the far East. Nat Rev Genet 3, 53-64.

Wong, R.C., Pera, M.F., Pebay, A., 2008. Role of gap junctions in embryonic and somatic stem cells. Stem Cell Rev 4, 283-292.

Wright, M.R., 1947. Regeneration and degeneration experiments on lateral line nerves and sense organs in anurans. J Exp Zool 105, 221-257.

Yasuoka, A., Hirose, Y., Yoda, H., Aihara, Y., Suwa, H., Niwa, K., Sasado, T., Morinaga, C., Deguchi, T., Henrich, T., Iwanami, N., Kunimatsu, S., Abe, K., Kondoh, H., Furutani-Seiki, M., 2004. Mutations affecting the formation of posterior lateral line system in Medaka, Oryzias latipes. Mech Dev 121, 729-738.

Yoshitomi, H., Zaret, K.S., 2004. Endothelial cell interactions initiate dorsal pancreas development by selectively inducing the transcription factor Ptf1a. Development 131, 807-81

Declaration

I herewith declare that I have written the PhD thesis “Embryonic and post-embryonic organogenesis in the medaka lateral line” on my own with no other sources and aids than quoted.

Heidelberg, 2022

List of Figures

List of Tables